



THE HONG KONG
POLYTECHNIC UNIVERSITY

香港理工大學

Pao Yue-kong Library

包玉剛圖書館

Copyright Undertaking

This thesis is protected by copyright, with all rights reserved.

By reading and using the thesis, the reader understands and agrees to the following terms:

1. The reader will abide by the rules and legal ordinances governing copyright regarding the use of the thesis.
2. The reader will use the thesis for the purpose of research or private study only and not for distribution or further reproduction or any other purpose.
3. The reader agrees to indemnify and hold the University harmless from and against any loss, damage, cost, liability or expenses arising from copyright infringement or unauthorized usage.

IMPORTANT

If you have reasons to believe that any materials in this thesis are deemed not suitable to be distributed in this form, or a copyright owner having difficulty with the material being included in our database, please contact lbsys@polyu.edu.hk providing details. The Library will look into your claim and consider taking remedial action upon receipt of the written requests.

Pao Yue-kong Library, The Hong Kong Polytechnic University, Hung Hom, Kowloon, Hong Kong

<http://www.lib.polyu.edu.hk>

**CELL BALANCING TECHNIQUES FOR
ELECTRIC VEHICLES AND ASSOCIATED
DISTRIBUTED MOBILE ENERGY STORAGE
CITY STUDY**

WANG XIAOLIN

PhD

The Hong Kong Polytechnic University

2019

**The Hong Kong Polytechnic University
Department of Electrical Engineering**

**Cell Balancing Techniques for Electric Vehicles
and Associated Distributed Mobile Energy Storage
City Study**

WANG XIAOLIN

A thesis submitted in partial fulfillment of the requirements
for the degree of Doctor of Philosophy

Aug. 2018

CERTIFICATE OF ORIGINALITY

I hereby declare that this thesis is my own work and that, to the best of my knowledge and belief, it reproduces no material previously published or written, nor material that has been accepted for the award of any other degree or diploma, except where due acknowledgement has been made in the text.

_____(Signed)

WANG Xiaolin (Name of student)

To my family

Abstract

Environmental protection has become a global priority as people are getting increasingly aware of the importance of sustainable development. Energy storage system is receiving increasing attention as it can store and buffer power with fast response. Due to the intermittence nature and stochastic user behavior, developing effective storage system is the cornerstone for integration of new energy sources, such as photovoltaic, wind power and electric vehicles (EV). Therefore, this thesis strives to provide novel control techniques for balancing voltages of hybrid new energy sources and facilitating new energy penetration to increase power efficiency.

Distributed energy sources, composed of distributed generation and energy storage, are another type of new energy sources penetrated in smart cities. For energy storage, supercapacitor (SC) has attracted increasing interest as it has advantages in high power density. In future energy storage systems, the types of energy sources will be hybrid for performance optimization which add extra challenges for cell balancing. Based on switched-capacitor and tapped-inductor principles, this thesis puts forward two novel and flexible topologies for balancing of hybrid energy sources which pave ways for the integration of SCs with other existing sources with higher compatibility and balancing accuracy.

EVs usually have various driving modes that balancing circuit should also equip energy loss reduction and multi-function capabilities. To overcome the problem of switching loss during balancing process, another novel cell balancing circuit is proposed with integration of zero-current switching technique. Moreover, the balancing circuit proposed can change between buck-boost pattern and switched-capacitor pattern with flexible control to cater the balancing requirements under different driving scenarios.

By solving the problem of cell balancing, EVs of high performance can play important roles in improving energy efficiency in smart city. In a combined urban transportation and power grid system, EVs are not only simple transport tools, but also mobile and distributed energy sources/consumers. However, there are mainly three challenges in utilizing energy from EVs: Firstly, the stochasticity of driving behavior, traffic and weather should be taken into account in the forecast of EV charging demand. Secondly, the control strategies adopted for peak shaving among all functioning urban districts shall be redesigned for optimized charging arrangement and energy utilization. Thirdly, the compensation to attract customer control acceptance should be considered as human may arbitrarily not follow control signals. This thesis strives to make a more practical forecast of EV charging demand with Markov chain model and propose an effective pricing control strategy with consideration of EV user behavior for improving the energy efficiency of the city.

Acknowledgements

First of all, I would like to express my sincere appreciation to my chief supervisor, Prof. K. W. Eric Cheng, for his continuous support and constructive suggestions throughout my PhD study. His enthusiasm, patience, erudition and creative way of thinking have profoundly promoted my academic abilities. It has been an honor to study under his supervision that I will cherish every moment discussing and learning with him.

I have spent four memorable and fruitful years with my research team. I really appreciate the selfless help from my colleagues and give my special thanks to Dr. Xu Cuidong and Mr. Wang Daohong who helped me with my experiments and encouraged me when facing difficulties. I would like to present my special thanks to Mr. Fong Yat-Chi, who gave me a lot of help on revising papers and drafting this thesis. Moreover, I would like to express my gratitude to my paper reviewers and thesis examiners for their invaluable comments to this research.

Finally, my genuine appreciation and love belong to my dear parents and husband who support me unconditionally in my Ph.D. study. Their encouragement keeps me moving forward with confidence.

Table of Contents

Abstract	I
Acknowledgement	III
Table of Contents	IV
Lists of Figures	VIII
Lists of Tables	XI
Lists of Abbreviations and Symbols	XII
Chapter I	
Introduction	1
1.1 Background and Incentives of Research	1
1.1.1 Current Problems on New Energy Utilization	1
1.1.2 Importance of Cell Balancing and Current Deficiency.....	1
1.1.3 Load control in Smart City Using EV Batteries.....	5
1.2 Primary Contributions	8
1.2.1 Series-Parallel Switched-Capacitor Balancing Circuit for Hybrid Source Package	8
1.2.2 Voltage Cell Balancing for Battery and SC Source Package with Tapped Inductor Techniques.....	9
1.2.3 Zero-Current Switching Switched-Capacitors Balancing Circuit for Battery/ SC Voltage Equalization	9
1.2.4 Forecast of Urban EV Charging Load and Smart Control Concerning Uncertainties.....	10
1.3 Thesis Layout	11
1.4 List of Publications	12
Chapter II	
Series-Parallel Switched-Capacitor Balancing Circuit for Hybrid Source Package	14
2.1 Introduction	14
2.2 Switched-Capacitor Voltage Balancing Circuit	15
2.2.1 Circuitry Description and Operation Principle	15
2.2.2 State Analysis in Clock Phase ϕ_a	16

2.2.3 State Analysis in Clock Phase ϕ_b	17
2.3 Modeling for Switched-Capacitor Voltage Equalizer	19
2.3.1 Equivalent Resistance Analysis	19
2.3.2 Energy Conversion Loss Analysis	23
2.3.3 Balancing Duration Analysis	24
2.4 Simulation Results of the Switched-Capacitor Voltage Equalizer	25
2.5 Experimental Results of the Switched-Capacitor Voltage Equalizer	27
2.6 Conclusion.....	31
Chapter III	
Non-Equal Voltage Cell Balancing for Battery and Super-Capacitor Source Package Management System Using Tapped Inductor Techniques	
	32
3.1 Introduction	32
3.2 Tapped Inductor Basic Circuit	29
3.2.1 Conventional Buck-Boost Balancing	29
3.2.2 The Tapped Inductor Basic Theory.....	29
3.3 The Tapped Inductor Balancing.....	35
3.3.1 Basic Cell Equalization	35
3.3.2 Generalized Cell Equalization.....	37
3.4 Modeling of Tapped Inductor Voltage Equalizer	39
3.4.1 Operation Principle and Average Current Analysis.....	39
3.4.2 Energy Conversion Loss Analysis	41
3.5 Simulation Study	42
3.6 Experimental Results	44
3.7 Conclusion.....	48
Chapter IV	
Zero Current Switching Switched-Capacitors Balancing Circuit for Energy Storage Cell Equalization and its Associated Hybrid circuit with Classical Buck-Boost.....	
	49
4.1 Introduction	49
4.2 Proposed cell balancing circuits.....	50
4.2.1 Circuit configuration	50

4.2.2	Balancing circuit operation analysis	51
4.2.3	Analysis of ZCS Operation	54
4.3	Modeling for balancing mode	57
4.3.1	Modeling for ZCS balancing mode.....	57
4.3.2	Modeling for Buck-Boost Balancing Mode.....	58
4.4	Simulation Results of the Multi-Function Voltage Equalizer	61
4.5	Experimental Results of the Multi-Function Circuit.....	63
4.6	Conclusion.....	66
Chapter V		
Forecast of Urban EV Charging Load and Smart Control Concerning		
	Uncertainties.....	68
5.1	Introduction	68
5.2	Methodology for Route Modeling.....	69
5.2.1	Travel Route Modeling	69
5.2.2	Transition Relationships	70
5.3	Methodology for Charging Load Forecast	72
5.3.1	Energy Consumption per km	72
5.3.2	Charging Frequency	73
5.3.3	Stochastic Load Forecast Model Using MCS	74
5.4	Minimizing impact on power system.....	75
5.4.1	Optimization Problem	75
5.4.2	Control Scheme.....	76
5.4.3	GA Implementation.....	77
5.5	Case Study.....	79
5.5.1	Influence of External Conditions	82
5.5.2	Influence of Cell Balancing Strategies.....	70
5.5.3	Stochastic Model Results	71
5.5.4	Impact of EV Load on Power System.....	84
5.5.5	Effect of Aggregator Control	88
5.6	Conclusion.....	91
Chapter VI		
	Conclusions and Future Work.....	78
6.1	Conclusions	78
6.2	Future Work	80

6.2.1 Energy management for Battery/SC Hybrid Vehicle.....	80
6.2.2 Promoting the Application of Zero-Current Switching	80
References	96

Lists of Figures

Fig. 1.1	Basic topology of cell-balancing	3
Fig. 1.2	Organization of the thesis	11
Fig. 2.1	Voltage balancing circuit of package series-parallel switched-capacitor	15
Fig. 2.2	Control signal of the switches	16
Fig. 2.3	Working principle of the proposed balancing system	17
Fig. 2.4	Equivalent circuit of each state	20
Fig. 2.5	Model of the Balance circuit	24
Fig. 2.6	The experimental application for hybrid source electric vehicle	28
Fig. 2.7	Double voltage ratio equalizer built in laboratory	29
Fig. 2.8	The balancing waveform from the experiment in the laboratory	30
Fig. 2.9	The voltage V_C and current I_C waveform of switched-capacitor C_I during the balancing progress	30
Fig. 3.1	General topology of tapped inductor for three basic SMPC topologies	34
Fig. 3.2	Tapped inductor balancing circuit	36
Fig. 3.3	Generalized tapped inductor cell equalization circuit	37
Fig. 3.4	Control signal of the switches	38
Fig. 3.5	Equivalent Model of the balance circuit	39
Fig. 3.6	Topologies for simulation	43
Fig. 3.7	The balancing waveforms and average current waveform from the experiment in the laboratory	46
Fig. 3.8	The voltage and current waveforms of tapped inductor L_I	47

	during the balancing progress	
Fig. 3.9	The voltage and current waveforms of tapped inductor L_2 during the balancing progress	47
Fig. 4.1	Different operating modes and requirements	50
Fig. 4.2	Proposed balancing circuit	51
Fig. 4.3	Working principle of the proposed balancing system	52
Fig. 4.4	Control signal of the switches	53
Fig. 4.5	Circuit of ZCS mode	54
Fig. 4.6	Model of the ZCS mode circuit	58
Fig. 4.7	Model of the Buck-boost mode circuit	59
Fig. 4.8	Multi-functional equalizer built in laboratory	63
Fig. 4.9	The ZCS mode balancing waveform from the experiment in the laboratory	64
Fig. 4.10	The voltage $V_{C1,2}$ and current I_{L1} waveform of switched-capacitor C_1 during the balancing progress of ZCS mode.	65
Fig. 4.11	The Buck boost mode balancing waveform from the experiment in the laboratory	65
Fig. 4.12	The voltage V_{L1} and current I_{L1} waveform of switched-capacitor C_1 during the balancing progress of Buck-boost mode.	65
Fig. 5.1	Route modeling process	69
Fig. 5.2	Calculation process of energy consumption per km	72
Fig. 5.3	The surface of energy consumption per km	80
Fig. 5.4	Charging load distribution under different balancing strategies	82
Fig. 5.5	Load demands in summer	83
Fig. 5.6	Load demands in winter	83
Fig. 5.7	Typical total grid load in summer weekdays	83
Fig. 5.8	33-node power system topology	86

Fig. 5.9	Voltage variation in summer weekday	87
Fig. 5.10	Daily charging power in H with smart control	88
Fig. 5.11	Daily voltage variation in W with smart control	89
Fig. 5.12	Total grid power with smart control methods adopted	90

Lists of Tables

Table 1.1	Example of cell voltage for Li-ion batteries	4
Table 2.1	Variation principles of V_C	22
Table 2.2	Simulation results of the Switched-capacitor voltage equalizer	26
Table 2.3	Parameters in the experiment	27
Table 3.1	Simulation results of the Tapped Inductor voltage equalizer	44
Table 3.2	Parameters in the experiment	45
Table 4.1	Switches control logical signal	53
Table 4.2	Simulation results of the Switched-capacitor voltage equalizer	62
Table 4.3	Parameters in the experiment	64
Table 5.1	Scenarios of charging duration at public stations	80
Table 5.2	Inputs under different scenarios	82
Table 5.3	Performance under different scenarios	85

Lists of Abbreviations and Symbols

Abbreviations (*in alphabetical order*)

AC	Air conditioning
BMS	Battery management system
DG	Distributed generation
EPA	United States Environmental Protection Agency
ESR	Equivalent series resistance
EV	Electric vehicle
GA	Genetic algorithm
H	Residential areas, Home
MCS	Monte Carlo Simulation
mmf	Magnetomotive force
MV	Medium voltage.
NHTS	National Household Travel Survey
O	Places for other family errands.
SC	Supercapacitor
SoC	State-of-charge
SoH	State-of-health
SP	Source package.
SMPC	Switched-mode power converter
SE	Shopping & Eating
SR	Social & Recreational
W	Work places
ZCS	Zero-current switching
EMI	Electromagnetic interference

Symbols (*in order of appearance*)

Chapter II

V_P	The voltage of the source package.
V_{SC}	The voltage of SC.
φ_a	Clock phase a .
φ_b	Clock phase b .
S_t	The t^{th} switch.
S_a	The a^{th} switch.
S_b	The b^{th} switch.
C_n	The n^{th} switched-capacitor.
v_c	The voltage of the switched-capacitor.
i_c	The current of the switched-capacitor.
V_p	The voltage of the source package.
V_{Bm}, V_{SCj}	The voltages of the batteries or SCs in the package.
i_p	The current of the source package.
r_{Bm}, r_{SCj}	The ESR of the batteries and SCs in the source package.
V_{Cs_min}	The minimum initial voltage of the switched-capacitor C_s when φ_a .
$R_{a,b}$	The total resistance including all the ESR of the switched-capacitors.
τ	The time constant.
r_S	The ON-resistance of the switch.
$C_{a,b}$	The capacitance of the series switched-capacitor string.
V_{Cp_max}	The maximum initial voltage of the switched-capacitor C_p when φ_a .
$v_{Ci}(t), i_{Ci}(t)$	The instantaneous voltage and current of the switched-capacitors.
i	The range from 1 to n .
$r_{b,i}$	The ESR in the i^{th} branch.
V_{Cs}	The switched-capacitor voltage during φ_a .
V_{Cp}	The switched-capacitor voltage during φ_b .
V'_{SC}	The internal voltage of the SC.

I_{SC}	The current of the SC.
V_{Cp_min}	The minimum initial voltage of the switched-capacitor when φ_b .
V_{Cs_max}	The maximum initial voltage of the switched-capacitor when φ_b .
f	The switching frequency of the switch.
q	The quantity of electric charge.
R_{eq}	The equivalent resistance.
V_{avg}	The equilibrium voltage value during the transition process between φ_a and φ_b .
E	Energy stored in the SC and source package.
E_{loss}	The energy conversion loss.
ΔV	The voltage difference during the balancing process.
t	The duration of the balancing process.

Chapter III

Q_1, Q_2	The switches.
SC_1, SC_2	The supercapacitors.
V_{SC1}, V_{SC2}	The voltage of SC_1 and SC_2 .
D_1, D_2	The duty ratio of Q_1 and Q_2 .
V_{in}	The input voltage.
V_o	The output voltage.
M_{on}, M_{off}	The mmf values when Q is turned on and off.
L_m, L_n	The inductance of the inductors with m and n turns.
D_x	The turn-on duty ratio.
V_{P1}, V_{P2}	The voltage of SP_1, SP_2 .
SP_x	The x^{th} source package .
L_x	The x^{th} tapped inductor.
V_{g-Q}, V_{g-S}	The switch signals.
V_{SPx}	The voltage of the SP_x .
V_x	The total voltage from SP_i to SP_x .
R_{on}	The on-resistance of the switch.
R_{Lm}, R_{Ln}	The ESR of the inductor in m and n turns.

R_P	The ESR of the source packages.
i_{on}, i_{off}	The instantaneous current across L when the switch is on and off.
I_{avg_on}	The average current across L when the switch is on and off.
I_{avg_off}	
Δi_{on}	The current difference during the on state.
E_{dch}	The energy discharged from SP_1 throughout one cycle.
Δi_{off}	The current difference during the off state.
E_{ch}	The energy charged to the SP_2 throughout one cycle.
E_{loss}	The energy conversion loss.

Chapter IV

f_s	Switching frequency.
f_r	Resonant frequency.
SC_k, C_k	The k^{th} SC and capacitor.
SC_j, C_j	The j^{th} SC and capacitor.
S_a, S_b	The switches in two groups.
L	The inductance of inductor.
V_{Ck}, V_{Cj}	Voltage between C_k and C_j .
$\Delta V_{Ck}, \Delta V_{Cj}$	the amplitude of V_{Sk} and V_{kj} .
i_r	The resonant current.
I_r	The amplitude of the i_r .
ω	The resonant angular frequency.
φ	The initial angle of the resonant state.
V_{Cmin}, V_{Cmax}	The minimum and maximum value of the initial voltage across C .
R_{ESR}	Total ESR in one resonant tank.
I_{avg}	The average current of one cycle.
R_{eq}	Equivalent resistance of each resonant tank.
E_{ch}, E_{disch}	Energy charged and discharged to SC throughout one cycle.
P_{loss}	The power loss of the circuit.
$M_{_ch}, M_{_disch}$	The mmf values for charging and discharging.

D_1, D_2	The turn-on duty ratio of transistor and diode.
i_{ch}, i_{disch}	The instantaneous current across L_l for charging and discharging.
$I_{avg_ch},$ I_{avg_disch}	The average current across L_l when it is charging or discharging.
$\Delta i_{ch}, \Delta i_{disch}$	The current difference during charging and discharging state.
E_{ch}, E_{disch}	The energy charged and discharged throughout one cycle.
E_{loss}	The energy loss.

Chapter V

X_n	The Markov process state.
$P_{n,n+1}$	The transition probability from state X_n to state X_{n+1}
p_{ij}	Transition probability from current state i to state j .
M_{ij}	Markov transition matrix
T_j	The end time of current trip
T_i	The end time of last trip
$w_{n,t}$	Energy consumption per km (kWh/km) to place n at time t .
C	Battery capacity.
L_t	Tested mileage under the same condition as time t .
Z_t	Normalized temperature at time t .
z_{min}, z_{max}	Critical temperature of feeling cold and feeling hot
p	The proportionality coefficient
SOC_n	Remaining SoC at place n .
l_{n+1}	Estimated length of next trip after place n .
T_s	Charging start time.
T_c	Charging duration.
$u_{n,t}^k$	Charging possibility of the k^{th} EV at place n , time t .
$P_{n,t}^k$	Daily charging load profile of the k^{th} EV
P_c	Charging power
$P_{n,t}$	Total daily load profile at place n , time t .
$I_{m,t}$	The line current of the m^{th} line, time t .

R_m	The line impedance of the m^{th} line
$V_{n,t}$	The voltage in node n at time t
V_{min}, V_{max}	Voltage limit in node n at time t
C_{max}	The maximum capacity of local network
T_p	Amount of time to be postponed.
T_l	Lasting duration of implementing control.
$c\%$	Percentage of EVs to be regulated.
$p\%$	Percentage of reduction in charging power
f	Fitness function
α_1, α_2	Weight coefficients

Chapter I

Introduction

1.1 Background and Incentives of Research

1.1.1 Current Problems on New Energy Utilization

Global warming and fossil fuel depletion have raised increasing attention from governments, researchers and industrial manufacturers [1]. There are cases that energy wastage and underutilization exist. On one hand, the daily power demand varies greatly between peaks and troughs, which largely increases the construction cost of power generation and transmission line [2]. Meanwhile, due to the intermittence nature of photovoltaic and wind power, and insufficient energy storage services, new energy sources are not fully utilized. On the other hand, as the transport sector relies on 95% liquid fossil fuels and is responsible for 25% of total greenhouse gas emissions related to energy, promoting electric vehicles (EV) can be one of the most effective ways to tackle the ever severe environmental pollution because it is zero-emission [3,4]. However, power storage limit, cell voltage balancing and underutilized energy charging service are the main obstacles to popularizing EV market [5].

1.1.2 Importance of Cell Balancing and Current Deficiency

Batteries and supercapacitors (SC) are widely used in electric vehicles, distributed generation systems and so on [6] [7]. As the power of a single cell of battery or SC cannot provide sufficient driving force to loads, a series string of battery or SC units are required to fulfill the voltage and power requirements for high power applications [8]. However, different SCs in the same series have different characteristics such as capacitance, equivalent series resistance (ESR)

equivalent series inductance (ESL) and self-discharging rate, which may lead to voltage imbalance between each cell in the system [9,10]. In practice, although sorting is used before packaging in order to reduce this phenomenon, the effect becomes more serious when the energy storage devices get aged [11]. This unbalancing phenomenon is now a well-known problem in the series connection [6], [8]. Due to unavoidable mismatch of each cell, the capability of the energy storage system cannot be fully used. In the charging cycle, the charging current stops when most or a portion of charged cells are full while in the discharging cycle, the energy devices stop when most or a portion of discharged cells are empty [13]. Voltage of cells shall be made equal to the required value to solve these unbalancing problems [12]. The balancing is important especially when a group of electric vehicle (EV) batteries are in series connection to make up the high voltage to drive the motor. Balancing for energy storage to the power distribution and renewable energy storage are in high demand and suitable technology of balancing is urgently needed for a number of energy storage applications.

A variety of cell voltage equalizers have been presented which can be classified into three main types, including battery selection, passive methods and active methods [14, 15]. Integrating cells with similar performance in one package is the simplest way, but the accuracy and efficiency during sorting are proved to be low. Passive method is the most widely used technology [16, 17]. Resistors in parallel with the cells are switched on when they have higher state-of-charge (SoC) than others or when the cells approach the peak withstanding voltage [18]. As the energy dissipates into the resistor, this method generates additional heating loss [19]. For energy-saving purpose, the charging/discharging current of each cell can be controlled to keep the same SoC among all cell units such that the higher energy can be transferred into the cells with lower energy using power converter circuit, instead of wasting as the heat loss [20]. This active method is proved to be more efficient so that many advanced equalizers have been designed

based on this concept it using transformers [21,22], converters [23, 24], inductors [25, 26], or switched-capacitors [27 -31].

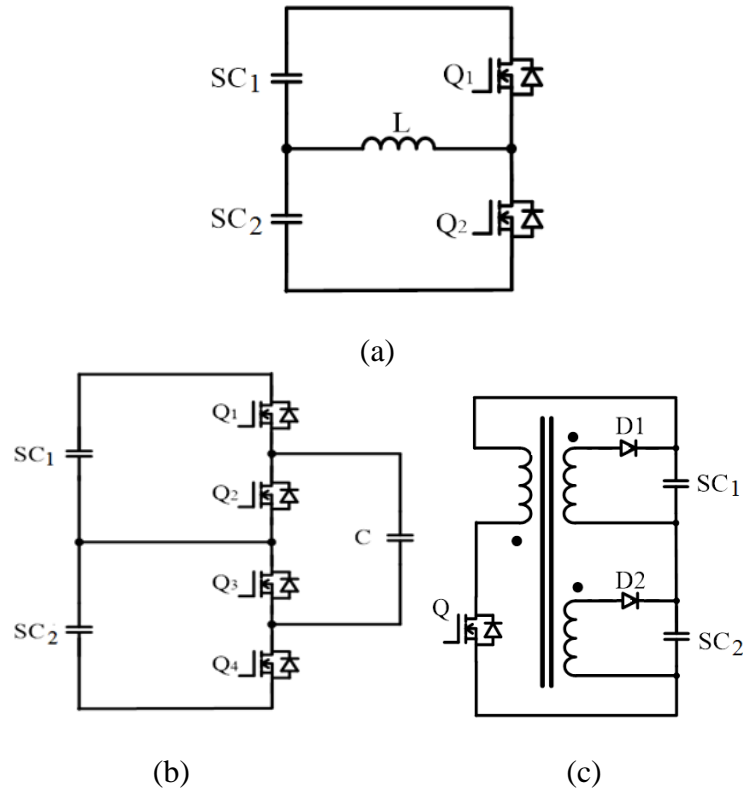


Fig. 1.1: Basic topology of cell-balancing.

(a) Buck-boost converter; (b) Capacitor balancing; (c) Transformer balancing.

One of the most common circuits of the active method is to use the classical buck-boost power converter illustrated in Fig.1.1a where an inductor is used to transfer the excess charge from one cell to another using the buck-boost power conversion. The concept has been further extended to the cases which couple an inductor to assist the balancing [32]. Fig. 1.1b and c are two improved cell balancing circuits that have been extensively adopted. Fig. 1.1b is based on switched-capacitor principles [33]-[34]. The operation of this method is similar to [35] where all cells are switched to common energy storage mode to equalize the voltage. Fig. 1.1c is transformer-based and uses windings to balance each cell. By adopting this topology, [36] and [37] use a bi-directional switch with two se-

ries MOSFETs to connect each cell to its balancing winding. Recently, a wireless power transfer approach for balancing is investigated in [38] that uses an air-gapped transformer to conduct the wireless power. Recent researches mainly focus on balancing cells of the same type with voltage ratio of 1:1 between two cells; therefore, they have difficulties in solving problems with combination of hybrid cells.

Table 1.1. Example of cell voltage for Li-ion batteries.

	LiCoO ₂	LiMn ₂ O ₄	LiNi _{1/3} Mn 1/3Co 1/3O ₂	LiFePO ₄	Li ₄ Ti ₅ O ₁₂
Name	Lithium Cobalt	Lithium Manganese	NMC	Lithium Iron Phosphate	LTO
Energy Density (Wh/kg)	180	100	180	140	100
Cell Volt- age (V)	3.7	3.8	3.8	3.2	2.2

Table 1.1 shows an example of different voltages of Li-ion cells [39]-[40]. Currently, the source package is mainly composed of standardized battery cells with the same chemical combination and initial voltage, where simple switched-capacitor circuit has acceptable balancing performance [41]-[47]. Recent papers mostly emphasize the balancing of single cells [48]-[56], and series-parallel connections are applied for converter and inverters [57]-[58]. Future EVs or distributed generation systems with hybrid energy systems are promising which take advantage of both battery and SC. As battery has high energy density while SC has high power density, they are combined to provide better performance of acceleration, emergency response [59] and energy storage [60] [61]. Besides, integrating retired batteries from aged EVs into grid energy storage will greatly promote environmental protection and the re-use concept [62]. However, the compatibility issue between different cell brands imposes restraints on the develop-

ment of energy storage system because cells have different background in age, brand and chemicals [63] [64].

Besides, researchers have done many state-of-the-art works on promoting balancing efficiency by decreasing balancing loss [65] [66]. Passive balancing method is the most widely used technology, however, the energy dissipates into the resistor such that this method generates additional heating loss [67]. For energy-saving purpose, the charging/discharging current of each cell can be controlled to keep the same SoC among all cell units so that the higher energy can be transferred into the cells with lower energy using power converter circuit, instead of wasting as the heat loss. This active method is proved to be more efficient so that many advanced equalizers have been designed based on it using switched-capacitors, inductors, transformers or converters [68]-[73]. Furthermore, majority of cell balancing circuits operate under hard switching [74]-[79], which will cause electromagnetic interference (EMI) and high switching loss [80]. On the other hand, the service life of energy sources will also be affected by current spike in hard switching circuits [81] [82].

With the increasing integration of hybrid energy sources and second-hand retired batteries, the cell balancing technique shall be promoted to a level of higher standard [83]. New problem is introduced when the voltage of a package of hybrid energy sources needs to be balanced with acceptable efficiency and energy conservation [84]. The balancing methods in the state-of-the-art literature lack optimization on the compatibility of hybrid cells, energy loss and accuracy of voltage equality. A multi-functional balancing circuit is also required for optimized energy efficiency at alterable working conditions and various driving states of EVs for example.

1.1.3 Load control in Smart City Using EV Batteries

Because of carrying a large number of cells, EV can be regarded as a mobile and distributed energy storage system that it can act as the role of “energy porter”

in future smart city. On one hand, to improve the energy efficiency and capacity of EVs under alterable working conditions, the voltage of EV internal batteries should be kept equal as it is illustrated in Section 1.1.2; On the other hand, to maximize the energy utilization in EV batteries, the orderly control of EV charging is essential for optimized load scheduling among different functioning districts of the city [86]. Therefore, the penetration of EVs in smart city cannot be successful without effective voltage balancing circuit or charging control strategy which is compatible to alterable circumstances [87]. Therefore, besides cell balancing problems, the stochastic charging behavior is another obstacle to EV storage system utilization [88] [89]. EV travelling route, the start time of charging, SoC and preferred charging duration of users can significantly influence the charging demand and available energy for discharging. The forecast of EV energy demand is the cornerstone for more reasonable investigation of its interaction with smart city [90].

Many existing papers have proposed methods or assumptions concerning EV charging forecast, however, most of them underestimate the stochasticity of EV user behavior in both traveling and charging. Inflexible charging start time and charging frequency are assumed in [91], [92] and [93] to illustrate uncontrolled charging. In reality, people may resort to multiple charging cycles when necessary and the home charging time could be profoundly influenced by travel history during daytime. [91] proposes a multiple charging simulation where drivers are expected to charge their EVs every time they stop. Nevertheless, this assumption may be unrealistic and the traveling patterns are not differentiated. Global Positioning System (GPS) recording devices are used in [94] to obtain the actual driving routes in the city of Winnipeg. The conditional probability density functions of travel distance and home arrival time are considered in the stochastic model whereas the charging demand in public areas and interrelationships between trips are also unclear. Besides, most studies assume full charging as the objective [95]-[110], but users may not follow given urgencies or personal neces-

sities in reality. A more practical EV charging forecast with higher compatibility to different outer conditions is urgently required for future EV market promotion.

Based on effective EV charging forecast, the city shall propose control schemes on EV user behaviors to smoothen the power demand by utilizing load shifting capacity of EVs. Operators in [111] assign compulsory EV charging plan without consideration on EV user behavior. Method in [112] introduces distributed generators (DG) to be installed locally for maximum integration of EVs. [112]-[116] have elaborated the significant difference between the charging load from system dispatching and the practical charging load aggregated from all individual EVs. To further enhance the credibility, these works have triggered the more important study on the stochasticity of EV behaviors including convenience of users, actual period for which each EV can stop at that specific place for control, and the exact incentive required to attract users to observe the control [117]. Some EV users may not accept the control signal from the grid operator and the contingency issues among different parts of the city may be very different. Stimulating customer participation will efficiently improve the control performance.

Controlling charging demand by economic incentives is one of the practical means to encourage customers to shift charging periods to off-peak hours while helping them save money. [118] mandatorily assumes negative correlation between charging price and local power demand which is not practical in real situation. Real-time (RT) pricing and day-ahead (DA) pricing are introduced in [113], [119]-[123] and the residential load is proved to timely follow the price variation. Especially, advanced metering infrastructure (AMI) which is introduced in [113] and [123] facilitates the mutual communication between operators and EV users, making the real-time flexible control with customer participation possible. However, the RT pricing control proposed in [113],[120] and [122] can only obtain the local optimum within the pre-defined controlling window. Furthermore, when considering a multi-area problem, the controlling windows in different areas cannot guarantee temporal synchronization in a dynamic environment. When

considering EVs in a smart city, the power grid should be meshed with transportation network and the pricing control strategies should be designed based on EV user behaviors along both networks.

1.2 Primary Contributions

The main focus of this thesis is to develop new and practical methodologies for facilitating the use of energy storage system by improving cell balancing circuits. Besides, regarded as the mobile storage systems in smart city, load shifting capacity of EVs is optimized by investigating EV charging forecast and smart control strategies. The original contributions of this thesis can be summarized in the following aspects:

1.2.1 Series-Parallel Switched-Capacitor Balancing Circuit for Hybrid Source Package

Current papers mainly focus on balancing voltage of a single type of cells; however, energy storage system usually consists of multiple cells. The associated cell voltage equalization is especially important for cell package design when non-sorted cell packages, like different combinations of various cell types and second-life retired batteries, are introduced. An innovative and efficient switched-capacitor balancing circuit is proposed in this chapter to achieve cell voltage balancing for a package of hybrid energy sources. The key feature is that the balancing is not just restricted to equal cell voltage but is extended to hybrid source or energy cell packages for performance improvement and cost reduction. Balancing techniques for different voltage ratios should be developed to improve the existing balancing methods and prepare for future vast applications of various balancing requirements. The circuit proposed could balance the voltage ratio not only 1:1 but also any preset $n:1$ ratio. Due to the increasing popularity of hybrid

energy systems, the balancing system proposed in this chapter is practical and useful for further development.

1.2.2 Voltage Cell Balancing for Battery and SC Source Package with Tapped Inductor Techniques

The battery management system (BMS) is the key development for energy storage systems, however, with rapid development of SC, future energy storage cells are not constrained within one type, while different types of cells may form a source package. Balancing hybrid sources requires high level of balancing accuracy. In the above switched-capacitor based circuit, although voltage ratio is extended to $n:1$, n is still constrained as integer. Therefore, a novel balancing circuit is proposed using tapped inductor techniques. Different from buck-boost converter and switched-capacitor, tapped inductor has advantages in step-free adjustment and is suitable for balancing hybrid source packages composed of SCs, batteries and aged batteries in any preset ratios with accuracy.

1.2.3 Zero-Current Switching Switched-Capacitors Balancing Circuit for Battery/ SC Voltage Equalization

Different states of EVs, such as drive state, brake state and park state, may have different requirements on balancing speed, accuracy and loss. At different states, the energy storage system of EV needs corresponding balancing mode in order to meet those requirements. In this thesis, a novel cell balancing circuit is proposed with integration of zero current switching technique to overcome the problem of energy loss and reduce the switching transient during balancing process. Besides, this balancing circuit is capable of working at different driving modes with flexible circuit switching and intelligent voltage control module. This chapter is the first attempt to use zero-current switching (ZCS) technique in the integrated buck-boost and switched-capacitor balancing circuit for rapid mode switching, accurate voltage tracking and loss reduction.

1.2.4 Forecast of Urban EV Charging Load and Smart Control Concerning Uncertainties

Cells in EV can be regarded as mobile energy storage systems. Effective balancing circuit guarantees the normal operation of cells, however, an accurate forecast of EV charging demand is the cornerstone to optimize control and utilization of load shifting capacity of EVs in smart city. To better interpret the uncertain mobility of EV charging, this thesis divides the user behavior into EV travel behavior and charging behavior. EV trips traveled along the day are categorized according to trip purposes and linked with Markov Chains. The geographical and temporal distribution of EV travel behavior is obtained while the possible range of charging demand at each location is estimated by the distance traveled earlier and the distance to be traveled for the next trip.

The strengths of this thesis concerning the forecast are: Firstly, data of the real world travel survey (the National Household Travel Survey [70], for example) can be fully utilized because the inputs of the forecast are in alignment with the items in the travel survey and the forecast in this thesis is conducted at a per-minute level. Secondly, the recorded trips are carefully categorized by different purposes and linked by possible occurrence sequence according to the fact that an EV may have several trips a day and those trips are not independent. Thirdly, to make the forecast more realistic under the situation that no relevant surveys found on investigating user charging preference, the estimated charging behavior at each location is dependent on both the forecast travel behavior and human arbitrary preference.

Variable start-time charging and variable power charging methods are proposed based on the forecast results to show the influence of cell balancing strategy on EV charging and the smart control performance.

1.3 Thesis Layout

Chapters II to IV present three novel cell balancing circuits, namely switched-capacitor circuit, tapped inductor circuit and a multi-functional circuit with zero-current switching, respectively. They have advantages in compatibility to hybrid source packages, higher accuracy and less switching loss. Chapters V provides new ideas on effective forecast and control strategies for EVs, which can be regarded as distributed and mobile storage systems. Chapter VI concludes the thesis.

Furthermore, the overall organization of this thesis is illustrated in Fig. 1.2.

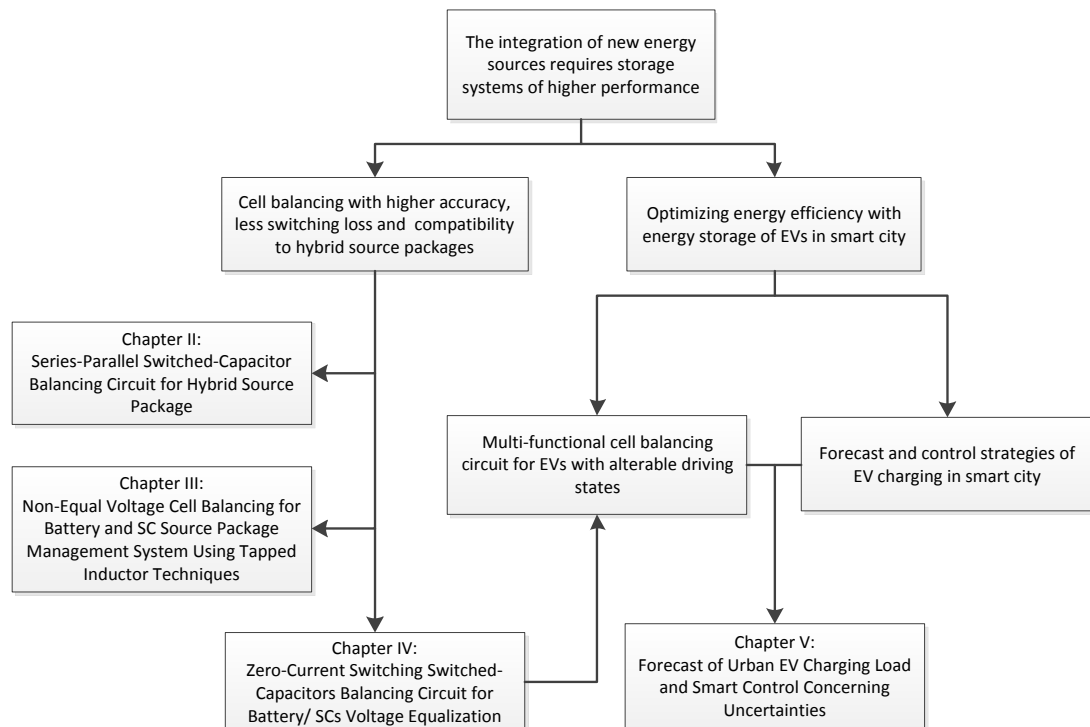


Fig. 1.2: Organization of the thesis

1.4 List of Publications

Journal papers:

1. Xiaolin Wang, K.W.Eric Cheng and Y.C.Fong, "Series-Parallel Switched-Capacitor Balancing Circuit for Hybrid Source Package," *IEEE Access*, vol.6, pp. 34254-34261, 2018.
2. Xiaolin Wang, K.W.Eric Cheng and Y.C.Fong, "Non-Equal Voltage Cell Balancing for Battery and Super-Capacitor Source Package Management System Using Tapped Inductor Techniques," *Energies*, vol.11, no.5, 2018.
3. Y. Nie, Xiaolin Wang (corresponding author) and K.W.Eric Cheng "Multi-Area Self-Adaptive Pricing Control in Smart City with EV User Participation," *IEEE Transactions on Intelligent Transportation Systems*, vol.19, no. 7, pp.2156-2164, 2018.
4. Xiaolin Wang, K.W.Eric Cheng and Y. Nie, "Distribution System Planning Considering Stochastic EV Penetration and V2G Behavior," *IEEE Transactions on Intelligent Transportation Systems*, 2017. (Accept after Minor Revision)
5. Xiaolin Wang, K.W.Eric Cheng and Y.C.Fong, "Zero Current Switching Switched-Capacitors Balancing Circuit for Energy Storage Cell Equalization and its Associated Hybrid circuit with Classical Buck-Boost, " *IET Power Electron.* (Submitted)

Conference papers:

1. Wang Xiaolin, Cheng K. W. E. and Xue X.D. "Electric Vehicle Performance and Design Index." *International Conference on Power Electronics Systems and Applications (PESA)*, Dec. 2017.
2. Xiaolin Wang, Y. Nie, K. W. E. Cheng and Jie Mei, "Forecast of Urban EV Charging Load and Smart Control Concerning Uncertainties," *International Symposium on Electrical Engineering (ISEE)*, Hong Kong, 2016.

3. X. Wang, K. W. Eric Cheng and Y. Nie, "Integration development for supercapacitor controlled distributed generation system." *International Conference on Power Electronics Systems and Applications (PESA)*, Dec. 2015.
4. Xiaolin Wang, George Sin and K.W. Eric Cheng "Future body design for electric vessel and aircraft." *International Conference on Power Electronics Systems and Applications (PESA)*, Dec. 2015.
5. Xiaolin Wang, K.W. Eric Cheng "Design Method of Outcome Based Learning for an Inverter Experiment in a Power Electronics Subject," *The 5th International Conference on Power Electronics Systems and Applications (PESA)*, Hong Kong, 2013.

Chapter II

Series-Parallel Switched-Capacitor Balancing Circuit for Hybrid Source Package

2.1 Introduction

Energy storage package usually consists of multiple cells. The associated cell equalization is important for cell package design. An innovative and efficient switched-capacitor balancing circuit is proposed in this chapter to achieve cell voltage balancing for a package of hybrid energy sources. The key feature is that the balancing is not just restricted to equalization of cell voltage but is extended to different cell combinations that will be beneficial for non-sorted cell packages, different types of Li-ion cells and for other application such as second-life retired batteries. The topology and operation process of each switching state for this voltage equalizer are analyzed in detail. The mathematical derivation, software simulation and laboratory experiment are conducted to verify the feasibility of this model. This proposed voltage equalizer is especially useful with the increasing establishment of hybrid systems which take advantages of different types of energy sources or energy storage devices.

The rest of this chapter is organized as follows. Section 2.2 describes the operation principle and the state analysis of the circuit. The modeling of the circuit will be obtained in Section 2.3. The simulation and experimental results will be presented in Sections 2.4 and 2.5, respectively.

2.2 Switched-Capacitor Voltage Balancing Circuit

2.2.1 Circuitry Description and Operation Principle

As indicated in Fig.2.1, the circuitry of the series-parallel switched-capacitor balancing circuit system consists of a package of hybrid energy sources and SC. Parameter n is defined in (2-1) where V_p is the voltage of the source package and V_{SC} is the voltage of SC. Three transistors (S_{a1} , S_{b1} , S_{b2}) and two capacitors (C_1 and C_2) form a balancing unit. The operation process of the proposed balancing system is divided into clock phase φ_a and clock phase φ_b with different switch positions as shown in Fig.2.2. The detailed operation principles of clock phase φ_a are shown in Section 2.2.2 while the illustration of clock phase φ_b is shown in Section 2.2.3. The number of SC cells, n , is therefore

$$n = \frac{V_p}{V_{SC}} \quad (2-1)$$

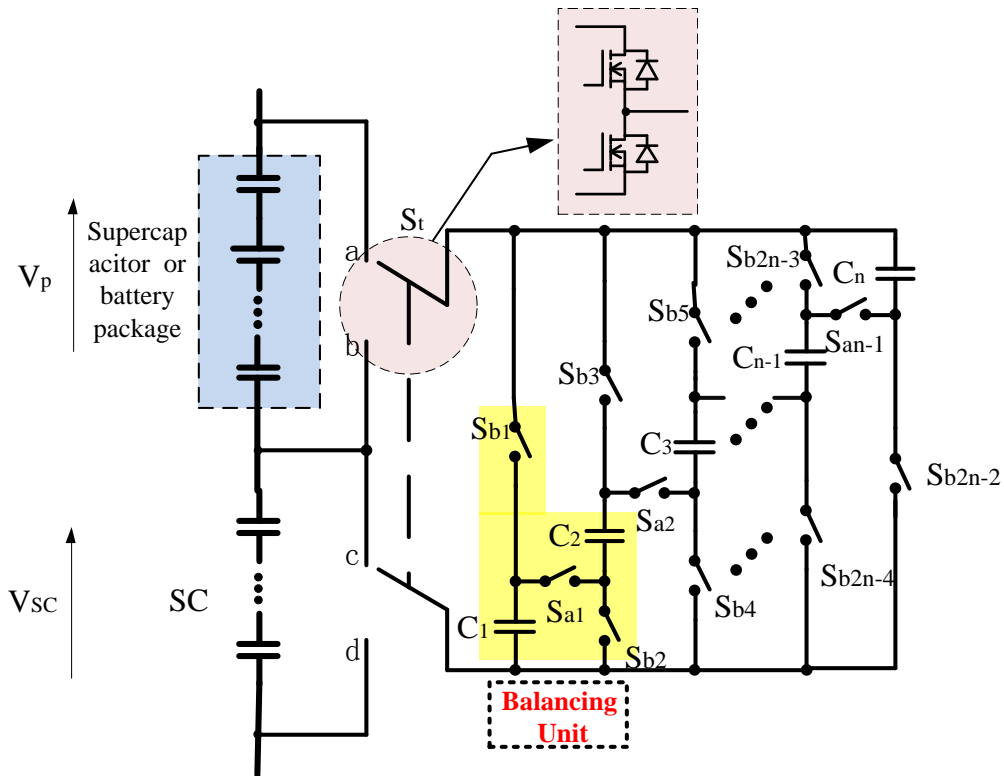


Fig. 2.1: Voltage balancing circuit of package series-parallel switched-capacitor.

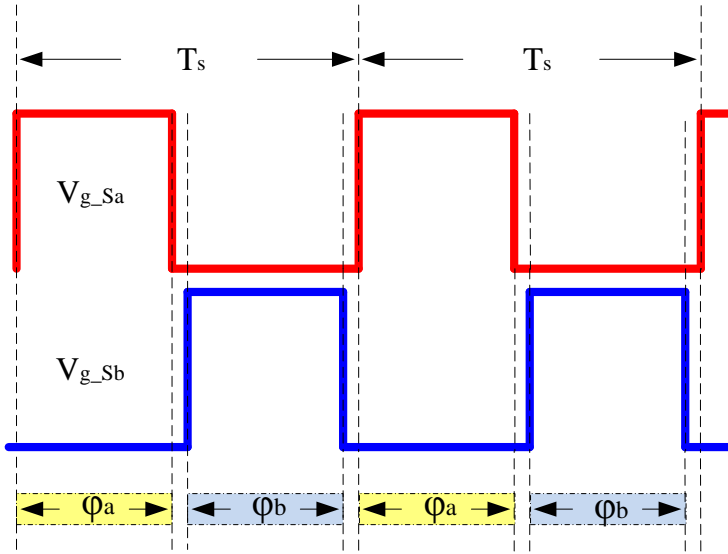


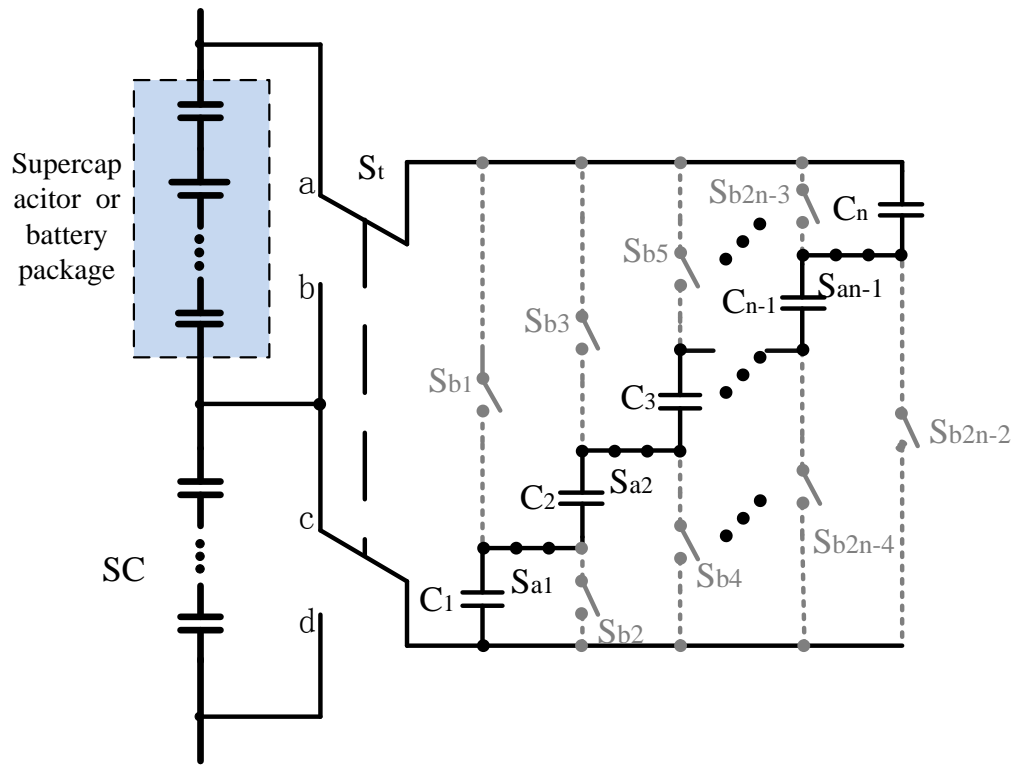
Fig. 2.2: Control signal of the switches

Fig.2.3 (a) illustrates the circuit in φ_a . When each pole of the main switch S_i is turned to connect a-c position, the source package is in series connection to the switched-capacitors. When S_i is turned to connect b-d position in φ_b , the SC is in parallel connection to the switched-capacitors as shown in the Fig.2.3 (b).

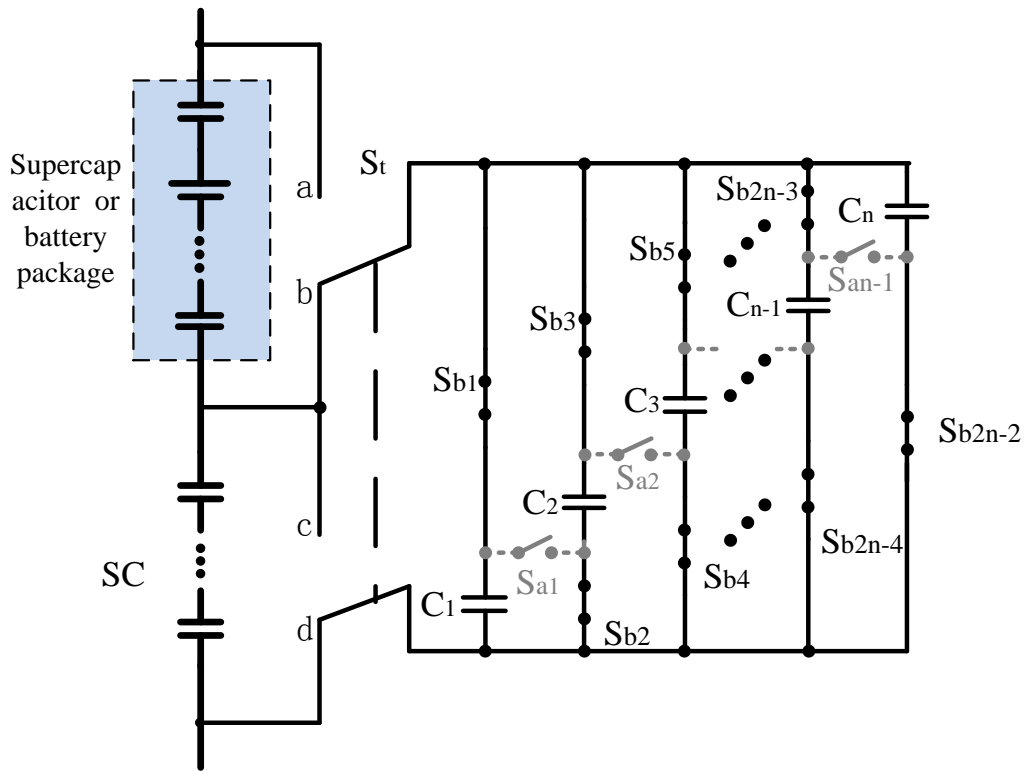
2.2.2 State Analysis in Clock Phase φ_a

All the switches S_i , S_a and S_b in Fig. 2.1 can be implemented by N-channel MOSFET and controlled by the signals shown in Fig. 2.2. Fig. 2.3(a) shows the connection of the switch S_i . During the clock phase φ_a , S_i is in a-c position and capacitors C_1, C_2 to C_n are in series connection to the source package. If the voltage of source package is higher than that of switched-capacitors C_1, C_2 to C_n , the switched-capacitors will be charged from the package. Fig. 2.4 (a) shows the charging flow between the package and switched-capacitors.

The voltage relationship in the package is shown in (2-2). The voltage of the switched-capacitor v_c and current of the switched-capacitor i_c vary during this state and are given in (2-3) and (2-4), respectively.



(a)



(b)

Fig.2.3: Working principle of the proposed balancing system.

(a) Series to the source package; (b) Parallel to the SC

$$V_p = V_{Bm} + V_{SCj} - i_p (r_{Bm} + r_{SCj}) \quad (2-2)$$

$$v_C(t) = \frac{V_p - (V_p - nV_{Cs_min}) e^{-\frac{t}{\tau_a}}}{n} \quad (2-3)$$

$$i_C(t) = \frac{V_p - nV_{Cs_min}}{R_a} e^{-\frac{t}{\tau_a}} \quad (2-4)$$

where V_p is the voltage of the package; V_{Bm} and V_{SCj} are the voltages of the batteries or SCs in the package; i_p is the current of the package, given that $i_p = i_C$; r_{Bm} and r_{SCj} are the ESR of the batteries and SCs in the package respectively; V_{Cs_min} is the minimum initial voltage of the switched-capacitor C_s which is one of all the switched-capacitors when $\frac{V_p}{n} > V_{SC}$.

R_a is the total resistance including all the ESR of the switched-capacitors. $n r_C$ and all the ON-resistance $(n-1)r_{Sa} + 2r_{St}$ of the S_{a1} to S_{an-1} and S_t in the ϕ_a , and the time constant τ_a in the ϕ_a are shown as

$$R_a = n r_C + (n-1)r_{Sa} + 2r_{St} \quad (2-5)$$

$$\tau_a = R_a C_a = C \left(r_C + \frac{n-1}{n} r_{Sa} + \frac{2r_{St}}{n} \right) \quad (2-6)$$

where C_a is the equivalent capacitance of the series switched-capacitor string, $C_a = \frac{C}{n}$.

Similarly, during the clock phase ϕ_a , if the voltage of source package is lower than that of the switched-capacitors C_1, C_2 to C_n , the switched-capacitors will be discharged. The variation of the voltage and current during ϕ_a is given below

$$v_C(t) = \frac{V_p + (nV_{Cp_max} - V_p)e^{-\frac{t}{\tau_a}}}{n} \quad (2-7)$$

$$i_C(t) = \frac{nV_{Cp_max} - V_p}{R_a} e^{-\frac{t}{\tau_a}} \quad (2-8)$$

where V_{Cp_max} is the maximum initial voltage of the switched-capacitor C_p , which is one of all the switched-capacitors when $\frac{V_p}{n} < V_{SC}$.

2.2.3 State Analysis in Clock Phase ϕ_b

In the duration of ϕ_b , S_t is changed to b-d position and all the switched-capacitors are in parallel as shown in Fig. 2.4 (b). When the voltage of the SC is higher than the voltage of the switched-capacitors connected in parallel, charge will transfer from the SC to switched-capacitors. Otherwise, SC will be charged by the switched-capacitors. $v_{Ci}(t)$ and $i_{Ci}(t)$ are the instantaneous voltage and current of the switched-capacitors.

Regarding the structure in the circuit,

When $i = 1$ or n ,

$$r_{b,i} = r_C + r_{Sb}$$

When $1 < i < n$,

$$r_{b,i} = r_C + 2r_{Sb}$$

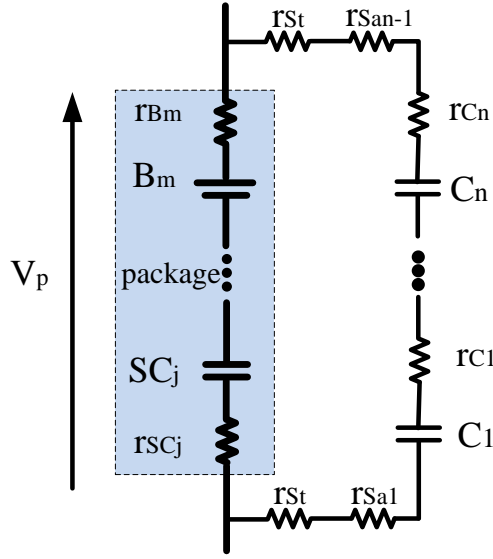
where i is the range from 1 to n ; $r_{b,i}$ is the ESR in the i^{th} branch; r_{Sb} is the on-resistance of S_{b1} to S_{b2n-2} .

In the topology analysis, the average resistance of $r_{b,i}$ is assumed to be equal in all branches in ϕ_b which is

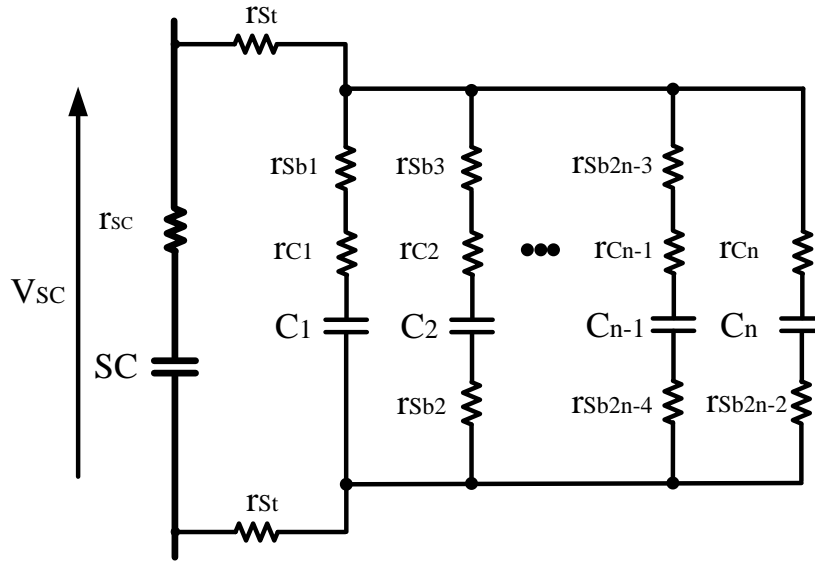
$$r_{b,i} = r_C + \frac{2n-2}{n} r_{Sb} \quad (2-9)$$

The time constant τ_b in ϕ_b is dominated by R_b , their relationship is shown below

$$R_b = \frac{r_C}{n} + \frac{2n-2}{n^2} r_{Sb} + 2r_{St} \quad (2-10)$$



(a)



(b)

Fig.2.4: Equivalent circuit of each state.

(a) state of φ_a ; (b) state of φ_b

$$\tau_b = R_b C_b = C \left(r_c + \frac{2n-2}{n} r_{sb} + 2nr_{st} \right) \quad (2-11)$$

where R_b is the sum of all the ESR of the switched-capacitors and all the ON-resistance of S_{b1} to S_{b2n-2} and S_i ; C_b is the sum of the capacitance of all the switched-capacitors, i.e. $C_b = nC$.

During the clock phase φ_b , if the switched-capacitor voltage V_{Cp} , is lower than the voltage of SC, the switched-capacitors C_1, C_2 to C_n will be charged. The variation of the voltage and the current is shown below

$$V_{SC} = V'_{SC} - i_{SC} r_{SC} \quad (2-12)$$

$$v_C(t) = V_{SC} - (V_{SC} - V_{Cp_min}) e^{-\frac{t}{\tau_b}} \quad (2-13)$$

$$i_C(t) = \frac{V_{SC} - V_{Cp_min}}{R_b} e^{-\frac{t}{\tau_b}} \quad (2-14)$$

where V'_{SC} is the internal voltage of the SC; I_{SC} is the current of the SC, given that $i_{SC} = ni_C$; r_{SC} is the ESR the SC; V_{Cp_min} is the minimum initial voltage of the switched-capacitor when $\frac{V_p}{n} < V_{SC}$.

If V_{Cp} is higher than the voltage of SC, the switched-capacitors C_1, C_2 to C_n will be discharged. The variation of the voltage and current is shown below

$$v_C(t) = V_{SC} + (V_{Cs_max} - V_{SC}) e^{-\frac{t}{\tau_b}} \quad (2-15)$$

$$i_C(t) = \frac{V_{Cs_max} - V_{SC}}{R_b} e^{-\frac{t}{\tau_b}} \quad (2-16)$$

where V_{Cs_max} is the maximum initial voltage of the switched-capacitor when $\frac{V_p}{n} > V_{SC}$.

2.3 Modeling for Switched-Capacitor Voltage Equalizer

2.3.1 Equivalent Resistance Analysis

During the progress of charge and discharge in one cycle, based on (2-3) and (2-15), V_{Cs} reaches maximum at the end of φ_a and reduces to minimum at the end

of φ_b . Similarly, based on (2-7) and (2-13), V_{Cp} reaches maximum at the end of φ_b and reduces to a minimum at the end of φ_a . Variation principles of V_C are expressed in Table 2.1.

Table 2.1. Variation principles of V_C

$\frac{V_p}{n} > V_{SC}$	$\frac{V_p}{n} < V_{SC}$
$V_{Cs_max} = \frac{V_p - (V_p - nV_{Cs_min})e^{-\frac{T_s}{2\tau_a}}}{n}$ <p style="text-align: center;">(2-17)</p>	$V_{Cp_min} = \frac{V_p + (nV_{Cp_max} - V_p)e^{-\frac{T_s}{2\tau_a}}}{n}$ <p style="text-align: center;">(2-19)</p>
$V_{Cs_min} = V_{SC} + (V_{Cs_max} - V_{SC})e^{-\frac{T_s}{2\tau_b}}$ <p style="text-align: center;">(2-18)</p>	$V_{Cp_max} = V_{SC} - (V_{SC} - V_{Cp_min})e^{-\frac{T_s}{2\tau_b}}$ <p style="text-align: center;">(2-20)</p>

where $T_s = \frac{1}{f}$, f is the switching frequency of the switch.

The difference between V_{C_max} and V_{Cs_min} , by subtracting (2-17) by (2-18), when $\frac{V_p}{n} > V_{SC}$, is then

$$V_p - nV_{SC} = n(V_{Cs_max} - V_{Cs_min}) \frac{1 - e^{-\frac{1}{2\tau_a f}} e^{-\frac{1}{2\tau_b f}}}{1 - e^{-\frac{1}{2\tau_a f}} - e^{-\frac{1}{2\tau_b f}} + e^{-\frac{1}{2\tau_a f}} e^{-\frac{1}{2\tau_b f}}} \quad (2-21)$$

$$R_{eq} = \frac{V_p - nV_{SC}}{I} \quad (2-22)$$

When (2-21) is substituted into (2-22), given that $I=qf$ and the quantity of electric charge in this cycle is $q=C(V_{C_max} - V_{Cs_min})$, the equivalent resistance R_{eq} could be further expressed as

$$R_{eq} = \frac{n}{Cf} \frac{1 - e^{-\frac{1}{2\tau_a f}} e^{-\frac{1}{2\tau_b f}}}{1 - e^{-\frac{1}{2\tau_a f}} - e^{-\frac{1}{2\tau_b f}} + e^{-\frac{1}{2\tau_a f}} e^{-\frac{1}{2\tau_b f}}} \quad (2-23)$$

Similarly, when $\frac{V_p}{n} < V_{SC}$, by subtracting (2-20) from (2-19), R_{eq} can be obtained to be the same as (2-23).

2.3.2 Energy Conversion Loss Analysis

After the balancing progress, all the quantity of electric charge Q transfers between source package and SC, from the higher voltage source to lower voltage source. In the end of the progress, total source package voltage is equal to n times voltage of SC which V_{avg} represents the equilibrium voltage value during the transition process between φ_a and φ_b .

V_{avg} can be expressed as

$$V_{avg} = V_p - \frac{Q}{C_p} = n \left(V_{SC} + \frac{nQ}{C_{SC}} \right) = \frac{n(nV_p C_p + V_{SC} C_{SC})}{n^2 C_p + C_{SC}} \quad (2-24)$$

Energy stored in the SC and source package before balancing is:

$$E(0) = \frac{1}{2} C_{SC} V_{SC}^2 + \frac{1}{2} C_p V_p^2 \quad (2-25)$$

Energy stored in the SC and source package after the process is:

$$E(\infty) = \frac{1}{2} V_{avg}^2 \left(\frac{C_{SC}}{n^2} + C_p \right) = \frac{1}{2} \frac{(nV_p C_p + V_{SC} C_{SC})^2}{n^2 C_p + C_{SC}} \quad (2-26)$$

The energy conversion loss is:

$$E_{loss} = E(0) - E(\infty) = \frac{1}{2} \frac{C_{SC} C_p (nV_{SC} - V_p)^2}{n^2 C_p + C_{SC}} \quad (2-27)$$

As it is shown in (2-27), the initial voltage and voltage ratio are the parameters that will affect energy conversion loss, instead of the capacitance and the ESR of the switched-capacitors or the switching frequency.

2.3.3 Balancing Duration Analysis

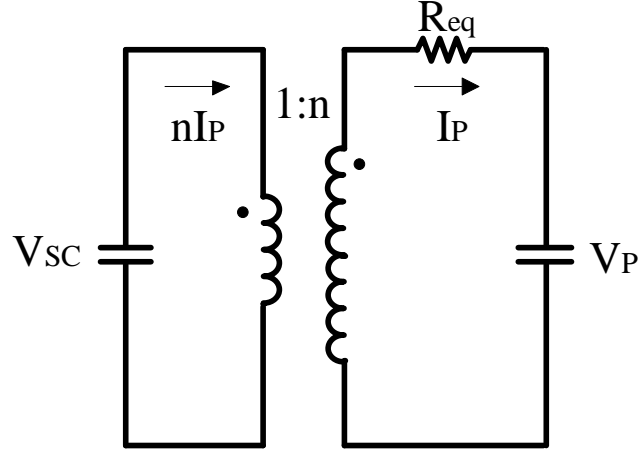


Fig.2.5: Model of the Balance circuit

As it is shown in Fig. 2.5, the source package and SC can be formulated to be charged or discharged between each other with a current conversion ratio, n . The voltage of the SC, V_{SC} , and source package V_P and the current of the source package I_P could be illustrated as:

$$V_{SC}(t) = V_{SC}(0) - \frac{n}{C_{SC}} \int I_P dt \quad (2-28)$$

$$V_P(t) = V_P(0) + \frac{1}{C_P} \int I_P dt \quad (2-29)$$

$$I_P = \frac{nV_{SC} - V_P}{R_{eq}} \quad (2-30)$$

By substituting (2-30) and solving (2-28) (2-29) with Laplace Transform, the voltage difference $\Delta V = nV_{SC} - V_P$ during the balancing process can be expressed as

$$\frac{\Delta V(t)}{\Delta V(0)} = e^{-\left(\frac{n^2}{C_{SC}} + \frac{1}{C_P}\right)\left(\frac{1}{R_{eq}}\right)t} \quad (2-31)$$

Therefore, by setting a termination voltage difference $\Delta V (end)$, the duration of the balancing process can be derived from (2-31) and given as

$$t = -\frac{1}{\left(\frac{n^2}{C_{SC}} + \frac{1}{C_P}\right)\left(\frac{1}{R_{eq}}\right)} \ln \frac{\Delta V (end)}{\Delta V (0)} \quad (2-32)$$

The balancing duration is mainly decided by the capacity of the source package, SC and also the equivalent resistance of the equalizer. If t is large enough, both nV_{SC} and V_P would be very close to V_{avg} when ΔV approaches zero.

2.4 Simulation Results of the Switched-Capacitor Voltage Equalizer

The proposed circuit is simulated by PSIM software which all the components are made ideal. The circuit topologies of voltage ratio $n=2, 3, 4$ are built in the simulation interface. Assume the source package is composed of the SCs with the same capacitance 1F. For the switched-capacitors two parameters $C=100\mu\text{F}$ and $220\mu\text{F}$ are used in simulation while $f=10$ kHz and 30 kHz of the control signal are used to operate the circuit. The above configuration is only used for case study. In practical application, the composition of source energy storage package can be scaled to one's requirement and the parameters of C and f can be optimized accordingly.

In the simulation analysis, all the components are assumed to be ideal, given that $\tau_a = \tau_b = 0$, the equivalent resistance R_{eq} in (2-23) could be further expressed as:

$$R_{eq} = \frac{n}{Cf} \quad (2-33)$$

Table 2.2. Simulation results of the Switched-capacitor voltage equalizer

Voltage ratio	$C=100\mu\text{F}, f=10\text{kHz}$	$C=200\mu\text{F}, f=10\text{kHz}$	$C=100\mu\text{F}, f=30\text{kHz}$
$n=2$			
$n=3$			
$n=4$			
X: Time(s); Y: Voltage(V)			

Table 2.2 illustrates the comparison of the waveforms in the simulation varied with capacitance C , switching frequency f and n . It is observed that both V_{sc} and $\frac{V_p}{n}$ finally converge to the same voltage level in all circumstances. When C is larger, the balancing duration is comparatively shorter because the charging/discharging capacity during one switch cycle is higher. When f is higher, the switching speed is faster that accelerates the equalization process. The balancing phenomenon conforms the principles in (2-32).

2.5 Experimental Results of the Switched-Capacitor Voltage Equalizer

The proposed circuit has the capability of performing balancing for different voltage ratios and it is highly suitable for energy storage cell package where different cell voltage units are integrated into an energy storage package. To verify the validity of mathematical derivation and software simulation, a double voltage ratio balancing circuit is built in the laboratory which is shown in Fig. 2.6, it is the energy storage package for a hybrid electric vehicle with different voltage levels. Two SCs are combined to simulate the performance of the energy source package. Topology of the equalizer is shown in Fig. 2.7 and the list of components is recorded in Table 2.3.

Table 2.3. Parameters in the experiment

Units	Quantity
Supercapacitor (DRL357S0TQ60SC)	3
Capacitance of SCs	350F
ESR of SCs	20m Ω
MOSFET (IRFR3607PBF)	7
ON-resistance of MOSFETs	7.34 m Ω
Switched-capacitor (EEHZA1H101P)	2
Capacitance of Switched-capacitors	100 μ F, 200 μ F
ESR of Switched- capacitors	28 m Ω
Switch frequency	10kHz, 30kHz



Fig.2.6: The experimental application for hybrid source electric vehicle.

The voltage balancing process of the experiment is shown in Fig. 2.8. The initial voltages of the source package and SC are 5.2V and 2.3V, respectively ($C=100\mu\text{F}$, $f=10\text{ kHz}$). After the voltage balancing is conducted, both $\frac{V_p}{2}$ and V_{sc} are balanced to the same voltage magnitude, which coincides with the results of theoretical analysis. The voltage of this case after balance operation is 4.96V and 2.49V. The initial energy stored in the package source and SC is 3291.8J, and energy stored after balance is 3237.7J. The energy conversion loss during the experiment is 54.1J which is close to the results calculated by (2-27) and the efficiency is 98.4%, 98.73% and 95.2% for other two cases. Fig. 2.9 depicts the voltage and current variations of switched-capacitors during different frequencies ($C=100\mu\text{F}$, $f=10\text{ kHz}$; $C=100\mu\text{F}$, $f=30\text{ kHz}$) and phases defined in Fig. 2.2. In the field test, voltage variation follows the functions (2-3) and (2-15) while current variation conforms to (2-4) and (2-16). The experiment results demonstrate that the variation of both voltage and current is conformed to the charging/discharging principles in each phase.

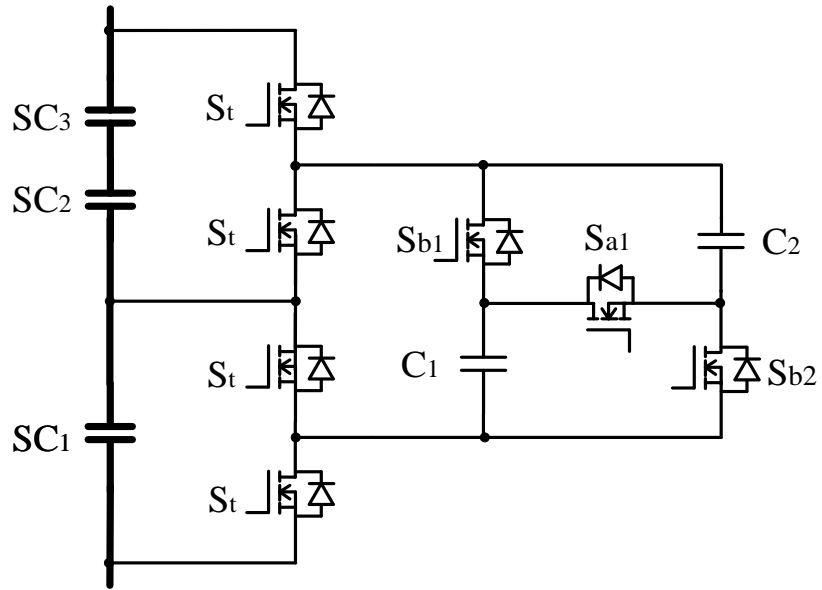
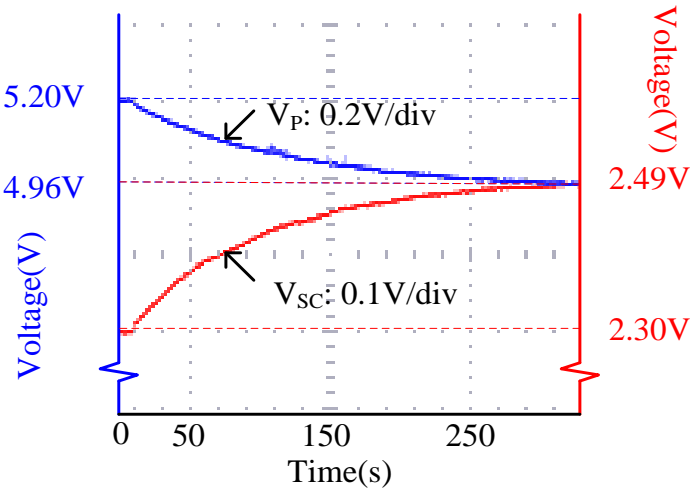
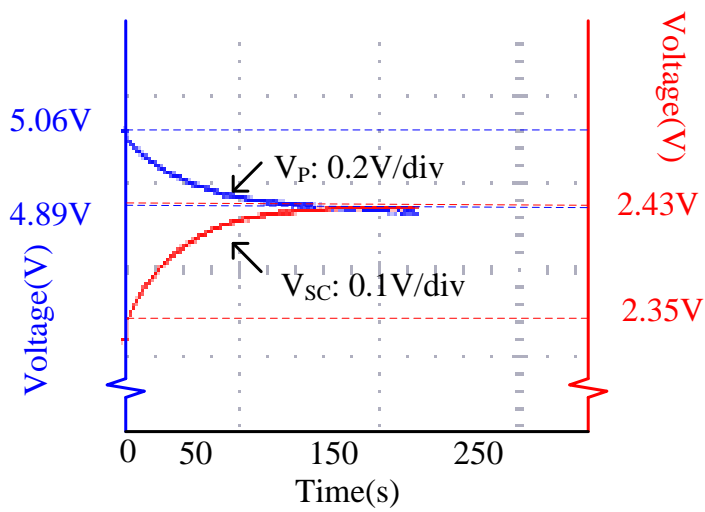


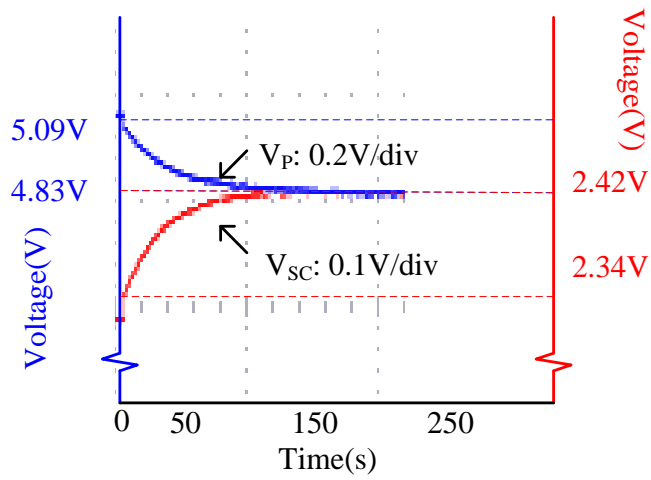
Fig.2.7: Double voltage ratio equalizer built in laboratory



(a)

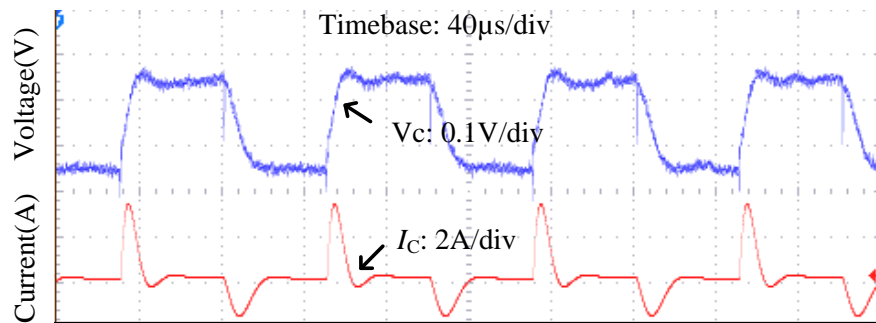


(b)

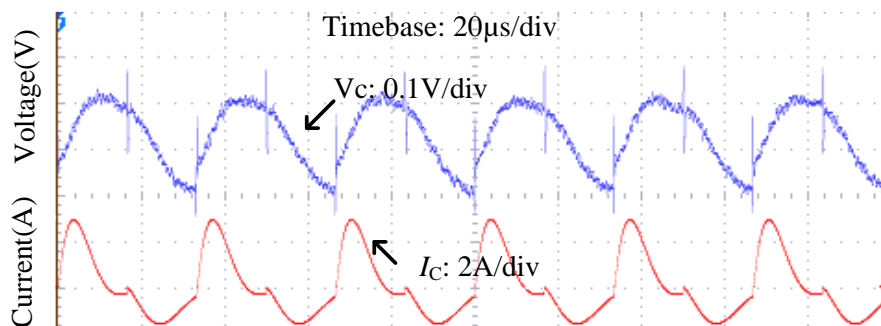


(c)

Fig. 2.8: The balancing waveform from the experiment in the laboratory (a) $C=100\mu\text{F}$, $f=10\text{ kHz}$; (b) $C=200\mu\text{F}$, $f=10\text{ kHz}$; (c) $C=100\mu\text{F}$, $f=30\text{kHz}$.



(a)



(b)

Fig. 2.9: The voltage V_c and current I_c waveform of switched-capacitor C_l during the balancing progress (a) $C=100\mu\text{F}$, $f=10\text{ kHz}$; (b) $C=100\mu\text{F}$, $f=30\text{kHz}$

2.6 Conclusion

In this chapter, series-parallel circuit configuration and operation principles of the innovative switched-capacitor voltage equalizer are demonstrated to effectively promote the use of hybrid source package composed of different cells. The equivalent circuit of the balancing model is described to show the process of voltage balancing. The key of the model is the use of an equivalent resistor which corresponds to the switching frequency and capacitance. The switching frequency and capacitance can be further adjusted to obtain the desired operation performance. An equalizer prototype for a package of energy sources with double voltage ratio is built in practical experiment to substantiate the validity of theoretical analysis. This innovative voltage equalizer is proved to be efficient and practical for industrial application. With the coming high demand in energy storage for mobility and renewable energy, the proposed technology provides a future development tool for non-equal cell integration. The components used in balancing is low-cost and of high efficiency.

Chapter III

Non-Equal Voltage Cell Balancing for Battery and Super-Capacitor Source Package Management System Using Tapped Inductor Techniques

3.1 Introduction

The battery management system (BMS) is the key development for energy storage systems, and battery balancing is an important subsystem of the BMS. However, with rapid development of SC, future energy storage cells are not constrained by one type, while different types of cells may form a source package (SP). Furthermore, the introduction of second-life batteries from retired electric vehicles promotes the demand of effective balancing systems for SPs with hybrid cells, as well as the requirement that balancing should be extended to any preset ratio rather than 1:1. This chapter proposes a novel tapped inductor balancing circuit that allows any ratio of voltage balancing for hybrid energy storage cells. The analysis of the circuit, simulation and experiment results are presented to demonstrate its effectiveness in handling hybrid source balancing.

The rest of this chapter is organized as follows. Section 3.2 describes the basic circuit of the tapped inductor. Section 3.3 presents the circuitry of the tapped inductor balancing circuit. The modeling of the circuit is obtained in Section 3.4. The simulation and experimental results will be presented in the Sections 3.5 and 3.6, respectively.

3.2 Tapped Inductor Basic Circuit

3.2.1 Conventional Buck-Boost Balancing

The conventional switched mode power conversion, buck-boost for example, can be used by adjusting different duty ratios of switches Q_1 and Q_2 to provide balancing for supercapacitors SC_1 and SC_2 in Fig.1.1(a). This is expressed as follows:

$$\frac{V_{SC_1}}{V_{SC_2}} = \frac{D_2}{D_1} \quad (3-1)$$

where V_{SC_1} and V_{SC_2} are the voltage of SC_1 and SC_2 , respectively. D_1 and D_2 is the duty ratio of Q_1 and Q_2 respectively. It is noted that idealized duty ratio, neglecting the dead-time is expressed as:

$$D_1 + D_2 = 1 \quad (3-2)$$

When the voltage ratios of SC_1 and SC_2 are different in more than 2, the efficiency of the voltage conversion between SC_1 and SC_2 is low [28],[29]. By using transformer concept or the isolated power converter such as forward converter or flyback converter, the efficiency of voltage conversion can be much higher when its transformer's turns ratio is much larger. The concept has been developed widely and realized by tapped inductor converter [30].

3.2.2 The Tapped Inductor Basic Theory

Fig. 3.1 shows a generalized circuit for three basic topologies in switched-mode power converter (SMPC). The transistor is connected to the tapped inductor L with the number of turns being m and the diode is connected to the tapped inductor with the number of turns being n . Since the magnetomotive force (mmf) is conservative for the tapped inductor, therefore, the voltage conversion ratio between input voltage V_{in} and output voltage V_o can be derived as follows.

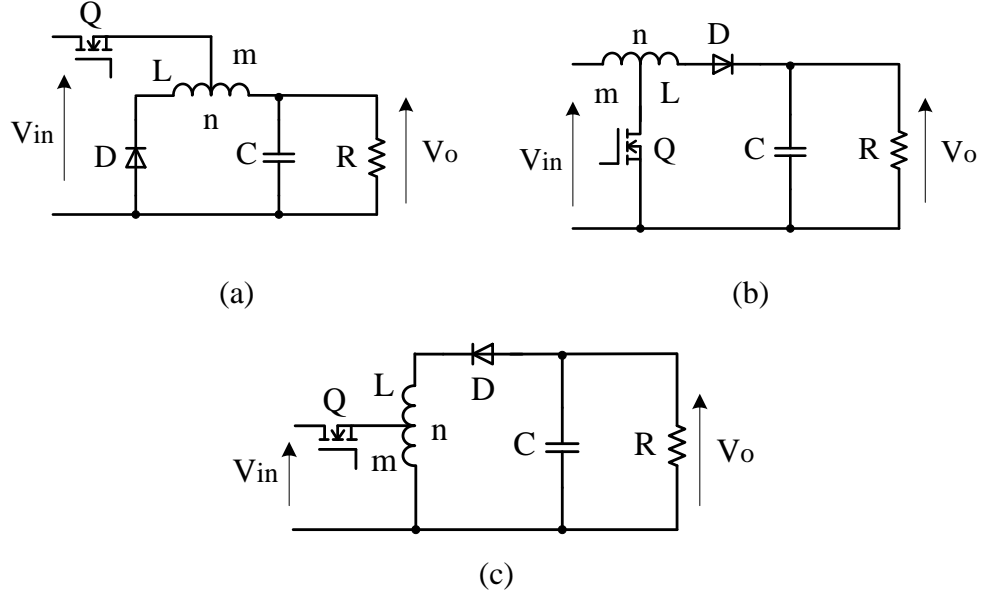


Fig. 3.1: General topology of tapped inductor for three basic SMPC topologies.

(a) Buck converter; (b) Boost converter; (c) Buck-boost converter.

To illustrate the voltage conversion for tapped inductor, the mmf values of M_{on} and M_{off} during the period when Q is turned on and off are:

$$M_{on} = m \frac{V_{Lm}}{L_m} D_1 T \quad (3-3)$$

$$M_{off} = n \frac{V_{Ln}}{L_n} D_2 T \quad (3-4)$$

where L_m and L_n are the inductance of the inductors with m and n turns, respectively. V_{Lm} and V_{Ln} are the voltage across L_m and L_n , respectively. D_1 and D_2 are the turn-on duty ratio of transistor and diode respectively.

(3-3) and (3-4) can be reduced to

$$\frac{V_{Lm}}{V_{Ln}} = \frac{m D_2}{n D_1} \quad (3-5)$$

and

$$\frac{V_{Lm}}{V_{Ln}} = \frac{m (1 - D_1)}{n D_1} \quad (3-6)$$

$$D_1 + D_2 = 1 \quad (3-7)$$

For the application to the three basic topologies, the voltage conversion ratio k is then:

Buck converter:

$$\frac{V_o}{V_{in}} = k + 1 \quad (3-8)$$

Boost converter:

$$\frac{V_o}{V_{in}} = \frac{k - 1}{k} \quad (3-9)$$

Buck-boost converter:

$$\frac{V_o}{V_{in}} = -k \quad (3-10)$$

where

$$k = \frac{m D_2}{n D_1} \quad (3-11)$$

3.3 The Tapped Inductor Balancing

3.3.1 Basic Cell Equalization

Fig. 1.1a and Fig. 3.1c can be combined into a tapped inductor balancing that makes use of the large voltage conversion for input and output. The diode is changed into a MOSFET and therefore a bi-directional power flow can be obtained that allows the energy balancing between two different source packages. Fig. 3.2a shows the topology that is also a buck-boost version. m and n are the number of turns obtained from the tapped inductor when the transistors Q_1 and Q_2 are on respectively.

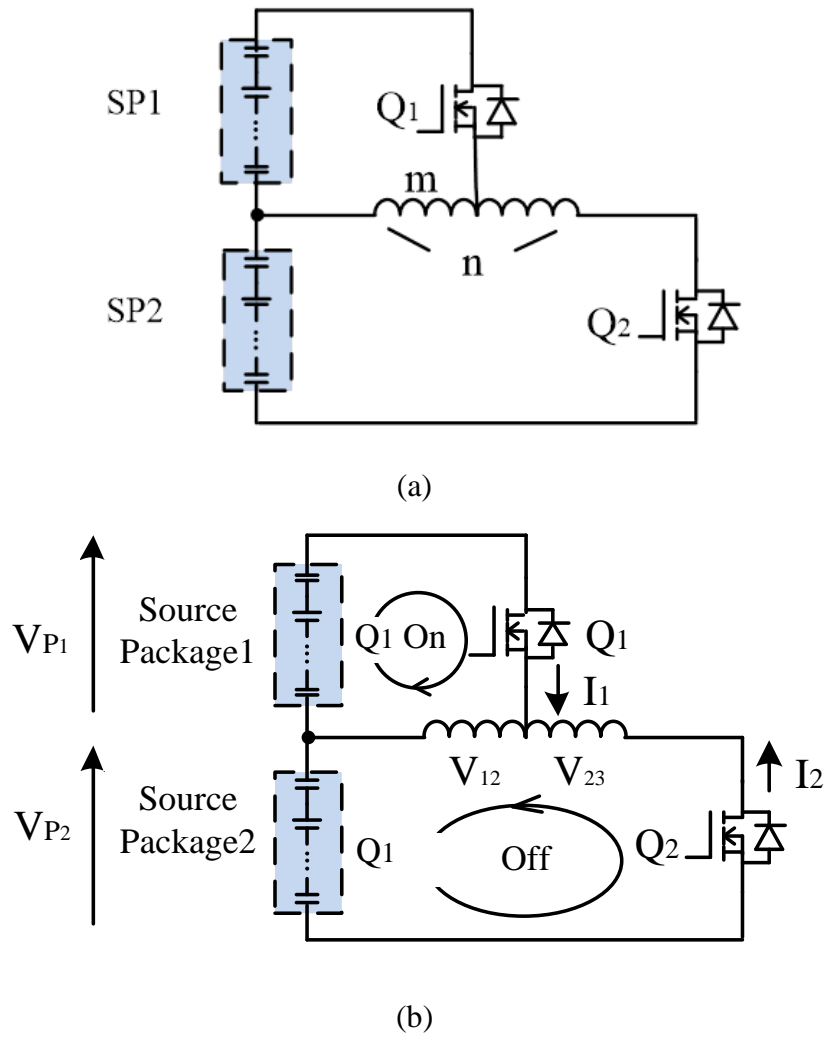


Fig. 3.2: Tapped inductor balancing circuit. (a) Basic circuit; (b) Current flow during on and off states of transistor.

The circuit analysis is similar to the conventional analysis of an SMPC. The voltage balancing equation then becomes:

$$\frac{V_{P_1}}{V_{P_2}} = \frac{m(1-D_1)}{n D_1} \quad (3-12)$$

where V_{P_1} is the voltage of SP_1 and V_{P_2} is the voltage of SP_2 .

In particular cases, if $D_1 = 0.5$, it is reduced to a simply transformer turns ratio to voltage ratio relationship:

$$\frac{V_{P_1}}{V_{P_2}} = \frac{m}{n} \quad (3-13)$$

In this case, each transistor is turned on for half a cycle in a complementary manner. The efficiency of such tapped inductor power conversion is high and using coupled-inductor's turns ratio, any voltage conversion can be obtained, that is, balancing of battery or SC hybrid source packages under any voltage ratios can be achieved.

3.3.2 Generalized Cell Equalization

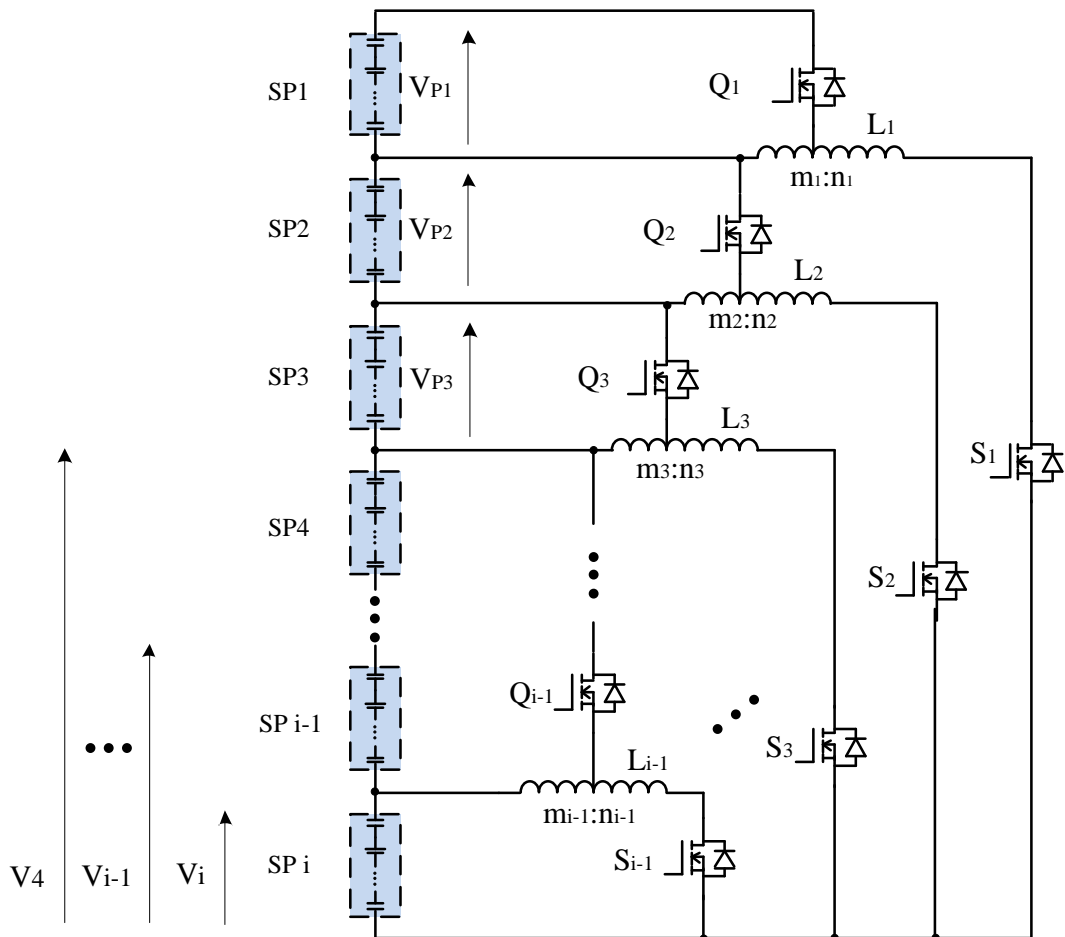


Fig. 3.3: Generalized tapped inductor cell equalization circuit.

The above circuit can be extended to a string of i packages as shown in Fig. 3.3. The x^{th} tapped inductor L_x , coupled with source package SP_x , has a tapping

and the turns ratio is $m_x : n_x$ where x varies from 1 to $i - 1$. The operation process of the proposed balancing system is divided into on state and off state with different switch signals V_{g_Q} and V_{g_S} in one cycle T as demonstrated in Fig. 3.4. The balancing is self-adaptive and automatically converges to equilibrium. The current between the source packages could be close to zero when the voltages of the source packages are equal after balancing progress and the loss is small. The detailed operation principles of the two states are shown in Section 3.4.

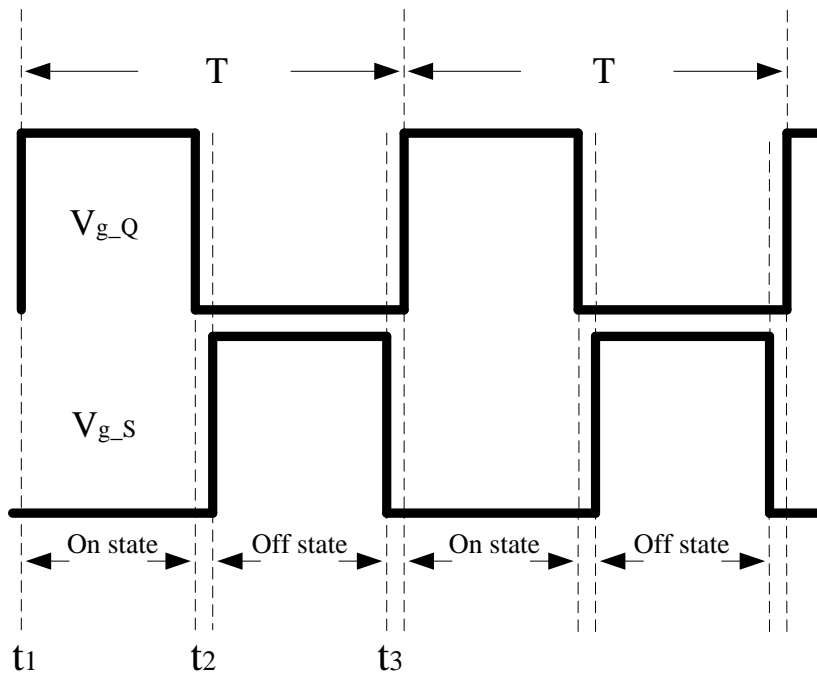


Fig. 3.4: Control signal of the switches.

The equalization equation for SP_x is:

$$\frac{V_{P_x}}{V_x} = \frac{m_x (1 - D_x)}{n_x D_x} \quad (3-14)$$

where V_{P_x} is the voltage of the SP_x . V_x is the total voltage from SP_i to SP_x . D_x is the duty ratio of Q_x and S_x .

When all the SP voltages are balanced, $D = 0.5$ is adopted to maintain the equalization of the cell voltage. Based on (3-14), the voltage ratio could be further edited as:

$$\begin{aligned}
& V_{P_1} : V_{P_2} : \dots : V_{P_{i-2}} : V_{P_{i-1}} : V_{P_i} \\
& = \frac{m_1}{n_1} \left(\frac{m_{i-1}}{n_{i-1}} + 1 \right) \left(\frac{m_{i-2}}{n_{i-2}} + 1 \right) \dots \left(\frac{m_2}{n_2} + 1 \right) : \frac{m_2}{n_2} \left(\frac{m_{i-1}}{n_{i-1}} + 1 \right) \left(\frac{m_{i-2}}{n_{i-2}} + 1 \right) \dots \left(\frac{m_3}{n_3} + 1 \right) : \\
& \dots : \frac{m_{i-2}}{n_{i-2}} \left(\frac{m_{i-1}}{n_{i-1}} + 1 \right) : \frac{m_{i-1}}{n_{i-1}} : 1
\end{aligned} \tag{3-15}$$

3.4 Modeling of Tapped Inductor Voltage Equalizer

3.4.1 Operation Principle and Average Current Analysis

During the progress of charging/discharging in one cycle, the charge is transferred between SP_1 and SP_2 . When the transistor is turned on and off and the equivalent circuit parameters vary accordingly. The equivalent model of the balancing circuit is shown in Fig. 3.5. All the analyses are under continues inductor current mode. The equivalent series resistance and on-state voltage for the diode are included to assist the modeling.

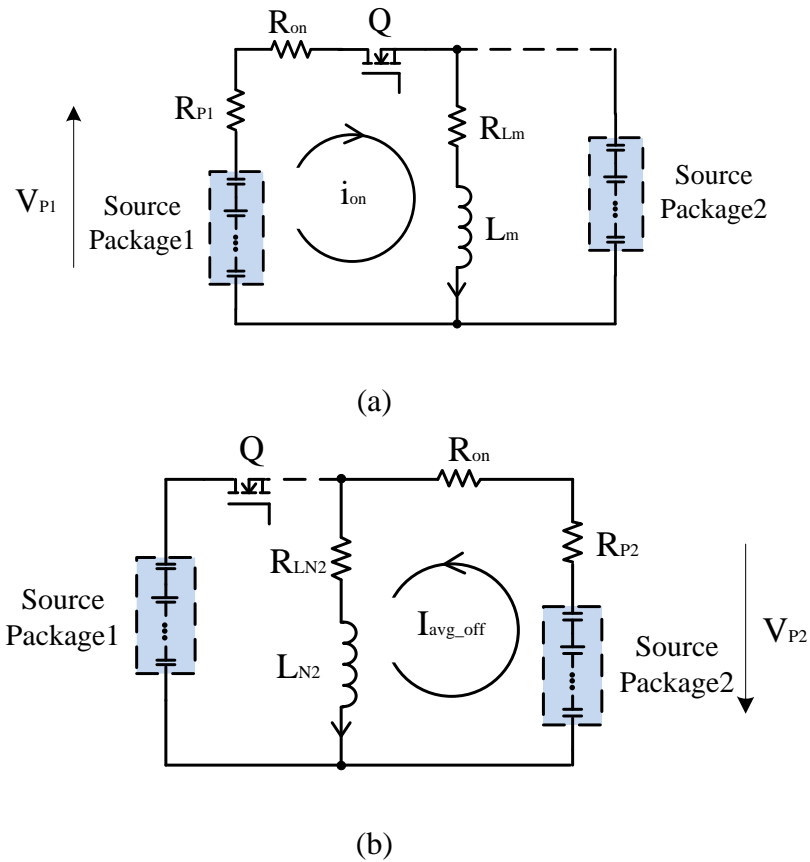


Fig. 3.5: Equivalent Model of the balance circuit. (a) on-state; (b) off-state.

Based on the relationship of (3-3) and (3-4), the mmf between SP_1 and SP_2 are

$$\frac{m}{L_m} \int V_{L_m} dt = \frac{n}{L_n} \int V_{L_n} dt \quad (3-16)$$

where $\frac{L_m}{L_n} = \frac{m^2}{n^2}$.

According to KVL, (3-16) could be further expressed as

$$\frac{V_{P_1} m}{L_m} DT - \frac{R_1 m}{L_m} \int i_{on} dt = \frac{V_{P_2} n}{L_n} (1-D)T - \frac{R_2 n}{L_n} \int i_{off} dt \quad (3-17)$$

where $R_1 = R_{on} + R_{Lm} + R_{P_1}$, $R_2 = R_{on} + R_{Ln} + R_{P_2}$. R_{on} is the on-resistance of the switch; R_{Lm} , R_{Ln} are the equivalent series resistance (ESR) of the inductor in m and n turns respectively, such that $\frac{R_{Lm}}{R_{Ln}} = \frac{m}{n}$; R_{P_1} and R_{P_2} are the ESR of the source packages P_1 and P_2 respectively; i_{on} and i_{off} are instantaneous current across L when the switch is on and off respectively.

I_{avg_on} and I_{avg_off} are the average current across L when the switch is on and off, respectively, so that $\frac{I_{avg_on}}{I_{avg_off}} = \frac{n}{m}$.

Assume when $\int i_{on} dt \approx I_{avg_on} DT$ and $\int i_{off} dt \approx I_{avg_off} (1-D)T$, I_{avg_on} could be obtained from (3-17) as:

$$I_{avg_on} = \frac{-\frac{m}{n} V_{P_2} (1-D) + V_{P_1} D}{\left(\frac{m}{n}\right)^2 R_2 (1-D) + R_1 D} \quad (3-18)$$

The average current I_{avg} of SP_1 is

$$I_{avg} = \frac{-\frac{m}{n}V_{P_2}(1-D)D + V_{P_1}D^2}{\left(\frac{m}{n}\right)^2 R_2(1-D) + R_1D} \quad (3-19)$$

3.4.2 Energy Conversion Loss Analysis

During balancing progress, all the energy transfers between source packages, from the higher voltage source to lower voltage source. In the end of the progress, each of the SP voltage is under the ratio shown in (3-15).

The variation of i_{on} is

$$i_{on}(t) = I_{avg_on} + \Delta i_{on} \left(t - \frac{DT}{2} \right) \quad (3-20)$$

where Δi_{on} is the current difference during the on state.

The energy discharged E_{dch} from SP_1 throughout one cycle is:

$$E_{dch} \approx V_{P_1} \int i_{on} dt \quad (3-21)$$

The variation of i_{off} is

$$i_{off}(t) = I_{avg_off} + \Delta i_{off} \left(t - \frac{DT}{2} \right) \quad (3-22)$$

where Δi_{off} is the current difference during the off state.

The energy charged E_{ch} to the SP_2 is

$$E_{ch} \approx V_{P_2} \int i_{off} dt \quad (3-23)$$

The energy transferred in the tapped inductors is $E_{Lm}=E_{Ln}$. The variation of E_{Lm} and E_{Ln} are presented below

$$E_{Lm} \approx \int_{t_1}^{t_2} (V_{P1} - i_{on} R_1) i_{on} dt \quad (3-24)$$

$$E_{Ln} \approx \int_{t_2}^{t_3} (V_{P2} - i_{off} R_2) i_{off} dt \quad (3-25)$$

By equaling (3-24) to (3-25), the energy conversion loss is

$$\begin{aligned} E_{loss} &\approx V_{P1} \int_{t_1}^{t_2} i_{on} dt - V_{P2} \int_{t_2}^{t_3} i_{off} dt \\ &= R_1 \int_0^{DT} i_{on}^2 dt + R_2 \int_0^{(1-D)T} i_{off}^2 dt \\ &= T \left(I_{avg_on}^2 + \frac{3\Delta i_{on}^2}{4} \right) \left[R_1 D + R_2 \left(\frac{m}{n} \right)^2 (1-D) \right] \end{aligned} \quad (3-26)$$

where $\Delta i_{on} \approx \frac{V_{P1}}{2L_m f}$, $\frac{\Delta i_{on}}{\Delta i_{off}} = \frac{n}{m}$.

As shown in (3-26), the initial voltage of *SPs*, voltage ratio, frequency, inductance, duty ratio and ESR will affect the energy conversion loss.

3.5 Simulation Study

The above balancing process has been simulated by PSIM software to study the performance of the circuit. Assume that the source packages are composed of the *SCs* with the same capacitance 350F. For the tapped inductor, $L = 400 \mu\text{H}$ is simulated while $f = 30 \text{ kHz}$ and $D = 0.5$ of the control signals are used to operate the circuit. The voltage ratios of $V_{P1}:V_{P2}:V_{P3}$ are simulated by three cases of 1:2:3, 1:2:4, 1:3:9 while according to (3-15), the turn ratios are 1:5, 1:6, 1:12 for L_1 and 2:3, 1:2, 1:3 for L_2 .

Table 3.1 indicates simulation results of the waveforms for voltage balance and the average current under the schematic in Fig. 3.6 with different voltage ratios. Because of the preset voltage ratio and initial voltages, SP_1 is discharged and SP_2 and SP_3 are charged for voltage ratio of 1:2:3; the SP_1 and SP_2 are discharged and SP_3 is charged for voltage ratio of 1:2:4 and 1:3:9. The voltage of each source package varies under the voltage ratio in the equalization process, and it is apparent that the balancing phenomenon conforms to the principles in (3-15). The variation of average current and energy loss in the simulations are consistent with the principles in (3-19) and (3-26).

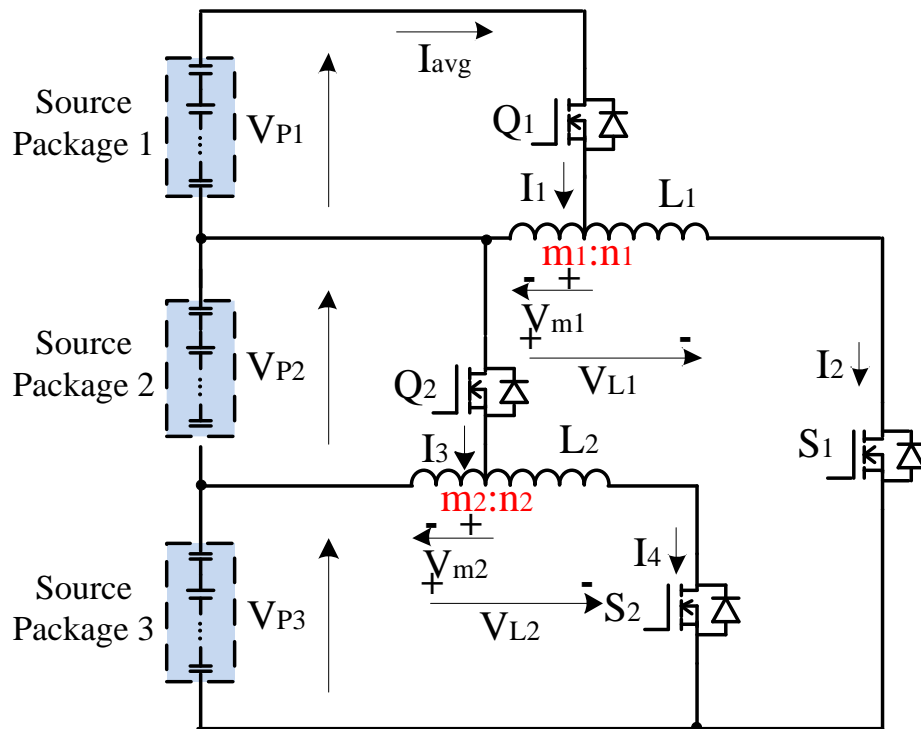


Fig. 3.6: Topology for simulation.

Table 3.1. Simulation results of the Tapped Inductor voltage equalizer.

Voltage Ratio	1:2:3	1:2:4	1:3:9
Voltage Balance Wave-form			
X: Time(s); Y: Voltage(V)			
Average Current Wave-form			
X: Time(s); Y: Current (A)			

3.6 Experimental Results

To verify the validity of mathematical derivation and software simulation, a 1:2:3 voltage ratio tapped inductor balancing circuit is built in laboratory and all the SP_s are tested in the same ambient temperature (20 °C). The inductors are made in the laboratory with 1:5 and 2:3 turns ratio. All the transistors are continuously pulsed as the method in Section 3. Although the control method could be used to trigger the unbalanced cells to accelerate the balancing speed, because the unbalancing speed is slow as compared with the speed of balancing of proposed balancing circuit, therefore the present control is to use continuous triggering to all transistors, and hence it reduces the control complication and the system is therefore absolutely stable. The balancing current will be reduced to zero when the equalization is achieved. Topology of the equalizer is shown in Fig. 3.6 and the list of components is recorded in Table 3.2. SP_1 , SP_2 , SP_3 are formed by

one SC, two SCs and three SCs connected in series and the list of components is recorded in Table 3.2. The size of the components in the control circuit of this balancing circuit is much smaller than the SPs because the balancing current is only a very small percentage of the main current of the SP. The circuit is suitable for practical use.

Table 3.2. Parameters in the experiment.

Units	Quantity
Supercapacitor (DRL357S0TQ60SC)	6
Capacitance of SCs	350 F
ESR of SCs	6 m Ω
MOSFET (IRFR3607PBF)	4
On-state resistance of MOSFETS	7.34 m Ω
Inductance of L_1	390.4 μ H
Turns ratio of L_1	1:5
Inductance of L_2	386.9 μ H
Turns ratio of L_2	2:3
Switching frequency	30 kHz

The source packages, SP_1 , SP_2 and SP_3 are charged to the initial voltages of around 2.01 V, 4.22 V and 7.18 V, respectively. The balancing process is started by enabling the gating signals of the equalizer prototype. The voltage balancing process of the experiment is shown in Fig. 3.7. After the voltage balancing progress, all V_{SP1} , $\frac{V_{SP2}}{2}$ and $\frac{V_{SP3}}{3}$ are balanced to the same voltage magnitude, which coincides with the results of theoretical analysis. Besides, the average current and energy loss are close to the principles in (3-16) and (3-23).

Fig. 3.8 and 3.9 depict the voltage and current variation of tapped inductor L_1 and tapped inductor L_2 during 30 kHz frequency. The ripple of currents I_1 , I_2 , I_3 and I_4 is small. The experiment results demonstrate that the variation of all volt-

age and current conforms to the charging/discharging principles in the balance progress.

Retired batteries from electric vehicles have different voltage characteristics. For convenience of experiment, this chapter took SC combination as the energy sources. However, as the tapped inductor balancing circuit proposed in this chapter can be applied with any preset voltage ratio, the integration of second life batteries will not weaken the effectiveness of this non-equal voltage balancing technique. In practical design with PCB implementation, it is possible to keep the size of the balancing system at much less than one-tenth of the size of the whole packages with the proposed circuit topology. In theory, the inductor size can be further reduced by increasing the switching frequency. Therefore, the proposed method is a practical cell balancing solution for managing hybrid source packages with difference voltage ratios.

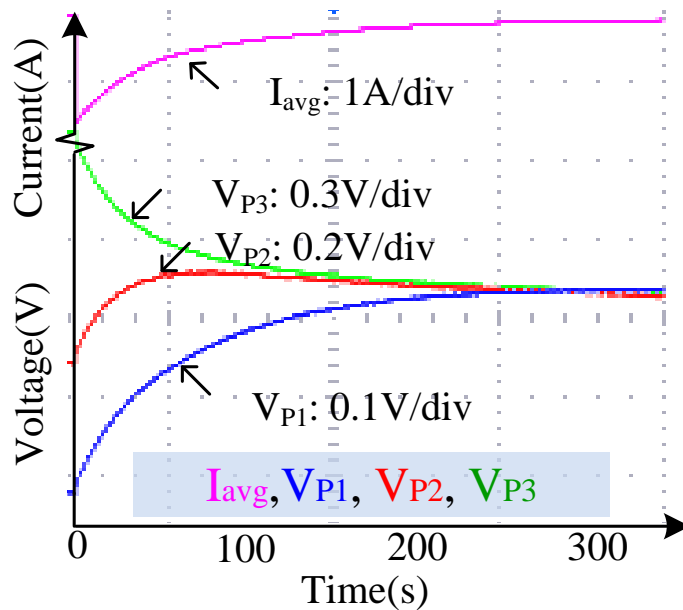


Fig. 3.7: The balancing waveforms and average current waveform from the experiment in the laboratory.

(CH1: I_{avg} is average discharge current; CH2: V_{P1} is voltage of source package1; CH3: V_{P2} is voltage of source package2; CH4: V_{P3} is voltage of source package3).

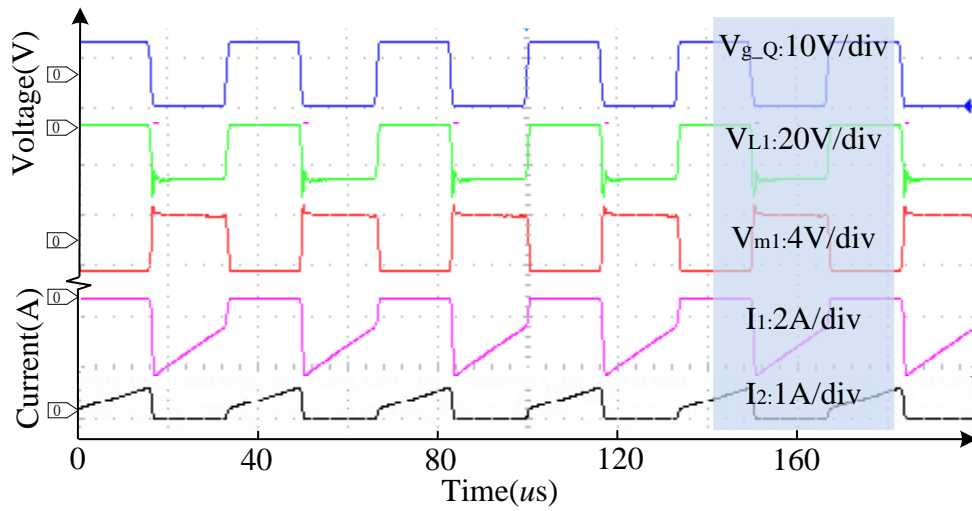


Fig. 3.8: The voltage and current waveforms of tapped inductor L_1 during the balancing progress.

(CH1: V_{g_Q} is gate signal of switches Q_1 and Q_2 ; CH2: V_{L1} is voltage between the whole turns of the L_1 ; CH3: V_{m1} is voltage between the left side of the L_1 ; CH4: I_1 is current flows across Q_1 ; CH5: I_2 is current flows across S_1).

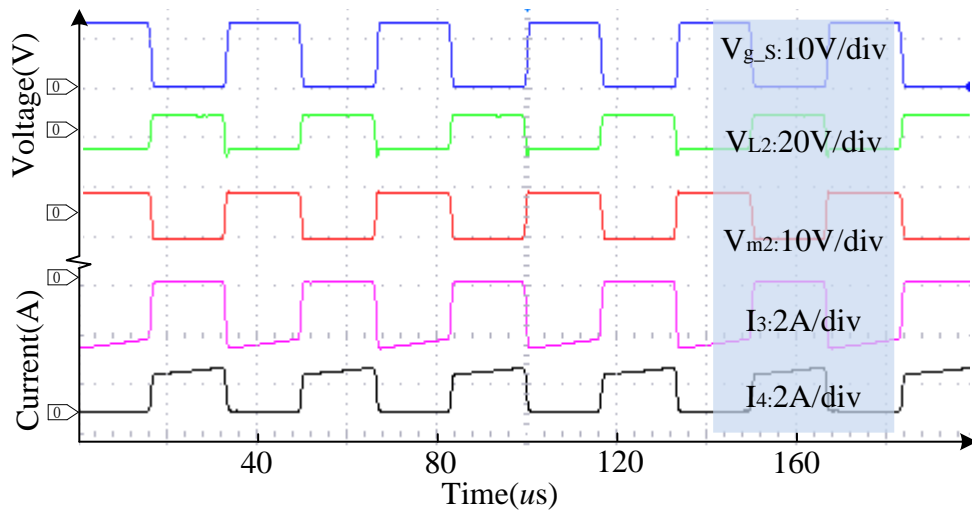


Fig. 3.9: The voltage and current waveforms of tapped inductor L_2 during the balancing progress.

(CH1: V_{g_S} is gate signal of switches S_1 and S_2 ; CH2: V_{L2} is voltage between the whole turns of the L_2 ; CH3: V_{m2} is voltage between the left side of the L_2 ; CH4: I_3 is current flows across Q_2 ; CH5: I_4 is current flows across S_2).

3.7 Conclusion

A new concept of source package equalization has been reported using a tapped inductor method. The method is derived from conventional tapped inductor converter. The advantage of the method is that it can allow cell balancing of any ratio with high efficiency. The proposed concept can be extended to several hybrid cells connected. Simulation and experimental results have been presented to demonstrate the effectiveness of this circuit. The scenario of successful balancing is extended to voltage ratio of 1:2:3 and the ripple of currents during balancing process is small enough. The proposed scheme is especially useful when second-life battery and other new types of energy are universally applied to energy storage systems, peak power compensation and even uninterruptible power supply.

Chapter IV

Zero Current Switching Switched-Capacitors Balancing Circuit for Energy Storage Cell Equalization and its Associated Hybrid circuit with Classical Buck-Boost

4.1 Introduction

To overcome the problem of switching loss during balancing process, a novel cell balancing circuit is proposed with integration of zero current switching technique. Moreover, the balancing circuit proposed can change between classical buck-boost pattern and resonant switched-capacitor pattern with flexible control to cater for the balancing requirements under different driving scenarios. The results of simulation of field experiments demonstrate successful balancing, speed and energy loss under various testing situations. The proposed balancing circuit is proved to be effective for wide range application.

In the rest of this chapter, a novel balancing circuit is introduced to overcome the problem of energy loss during balancing process. Besides, this balancing circuit is capable of working at different driving modes with flexible circuit switching and intelligent voltage control module. This paper is the first attempt to use ZCS technique in the integrated balancing circuit for rapid mode switching, accurate voltage tracking and loss reduction. Circuit configuration, operation principle, equations are presented in Sections 4.2 and 4.3. The effectiveness of the proposed balancing circuit is demonstrated by the results of simulation and field experiment in Sections 4.4 and 4.5. Section 4.6 concludes the chapter.

4.2 Proposed cell balancing circuits

4.2.1 Circuit configuration

In this section, a series multi-functional balancing circuit is presented for analysis. Different states of EVs, such as drive state, brake state and park state, may have different requirements on output power, balancing speed and balancing loss. Fig. 4.1 demonstrates six different operating modes with different cell balancing requirements for the corresponding driving states, for example, EVs in acceleration desire high balancing speed and low loss while park state does not have requirements on balancing speed. The circuitry of Fig. 4.2 shows the SC cells in series connection with two operation states, buck-boost balancing and switched-capacitor balancing. This multi-functional balancing circuit change its topology and parameters to cater the operation requirements of different operation modes, such as common drive mode, drive with air-conditioning (AC) mode, acceleration mode, brake mode and park mode for EVs.

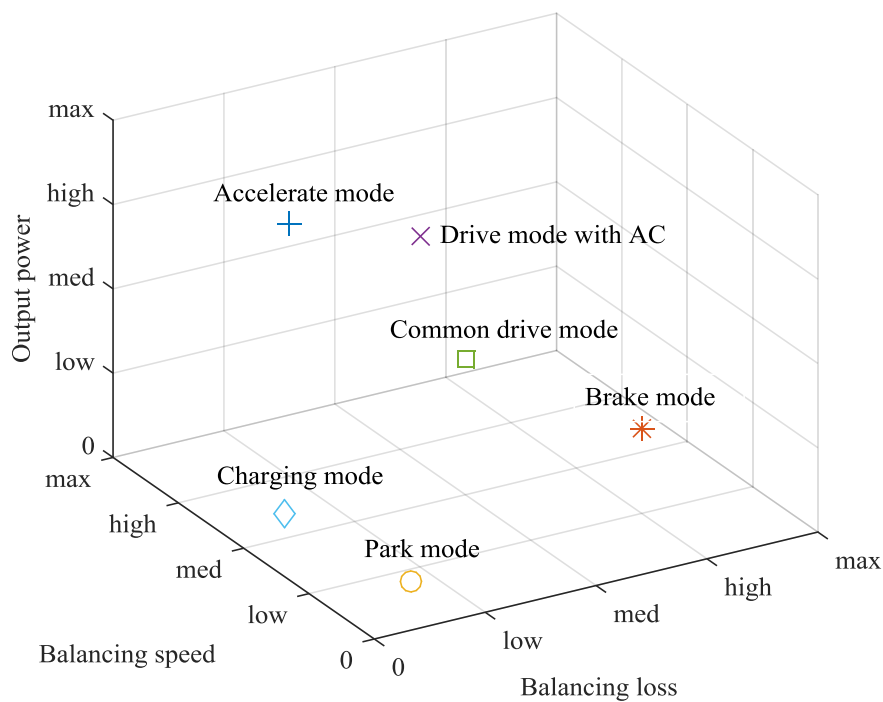


Fig. 4.1: Different operating modes and requirements

4.2.2 Balancing circuit operation analysis

In ideal case, the switching frequency f_s should be equal to the resonant frequency f_r .

$$f_s = f_r = \frac{1}{2\pi} \sqrt{\frac{1}{LC} - \theta^2} \quad (4-1)$$

where, $\theta = \frac{R}{2L}$; L is the inductance of the inductor and C is the capacitance of the switched-capacitor.

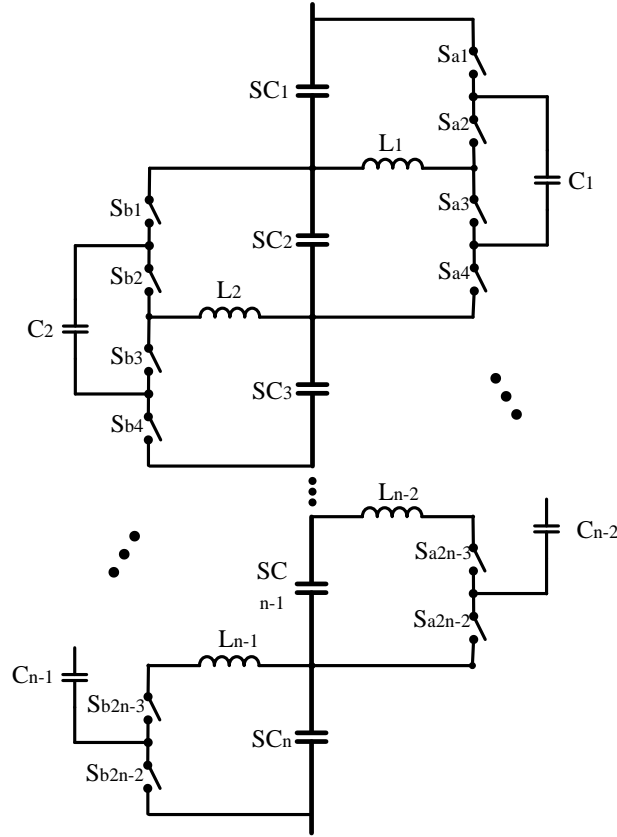


Fig. 4.2: Proposed balancing circuit

However, it is arduous to precisely match the RLC parameters of different balancing branches in real implementation. To avoid reverse current of the resonant inductor, the switching frequency in the proposed switched-capacitor circuit should be slightly higher than the resonant frequency with regards to the tolerances of the RLC parameters.

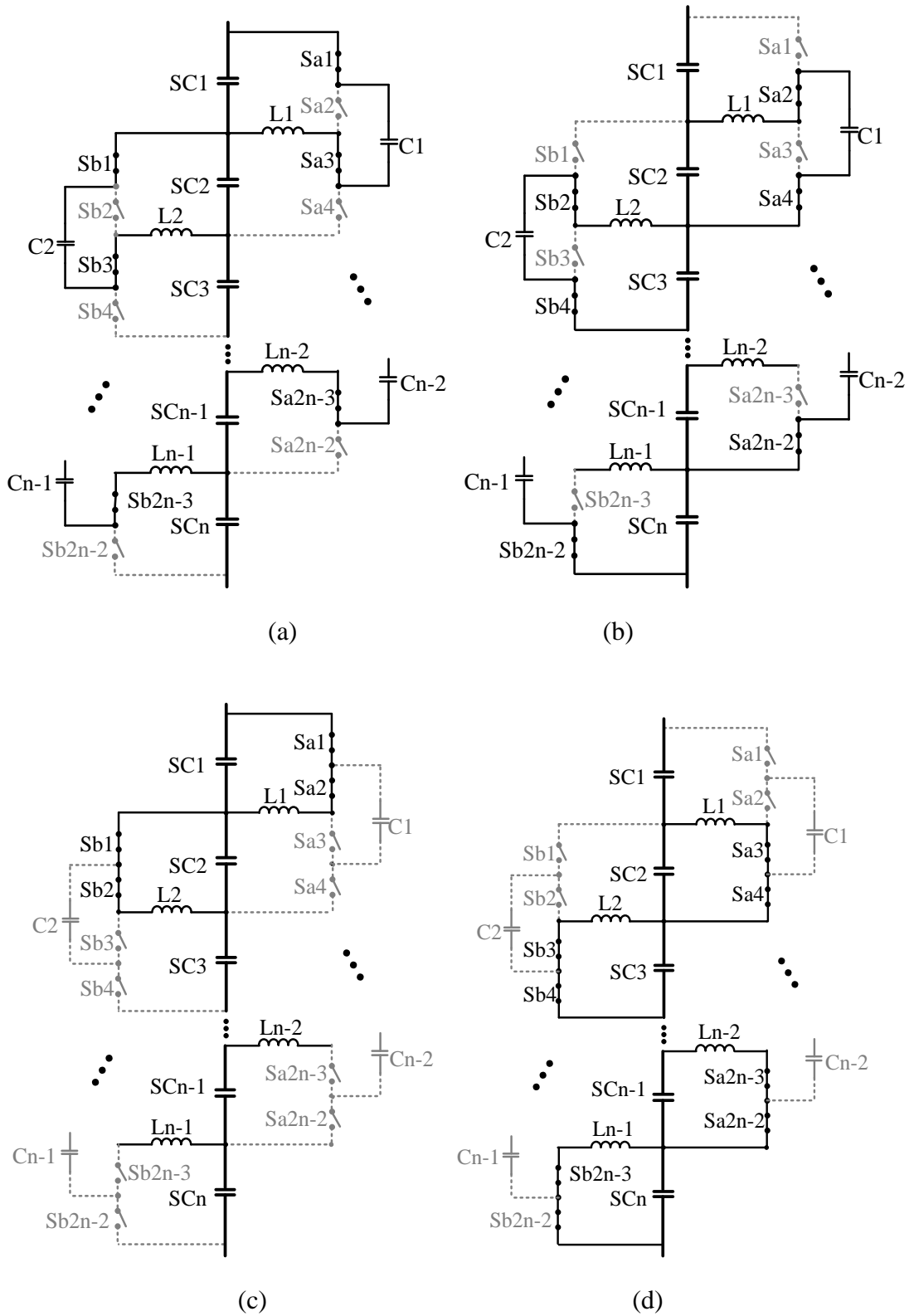


Fig. 4.3: Working principle of the proposed balancing system.

- (a) ZCS mode state I; (b) ZCS mode state II; (c) Buck-boost mode state I;
- (d) Buck-boost mode state II

Table 4.1. Switches control logical signal

Function Mode	Switching States							
	S_{a2}	S_{a2}	S_{a2}	S_{a2}	S_{b2}	S_b	S_{b2}	S_{b2}
	$m-1$	m	$m+1$	$m+2$	$m-1$	$2m$	$m+1$	$m+2$
ZCS mode	1	0	1	0	1	0	1	0
Buck boost mode	1	1	0	0	1	1	0	0

In the n -cells voltage balancing system as shown in Fig. 4.3, there are $4n-4$ switches which are dominated by the main intelligent control box to operate the circuit in different modes. All the switches are named in two groups S_a and S_b , the switches in each group are divided as S_{a2m-1} , S_{a2m} , S_{a2m+1} and S_{a2m+2} , where m varies from 1 to $n-1$; In S_{b2m-1} , S_{b2m} , S_{b2m+1} and S_{b2m+2} , m varies from 1 to $n-1$. The two functioning modes are ZCS mode and buck-boost mode with different switch positions as shown in Fig. 4.4.

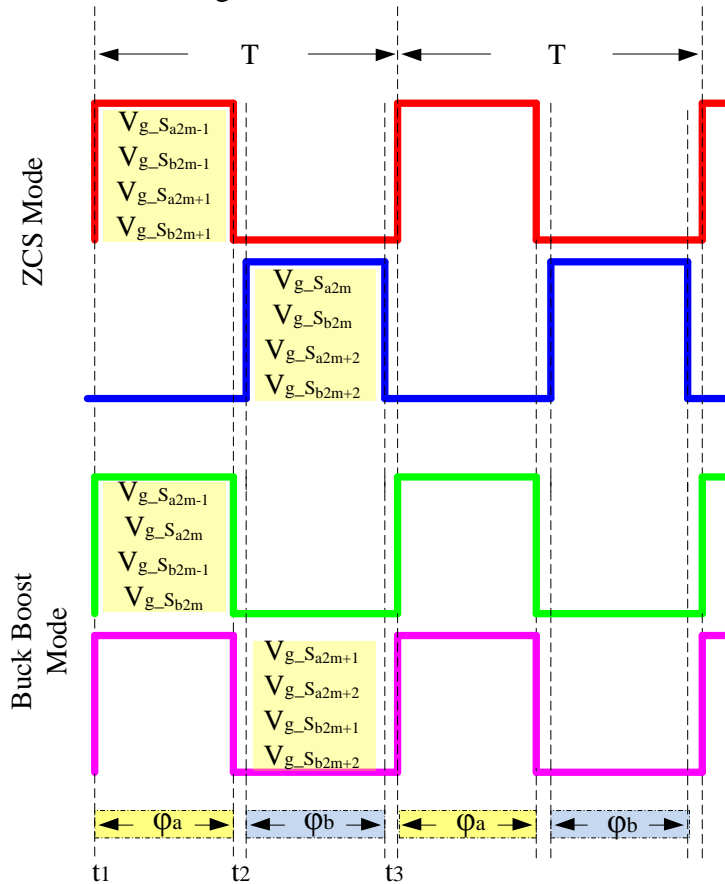


Fig. 4.4: Control signal of the switches

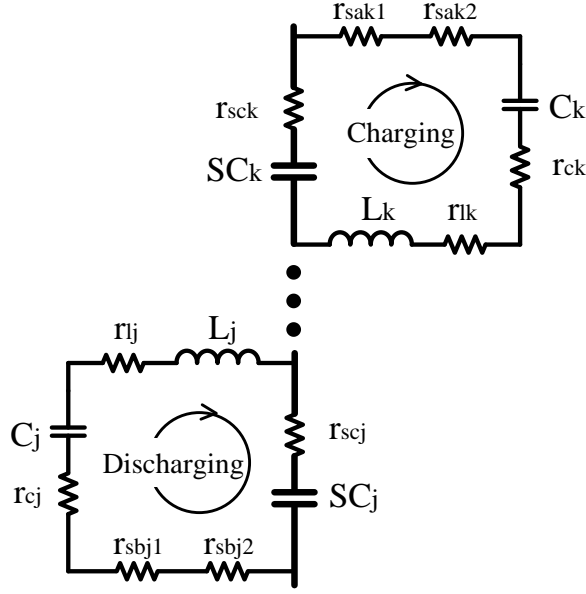


Fig. 4.5: Circuit of ZCS mode

When the switches S_{a2m-1} , S_{b2m-1} and S_{a2m+1} , S_{b2m+1} are turned on, the circuit forms the switched capacitors resonant tanks as shown in Fig. 4.5. In the state of the ZCS-SC, charge will transfer from SC_k to C_k switched-capacitor tank when the voltage of SC_k is higher than the initial voltage of C_k . Therefore, C_k is charged and the control signal during the process is shown in the top curve of Fig. 4.5 and Table 4.1. In the similar way, charge will transfer from C_j to SC_j when the voltage of SC_j is lower than the initial voltage of C_j . C_j is discharged in this process and the control signal is shown in the bottom curve of Fig. 4.5 and Table 4.1. SC_k , C_k , L_k and SC_j , C_j , L_j form the resonant loops.

4.2.3 Analysis of ZCS Operation

1) State I [See Fig. 4.3(a)]

In the state when S_{a2m-1} and S_{a2m+1} are turned on and S_{a2m} and S_{a2m+2} are turned off. The voltage V_{Ck} of C_k and the resonant current i_r are both increasing. Assume that all the components here are ideal and there are zero internal resistance for the SCs, switched-capacitors, inductors and switches in this analysis. The relationship between the current and the voltage are as shown below:

$$i_r = C_k \frac{dV_{C_k}}{dt} \quad (4-2)$$

$$L_k \frac{di_r}{dt} + V_{C_k} = V_{SC_k} \quad (4-3)$$

where L_k is the inductance of inductor L_k ; V_{SC_k} is the voltage between SC_k .

Then, the solutions of above are

$$V_{C_k} = V_{SC_k} + \Delta V_{C_k} \cos(\omega t + \phi) \quad (4-4)$$

$$i_r = I_r \sin(\omega t + \phi) \quad (4-5)$$

where ΔV_{C_k} is the amplitude of V_{SC_k} ; I_r is the amplitude of the i_r ; ω is the resonant angular frequency which is $\omega = \frac{1}{\sqrt{L_k C_k}}$, C_k is the capacitance of C_k ; ϕ is the initial angle of the resonant state.

In this resonant period, assume that the initial voltage $V_{C_{min}}$ across the capacitor C_k is minimum voltage, which is lower than the voltage V_{SC_k} across the SC_k . The voltage V_{L_k} and the amplitude of the i_r are illustrated as

$$L_k \frac{di_r}{dt} = V_{SC_k} - V_{C_{min}} \quad (4-6)$$

$$I_r = \frac{V_{SC_k} - V_{C_{min}}}{\omega L_k} = (V_{SC_k} - V_{C_{min}}) \sqrt{\frac{C_k}{L_k}} \quad (4-7)$$

After half a resonant period, the voltage of the V_{C_k} could reach maximum $V_{C_{k_max}}$, which is shown below:

$$V_{C_{k_max}} = 2V_{SC_k} - V_{C_{min}} \quad (4-8)$$

2) State II [See Fig. 4.3(b)]

In the state when S_{b2m-1} and S_{b2m+1} are turned on and S_{b2m} and S_{b2m+2} are turned off, switched capacitor C_j is discharging SC_j and the resonant current i_r is increasing in the opposite direction. The relationship between the current and the voltage are as shown below:

$$i_r = C_j \frac{dV_{C_j}}{dt} \quad (4-9)$$

$$L_j \frac{di_r}{dt} + V_{C_j} = V_{SC_j} \quad (4-10)$$

Then, the solutions of above are

$$V_{C_j} = V_{SC_j} - \Delta V_{C_j} \cos(\omega t + \phi) \quad (4-11)$$

$$i_r = -I_r \sin(\omega t + \phi) \quad (4-12)$$

In this resonant period, $V_{C_{max}}$ is the initial voltage across C_j at the discharge state which reaches the maximum value. The amplitude of the resonant current is

$$I_r = \frac{V_{C_{max}} - V_{SC_j}}{\omega L_j} = (V_{C_{max}} - V_{SC_j}) \sqrt{\frac{C_j}{L_j}} \quad (4-13)$$

The voltage of V_{C_j} could reach minimum $V_{C_{j_min}}$ at the end of this resonant period.

$$V_{C_{j_min}} = 2V_{SC_j} - V_{C_{max}} \quad (4-14)$$

In fact, there are equivalent series resistance (ESR) for the components and the voltage drop across the switches cannot be ignored. The r_{SC} , r_C , r_S and r_L internal resistors for SCs, switched-capacitors, ON-resistance of the switches and inductors respectively should be considered in the following analysis. The total ESR R_{ESR} in one resonant tank of the circuit is $R_{ESR} = r_{SC} + r_C + r_L + 2r_S$.

The resonant current of charging and discharging state should be revised as:

State I:

$$i_r = \frac{V_{SC_k} - V_{C_{min}}}{\omega_r L_k} e^{-\rho t} \sin \omega_r t \quad (4-15)$$

State II:

$$i_r = \frac{V_{C_{\max}} - V_{SC_j}}{\omega_r L_j} e^{-\rho t} \sin \omega_r t \quad (4-16)$$

where $\rho = \frac{R_{ESR}}{2L_{k,j}}$, $\omega_r = \sqrt{\frac{1}{L_{k,j}C_{k,j}} - \rho^2}$.

$L_{k,j}$ refers to either L_k or L_j in each of their state I and II and hence ρ and ω_r are calculated according to their respective L_k or L_j in State I and State II. The maximum and minimum voltage of $V_{C_{k,j}}$ are

$$V_{C_{\max}} = V_{SC_k} - (V_{SC_k} - V_{C_{\min}}) e^{-\rho\pi/\omega_r} \quad (4-17)$$

$$V_{C_{\min}} = V_{SC_j} - (V_{SC_j} - V_{C_{\max}}) e^{-\rho\pi/\omega_r} \quad (4-18)$$

4.3 Modeling for balancing mode

4.3.1 Modeling for ZCS balancing mode

As it is shown in Fig. 4.6, SC cells can be formulated to be charged or discharged between each other with the equivalent resistance. In the resonant circuit, C_k, L_k and C_j, L_j has same value C and L , respectively and all the switches are the same. The voltage of V_C could get to maximum $V_{C_{\max}}$ at the end of the state I and reduces to minimum at the end of state II. The voltage ripple ΔV_C can be obtained by subtracting (4-18) from (4-17).

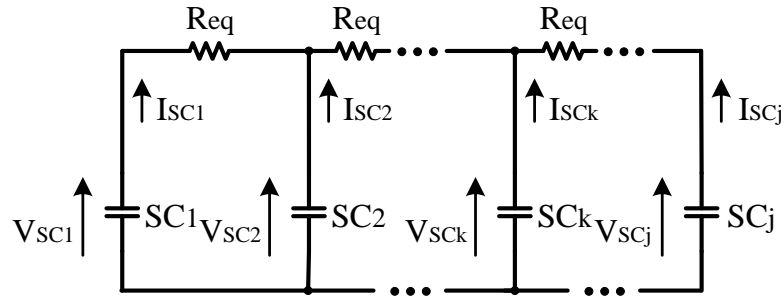


Fig. 4.6: Model of the ZCS mode circuit

$$\Delta V_C = (V_{SC_k} - V_{SC_j}) \frac{1 - e^{-\rho\pi/\omega_r}}{1 + e^{-\rho\pi/\omega_r}} \quad (4-19)$$

In one switching cycle, the quantity of electric charge is $C\Delta V_C$, flowing from higher voltage cell to lower voltage cell. The average current I_{avg_r} of one cycle is

$$I_{avg_r} = f_s \cdot C \cdot \Delta V_C \quad (4-20)$$

When (4-19) is substituted into (4-20), the equivalent resistance R_{eq} of each resonant tank is

$$R_{eq} = \frac{1 + e^{-\rho\pi/\omega_r}}{f_s C (1 - e^{-\rho\pi/\omega_r})} \quad (4-21)$$

The power loss P_{loss_r} of the ZCS mode is shown below

$$P_{loss_r} = I_{avg_r}^2 \cdot R_{eq} = f_s C (V_{SC_k} - V_{SC_j})^2 \frac{1 - e^{-\rho\pi/\omega_r}}{1 + e^{-\rho\pi/\omega_r}} \quad (4-22)$$

4.3.2 Modeling for Buck-Boost Balancing Mode

During the progress of buck-boost balancing mode, the charging/discharging vary in one cycle, the charge is transferred between SC_k and SC_j . The equivalent model of the balancing circuit is shown in Fig. 4.7, where the ESR and on-state voltage for the diode are included to facilitate modeling.

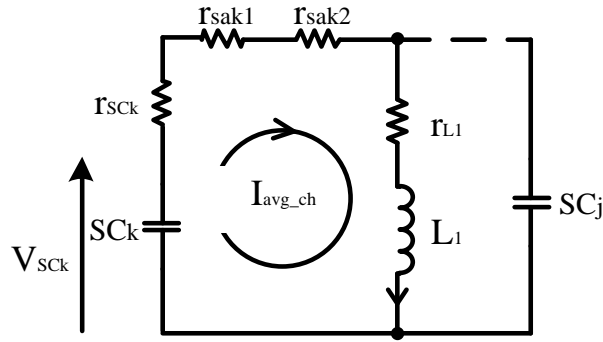
To illustrate the voltage conversion process for the inductor L_1 , the mmf values of M_{ch} and M_{disch} to investigate the voltage conversion of the converter circuit for charging and discharging, respectively, during one cycle are

$$M_{ch} = \frac{V_{SC_k}}{L_1} D_1 T \quad (4-23)$$

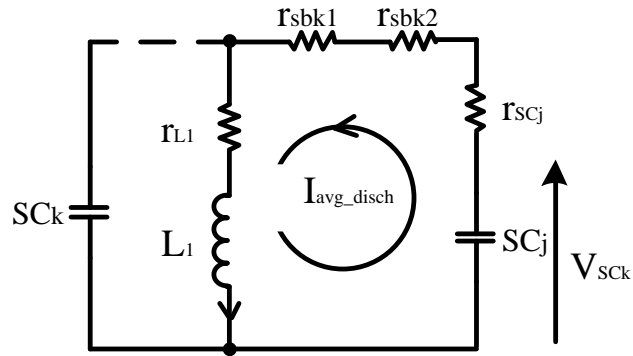
$$M_{_disch} = \frac{V_{SCj}}{L_1} D_2 T \quad (4-24)$$

where D_1 and D_2 are the turn-on duty ratio of transistor and diode respectively, $D_1 + D_2 = 1$.

According to KVL, the relationship between two cells is



(1)



(2)

Fig. 4.7: Model of the Buck-boost mode circuit

$$\frac{V_{SCk}}{L_1} DT - \frac{R_1}{L_1} \int i_{ch} dt = \frac{V_{SCj}}{L_1} (1-D)T - \frac{R_2}{L_1} \int i_{disch} dt \quad (4-25)$$

where $R_1 = 2r_s + r_L + r_{SCk}$, $R_2 = 2r_s + r_L + r_{SCj}$; i_{ch} and i_{disch} are instantaneous current across L_1 for charging and discharging, respectively. I_{avg_ch} and I_{avg_disch} are the average current across L_1 when it is charging or discharging.

When $\int i_{ch} dt \approx I_{avg_ch} DT$ and $\int i_{disch} dt \approx I_{avg_disch} (1-D)T$, I_{avg_ch} could be obtained from (4-25) as:

$$I_{avg_ch} = \frac{V_{SCj}(1-D) + V_{SCk}D}{R_2(1-D) + R_1D} \quad (4-26)$$

The average current I_{avg_b} of SC in this mode is

$$I_{avg_b} = \frac{V_{SCj}(1-D)D + V_{SCk}D^2}{R_2(1-D) + R_1D} \quad (4-27)$$

In the balancing progress, all the energy transfers between each cell, from the higher voltage SC cell to lower voltage cell. During these states, the variation of the i_{ch} is

$$i_{ch}(t) = I_{avg_ch} + \Delta i_{ch} \left(t - \frac{DT}{2} \right) \quad (4-28)$$

where Δi_{ch} is the current difference during charging state, $T = \frac{1}{f_s}$.

The variation of the i_{disch} is

$$i_{disch}(t) = I_{avg_disch} + \Delta i_{disch} \left(t - \frac{DT}{2} \right) \quad (4-29)$$

where Δi_{disch} is the current difference during discharging state.

The energy discharged E_{disch} from SC_k and the energy charged E_{ch} to the SC_j throughout one cycle are:

$$E_{disch} \approx V_{SCk} \int i_{ch} dt \quad (4-30)$$

$$E_{ch} \approx V_{SCj} \int i_{disch} dt \quad (4-31)$$

The energy transferred in the inductor L_l is

$$\int_{t_1}^{t_2} (V_{SCk} - i_{ch} R_1) i_{ch} dt \approx \int_{t_2}^{t_3} (V_{SCj} - i_{disch} R_2) i_{disch} dt \quad (4-32)$$

The energy loss E_{loss} could be obtained by (4-30) subtracting (4-31).

$$\begin{aligned} E_{loss} &\approx V_{SCk} \int_{t_1}^{t_2} i_{ch} dt - V_{SCj} \int_{t_2}^{t_3} i_{disch} dt \\ &= R_1 \int_0^{DT} i_{ch}^2 dt + R_2 \int_0^{(1-D)T} i_{disch}^2 dt \\ &= T \left(I_{avg_ch}^2 + \frac{3\Delta i_{ch}^2}{4} \right) [R_1 D + R_2 (1-D)] \end{aligned} \quad (4-33)$$

where $\Delta i_{ch} \approx \frac{DV_{SCk}}{2L_1 f_s}$.

The power loss P_{loss_b} of the buck-boost mode is

$$P_{loss_b} = \frac{[V_{SCk} (1-D) + V_{SCj} D]^2}{R_2 (1-D) + R_1 D} + \frac{3}{4} \left(\frac{DV_{SCk}}{L_1 f_s} \right)^2 [R_2 (1-D) + R_1 D] \quad (4-34)$$

4.4 Simulation Results of the Multi-Function Voltage Equalizer

In PSIM software, the proposed circuit is simulated. The circuit topologies of three series connected SCs with initial voltages of 2.0, 2.4, 2.6V, respectively and with the same capacitance 1F are built in the simulation shown in Fig. 4.8. Switched-capacitors $C=22\mu\text{F}$ are used in simulation while $f_s=15, 20, 25$ kHz and 90, 100, 110 kHz of the control signals are used to operate the circuit. The above configurations are the same with practical application, except the capacitance of the SCs because PSIM could not accept large Farad for capacitance.

Table 4.2. Simulation results of the Switched-capacitor voltage equalizer

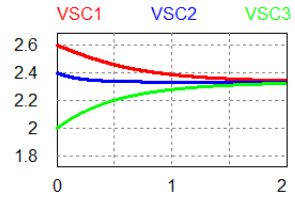
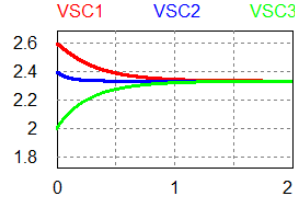
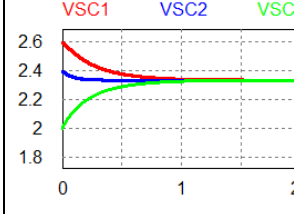
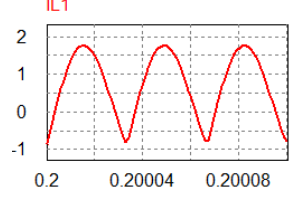
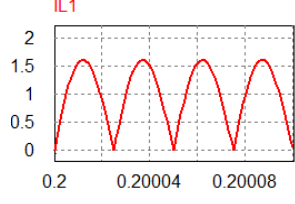
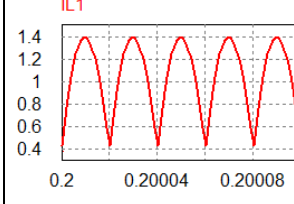
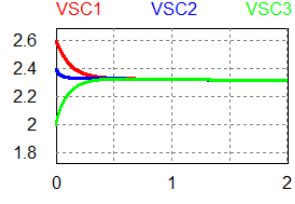
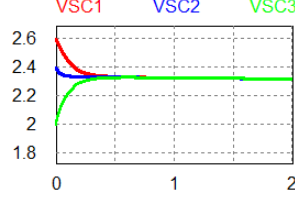
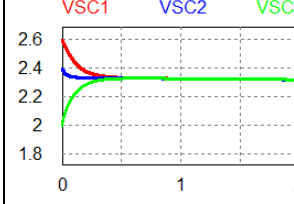
Mode	$f_s=15\text{kHz}$	$f_s=20\text{kHz}$	$f_s=25\text{kHz}$
ZCS mode			
	X: Time(s); Y: Voltage(V)		
			
X: Time(s); Y: Current(A)			
Buck-boost mode	$f_s=90\text{kHz}$	$f_s=100\text{kHz}$	$f_s=110\text{kHz}$
			
	X: Time(s); Y: Voltage(V)		

Table 4.2 illustrates the comparison of the waveforms in the simulation varied with different switching frequency f_s for ZCS and buck-boost mode. It is observed that V_{SC1} , V_{SC2} and V_{SC3} finally converge to the same voltage level in all circumstances. For ZCS mode, when f_s is larger, the switching speed is faster that accelerates the equalization process. The balancing phenomenon conforms to the principles in (4-20). When the switching frequency f_s is the same as the resonant frequency f_r the balancing progress could reach zero current when switches are turn on and off, this conforms to the principle in (4-1). But the variation of the f_s could not affect the balancing speed for buck-boost mode which is illustrated in (4-27).

4.5 Experimental Results of the Multi-Function Circuit

The proposed circuit has advantages in performing balancing for different EV driving modes so that it is more flexible for energy storage system which has different working conditions. To verify the mathematical derivation and software simulation, energy storage strings composed of three SCs are formulated with the multi-functional balancing circuit controlled by different switching signals. The topology is shown in Fig. 4.8 and the list of components is recorded in Table 4.3.

The voltage balancing process for ZCS mode of the experiment is shown in Fig.4.9. The initial voltages of the SCs are 2.6V, 2.31V and 1.88V, respectively. After the voltage balancing is conducted, V_{SC1} , V_{SC2} and V_{SC3} are all finally balanced to the same voltage magnitude, which coincides with the results in the above theoretical analysis. The integrated voltage magnitude after balancing is 2.23V. Fig. 4.10 depicts the voltage and current variations of C_1 , C_2 and L_1 . It is clearly shown that when the switch is turning on/off, the instantaneous current of the resonant loop is close to zero, which conforms to the principles of ZCS and loss reduction.

The voltage balancing process for buck-boost mode of the experiment is shown in Fig. 4.11. The initial voltages of the SCs are set as 2.42V, 2.29V and 2.03V, respectively. After conducting voltage balancing, V_{SC1} , V_{SC2} and V_{SC3} are also balanced to the same voltage magnitude as expected. The integrated voltage magnitude after balancing operation is 2.17V. Fig. 4.12 depicts the voltage and current variations of L_1 . The energy loss of ZCS mode decreases 35% compared with that in buck-boost mode.

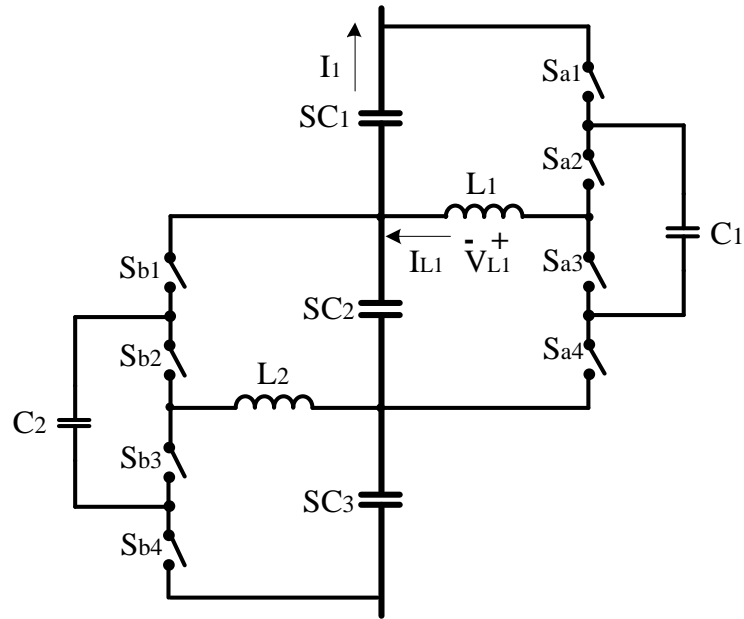


Fig. 4.8: Multi-functional equalizer built in laboratory

Table 4.3. Parameters in the experiment

Units	Quantity
Supercapacitor (DRL357S0TQ60SC)	3
Capacitance of SCs	350F
MOSFET(IRFR3607PBF) 75V 7.34mΩ	8
ON-resistance of MOSFETs	7.34 mΩ
Switched-capacitor (RNS1E220MDN1KX)	2
Capacitance of Switched-capacitors	22μF
ESR of Switched-capacitors	28mΩ
Inductor (WE-HCF)	2
Inductance of the inductor	33μH
ESR of Inductor	1.31mΩ
Switching frequency	20kHz, 100kHz

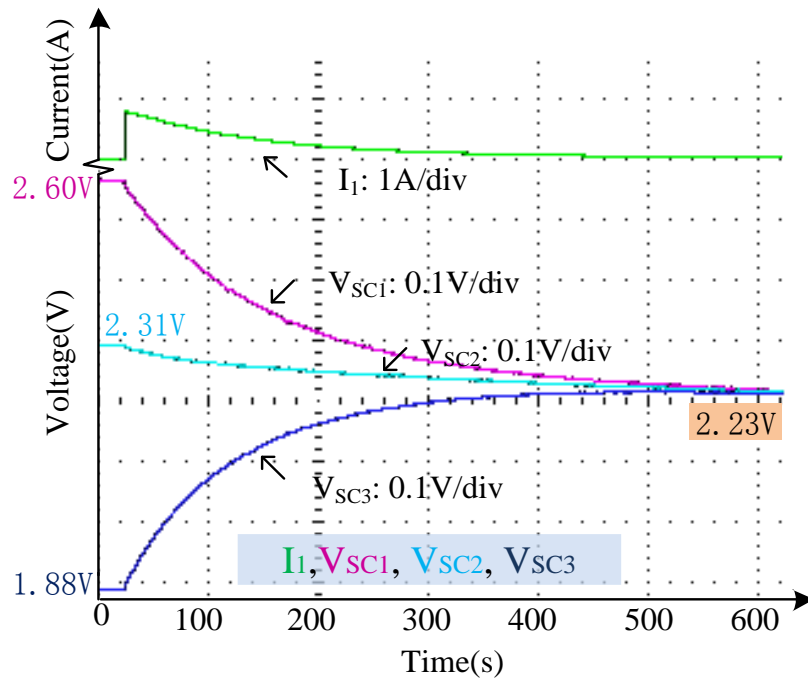


Fig. 4.9: The ZCS mode balancing waveform from the experiment in the laboratory

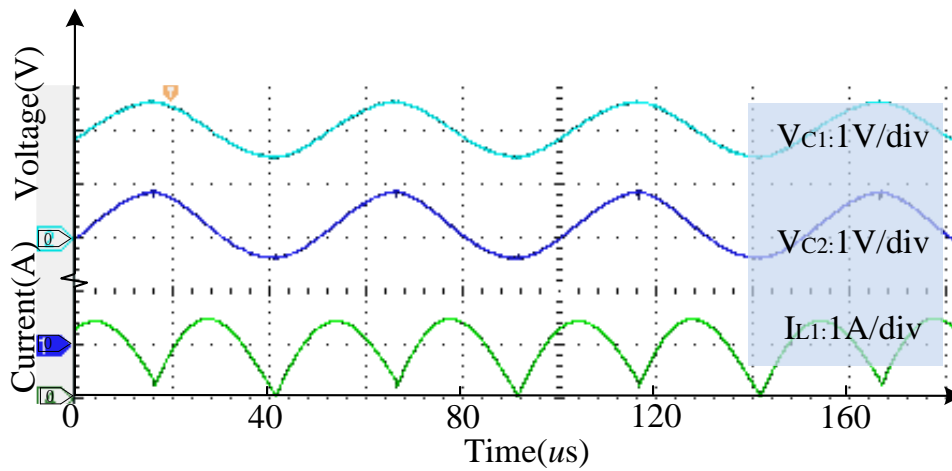


Fig. 4.10: The voltage $V_{C1,2}$ and current I_{L1} waveform of switched-capacitor C_1 during the balancing progress of ZCS mode.

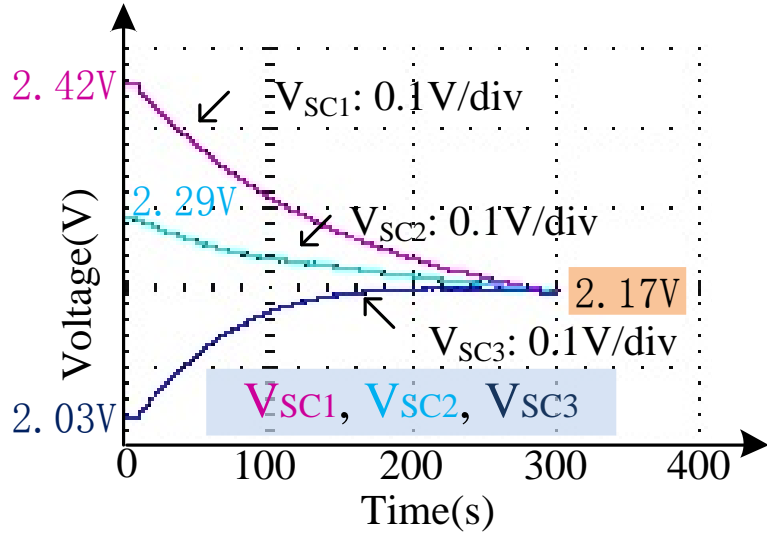


Fig. 4.11: The Buck boost mode balancing waveform from the experiment in the laboratory

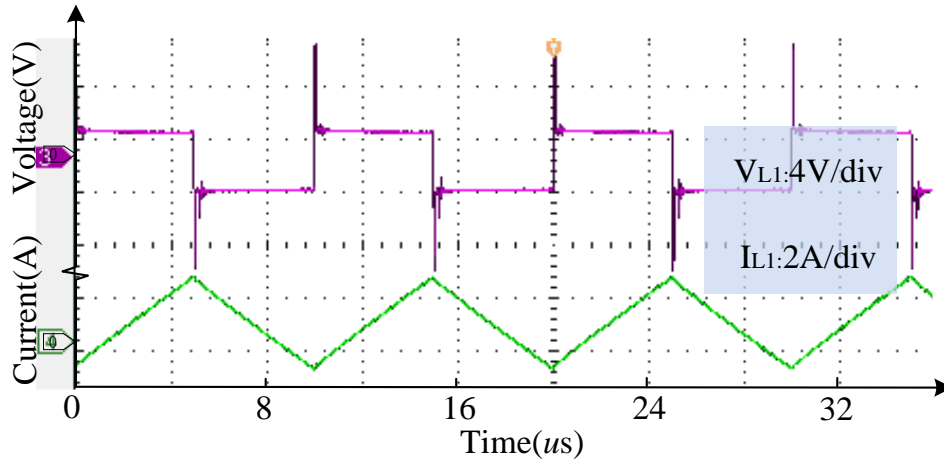


Fig. 4.12: The voltage V_{L1} and current I_{L1} waveform of switched-capacitor C_1 during the balancing progress of Buck-boost mode.

The experimental results demonstrate that the variations of both voltage and current in the proposed circuit conform to the charging/discharging principles analyzed in each phase.

4.6 Conclusion

A novel zero-current switching cell balancing circuit is proposed in this chapter to decrease switching loss during balancing process. Furthermore, in order to adjust to different requirements of EV operation states, the multi-

functional circuit is able to easily change between buck-boost and switched-capacitor pattern with flexible switching frequency and duty ratios. Simulation and field experiment are conducted to demonstrate its loss reduction effect and flexibility in various situations. The energy loss of ZCS mode decreases 35% compared with that in buck-boost mode. Future works may include voltage feedback control during balancing process to further increase speed and decrease loss.

Following good balancing design of battery cells and packaging, the next chapters are to study charging control forecast study of the battery EV in an urban charging plan with the influence of balancing strategies.

Chapter V

Forecast of Urban EV Charging Load and Smart Control Concerning Uncertainties

5.1 Introduction

Popularizing electric vehicles (EV) can be one of the most effective ways to deal with the ever severe air pollution. In smart city, EVs are not only transportation tools, but also mobile and distributed energy generation/consumption. However, the accumulated charging power from the increasing integration of EVs could add large pressure to the peak of power grid.

To make full use of the peak-shaving capacities of aggregated EVs, the voltage of EV internal battery packages and the battery cells should be kept equal for the best performance and safety. Especially, the multi-functional balancing circuit proposed in Section IV is able to switch modes according to different driving states and the full capacity of EV battery is guaranteed.

Besides voltage balancing of EV batteries, the stochastic charging behavior is another obstacle to EV storage system utilization. In this chapter, a novel EV load forecasting model is formulated based on Markov chain [81] allowing for the stochasticity of user behavior, traffic and weather. The impact of EV integration is assessed in a typical medium voltage (MV) system while the resulting peak load and power loss are mitigated with charging control schemes. The proposed model could help to forecast the future charging demands with probabilistic uncertainties. The smart control schemes shall instruct the aggregator to make optimal charging plan concerning security and efficiency issues.

The rest of this chapter is organized as follows. In Section 5.2, a general forecast model of EV traveling routes is formulated with Markov Chain. In Sec-

tion 5.3, urban EV charging load is forecast concerning stochastic travel behavior, road traffic and weather. In Section 5.4, smart charging control is proposed to determine optimal user charging schemes. In Section 5.5, the advantages of proposed voltage balancing circuits are verified and results of the charging load forecast and the urban EV charging optimization are demonstrated in the case study. Section 5.6 summarizes this chapter.

5.2 Methodology for Route Modeling

This section provides a general method for simulating the daily routes with multiple travel purposes. The theory of Markov Chain is applied to find out the interrelationship among consecutive trips.

5.2.1 Travel Route Modeling

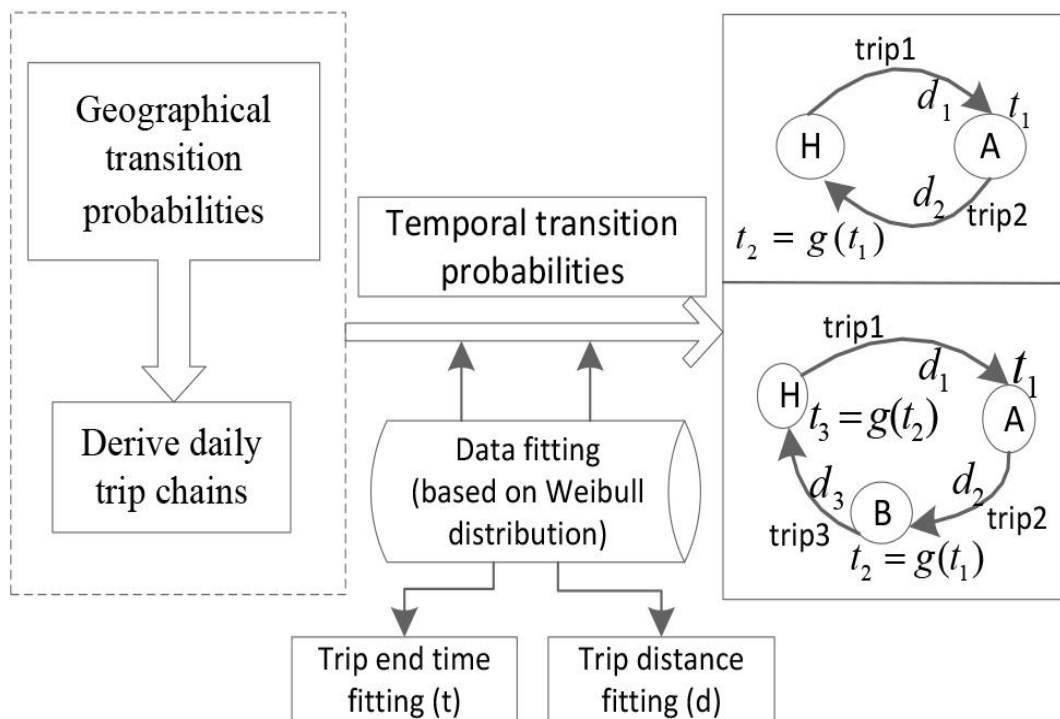


Fig. 5.1: Route modeling process

The route modeling process is described in Fig. 5.1. Daily trip chains are created to show the whole travel routes with spatial and temporal information. For private cars, Home (H) is generally both the daily starting place with full-charged battery and the daily last stop. Although an EV can have several trips a day, many of them, like picking someone up or buying a drink, are short trips with temporary parking. It is shown from National Household Travel Survey (NHTS) [100] that the average number of trips per vehicle per day with charging possibility is 2.42. Chains are divided into two categories to investigate the transitions. If the average number of effective trips is larger in other places, the length of the trip chain can be extended.

“Home - Activity - Home” form with two travels a day is the simplest trip chain which demonstrates a regular lifestyle. In the Fig.5.1, d_1 represents the leaving-home trip while d_2 or d_3 is the trip back to H. Complex chains with multiple consecutive trips depict people who are social or have business. A and B are chosen location from travel purposes W (Work), SE (Shopping & Eating), SR (Social & Recreational) or O (Other family errands), d_1 , d_2 and d_3 are consecutive trips traveling among A, B and H.

5.2.2 Transition Relationships

For the two kinds of chains in Fig. 5.1, the information of individual trips driving from one place to another is fitted with Weibull distribution [91]. Although people's travel behavior changes with time, it is predictable and may somehow be influenced by the last trip when considering a series of trips within a day. The Markov chain is widely used to describe the discrete-time stochastic progress of a system [111], therefore the daily trip chains are assumed to follow Markov process. The Markov property defines that the probability of the transition into state X_{n+1} only depends on its last state X_n , irrespective of other previous states. The transition probability $P_{n,n+1}$ in (5-1) represents the probability of a one-step transition from state X_n to state X_{n+1} :

$$\begin{aligned}
p_{n,n+1} &= P(X_{n+1} = x_{n+1} \mid X_1 = x_1, \dots, X_n = x_n) \\
&= P(X_{n+1} = x_{n+1} \mid X_n = x_n)
\end{aligned}
\tag{5-1}$$

1) *Geographical transition probabilities*: If each possible stopping place is regarded as one state, people's next travel destination only depends on their current stopping state according to Markov chain principles. For five places H, W, SE, SR and O, if they are assigned to be state 1, 2, 3, 4 and 5 respectively, a Markov transition matrix M_{ij} is formed in (5-2):

$$M_{ij} = \begin{bmatrix} p_{11} & \cdots & p_{15} \\ \vdots & \ddots & \vdots \\ p_{51} & \cdots & p_{55} \end{bmatrix}
\tag{5-2}$$

where p_{ij} represents the transition probability to state j while the vehicle's current state is i .

People's travel route within a day can be forecast based on the Markov transition matrix [125]-[127]. In this chapter, the data of Markov chain is generally formulated from local travel survey which collects travel behavior information of regional representative samples including trip origin and purpose with trip distance and arriving time. Firstly, the complete consecutive chains are selected from travel survey. The value of each element in the matrix is then represented as the ratio of the next travel preference after one specific stop. The Markov chain varies with external properties like seasons or working days, but is time homogeneous in a day's view once established because the trips are closely related.

2) *Temporal transition probabilities*: Although the separate end time distribution of each transition is determined beforehand, the end time of last trip could greatly influence the distribution of current trip end time when considered in a complete chain. According to the theory of Markov Chain, the end time of current trip T_j can be represented by a function $g(\cdot)$ of the end time of last trip T_i , as shown in (5-3) and Fig. 5.1.

$$T_j = g(T_i) \quad (5-3)$$

where $g()$ in the mathematical model can be determined from historical travel surveys.

5.3 Methodology for Charging Load Forecast

Having obtained the modeling of daily routes, including their temporal and geographical information, researching the power consumption of each trip is of importance to forecast the state-of-charge (SoC) upon each destination. Multiple charging is then considered when necessary. The geographical distribution of daily charging load demand is obtained by Monte Carlo Simulation (MCS).

5.3.1 Energy Consumption per km

Driving style, load, traffic conditions and weather may influence the power consumption at certain extent, so obtaining an exact value of mileage is unrealistic. The time-variant energy consumption per km, denoted in (5-4), varies in accordance with the temporal external conditions.

$$w_{n,t} = \frac{C}{L_t} \quad (5-4)$$

where $w_{n,t}$ is the energy consumption per km (kWh/km) heading to place n at time t ; C is battery capacity (kWh); L_t is the tested mileage (km) under the same condition as time t .

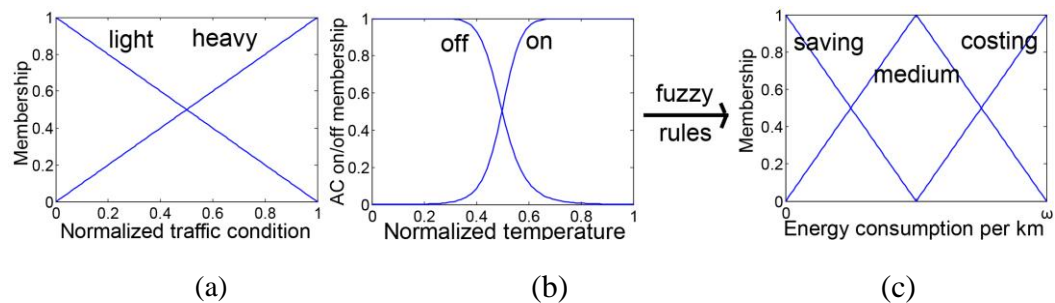


Fig. 5.2: Calculation process of energy consumption per km

The calculation process is depicted in Fig. 5.2. The authors in [112] have mentioned the impact of ambient temperature and road slope but the accurate parameters are hard to define. A method based on fuzzy logic is proposed for estimation concerning integrated traffic and weather effects.

The traffic condition is normalized from light to heavy based on linearization to [0,1] and also defined in Fig. 5.2(a), so its membership function is of a triangular shape. As both hot and cold weather require the operation of air conditioning (AC), the outer temperature of vehicle is normalized in (5-5):

$$Z_t = 0.5 + p \cdot \text{sgn}[(z_t - z_{\min})(z_t - z_{\max})] \quad (5-5)$$

where Z_t is normalized ambient temperature at time t ; z_{\min} and z_{\max} represent the critical temperature of feeling cold and feeling hot respectively; p is the proportionality coefficient.

As almost all people prefer driving comfort to saving energy when outside temperature exceeds certain threshold, the tendency to turn on AC follows the generalized bell-shaped membership function defined in [113] and also defined in Fig. 5.2(b). The adjectives “saving”, “medium” and “costing” listed in Fig. 5.2(c) represents peoples’ perception on the degree of energy consumption per km by different membership curves.

The fuzzy rules can be tuned with real tested results under different scenarios, and the centroid defuzzification method [113] is used to obtain the surface of output energy consumption per km $W_{n,t}$.

5.3.2 Charging Frequency

The choice of whether charging at a specific stop largely depends on the energy adequacy for the next trip. Normally the SoC of battery shall be kept no less than 30% for safety driving and battery life time [114] and therefore, if at one charging station (5-7) is fulfilled, suitable mode of charging should be performed on the EV; otherwise there is no need for charging until back home.

$$SOC_n \cdot C = SOC_{n-1} \cdot C - w_{n,t} \cdot l_n \quad (5-6)$$

$$SOC_n \cdot C - w_{n+1,t} \cdot l_{n+1} < 30\% \cdot C \quad (5-7)$$

where SOC_n is the remaining SoC at place n ; l_{n+1} is the length of next trip after place n and should be estimated when reaching place n .

5.3.3 Stochastic Load Forecast Model Using MCS

Having obtained the travel route and charging information for each vehicle, the load demand in each destination can be forecast.

If (5-7) is fulfilled at place n , the charging start time equals to the trip end time and is derived from (5-3) to be T_j while charging duration is T_c . The charging possibility $u_{n,t}^k$ of the k^{th} EV is defined in (5-8) and the daily charging load profile $P_{n,t}^k$ is presented in (5-9).

$$u_{n,t}^k(T_j \leq t \leq T_j + T_c) = 1; u_{n,t}^k = 0, \text{ otherwise} \quad (5-8)$$

$$P_{n,t}^k = P_c \cdot u_{n,t}^k \quad (5-9)$$

where P_c is the charging power.

This process is repeated for all K EVs. Their individual daily load profiles are then summed up for constituting total daily load profile $P_{n,t}$ at different charging stations in (5-10).

$$P_{n,t} = \sum_{k=1}^K P_c \cdot u_{n,t}^k \quad (5-10)$$

5.4 Minimizing impact on power system

With the increasing integration of EV, the load demand is placing ever more pressure on the established power system. Considering the performance of the system regarding efficiency and security issues, optimized schemes are then proposed aiming at alleviating the impact on the regional network in the most severe scenario.

5.4.1 Optimization Problem

For maneuverability and feasibility, load demand in H during the day is chosen to be optimized because all EVs are assumed to be charged at H in the end and vehicles would stay in home garage for the whole night [128]-[129]. Consider a distribution power system in a city with different functioning areas, such as H, W, SE, SR and O. EVs travel consecutively along those potential areas and charge at power nodes of the distribution grid connecting those areas. This chapter aims to devise a control scheme based on minute basis for the residential aggregator to minimize the total power loss of the distribution grid while avoiding the voltage and charging power from exceeding the predefined limits. The optimization problem is described as follows.

Objective:

$$\text{Min} \sum_{t=1}^{1440} \sum_{m=1}^M I_{m,t}^2 R_m \quad (5-11)$$

Constraints:

$$V_{\min} \leq V_{n,t} \leq V_{\max} \quad (5-12)$$

$$\overline{P}_{n,t} \leq C_{\max} \quad (5-13)$$

where $I_{m,t}$ represents line current of the m^{th} distribution line at time t ; R_m is the line impedance; $V_{n,t}$ is the voltage in node n at time t .

Inequality (5-12) represents the voltage limit (V_{\min}, V_{\max}) in node n at time t while (5-13) denotes the maximum charging power $P_{n,t}$ at node n constrained by the maximum capacity C_{\max} of local network, including transformers. The aggregator installed at each area acts as the medium for receiving smart control signals and put them into effect on the local cluster of EVs, following two control methods shown below.

5.4.2 Control Scheme

Two methods are considered for coordination of the best daily EV charging profile in order to search the best total distribution power flow, including base power load and EV charging power. Their control variables and basic assumptions are clarified below:

1) *Variable start-time charging*: In this control scheme, EV will not be charged once connected to the aggregator but may be postponed some time in case of congestion. By regulating the charging start time in peak hours, some load demand could be shifted to unbusy hours when the system is in its valley. To fulfill this goal, four variable input parameters are selected as below:

$$T_p, T_s, T_l, c\%,$$

where T_p is the amount of time to be postponed; T_s is the start time of period under control when EVs are not charged immediately after arrival; T_l is the lasting duration of implementing this control scheme; $c\%$ is the percentage of EVs which will be regulated during that period.

2) *Variable power charging*: In this control strategy, the charging power will no longer be the same at all time but subject to change with the severity of overload at the connecting time. In this variable power charging, the charging power for EV can be changed by adjustment of the central aggregator. During over-loaded hours, the central aggregator at residential district is able to lower the overall charging power to decrease the peak load of the system while pro-

longing the needed charging duration accordingly. There are also four control inputs in this scheme:

$$p\%, T_s, T_l, c\%,$$

where $p\%$ is the percentage of reduction in charging power and the resulting extension in charging duration varies with the $p\%$, during the controlled period determined by T_s and T_l .

5.4.3 GA Implementation

The optimization problem is formulated in this section. A central aggregator at H is established so that it is able to communicate with the regional network for the information of base power flow and send control signals to local chargers to adjust the above inputs when necessary. In this chapter, Genetic Algorithm (GA) is adopted to search the optimal solution [116], [130]-[131] with fitness function f as follows:

$$\text{Min } f = f_1 + f_2 + f_3 \quad (5-14)$$

$$f_1 = \sum_{t=1}^{1440} \sum_{m=1}^M I_{m,t}^2 R_m \quad (5-15)$$

$$f_2 = \sum_{t=1}^{1440} \sum_{n=1}^N \alpha_1 G(V_{\min} - V_{n,t}) \quad (5-16)$$

$$f_3 = \sum_{t=1}^{1440} \sum_{n=1}^N \alpha_2 G(\overline{P}_{n,t} - C_{\max}) \quad (5-17)$$

$$G(x) = \begin{cases} x, & x > 0 \\ 0, & \text{otherwise.} \end{cases} \quad (5-18)$$

where f_1 represents the value of total line loss in (5-15). Values of f_2 and f_3 are derived from the extents of voltage drop violation ($V_{\min} - V_{n,t}$) shown in (5-16) and overload ($\overline{P}_{n,t} - C_{\max}$) shown in (5-17), respectively. f_2 and f_3 are added as

penalties to the fitness function (5-14) where penalty coefficients α_1 and α_2 are set large enough that violation of voltage and power limit will severely impair the minimization of (5-14), which is the objective of smart EV charging control.

The inputs of GA vary with the control scheme selection in Section 5.4.2. The property of each input is distinct and the variation range may be too large for binary coding, so a real-coded GA is therefore employed to enhance efficiency. The detailed process of GA is described by the following pseudo-codes taking variable power charging as an example. The value of *gen* represents the current generation of offspring. Carefully determine the variation range of each input in Section 5.4.2;

Set *gen*=0;

Randomly sampling input values to change the charging scheme in H: For *c*% of the EVs connected to H during period [T_s , T_s+T_l], $P_c = P_c * p\%$. // reusing (5-6) -(5-10);

Power flow calculation with updated power demand in H and other original data obtained from the configuration of power grid;

Calculating fitness of each pair of inputs // using (5-14) -(5-18);

While (*gen*<maximum generation)

Selection based on ranking of the fitness;

Update input values via Crossover and Mutation to optimize charging scheme in H // reusing (5-6) -(5-10);

Power flow calculation with updated power demand;

Calculating fitness of current generation // using (5-14) -(5-18);

Fitness-based reinsertion to reduce recomputation;

gen=*gen*+1;

End

Local optimization methods can be fast in handling large-scale problems, and are widely applicable [115]. The processor of the aggregator shall make quick decision responding to the changes of bulk regional grid, so obtaining globally optimal solution is not realistic. The algorithm in this chapter focuses on local optimization which quickly finds a good solution for application, if not the very best. Therefore, the variation range of each input should be determined carefully based on accurate forecast of peak (valley) periods and occurring places derived in Sections 5.2 and 5.3. The maximum generation shall be set properly to guarantee a good control plan obtained in acceptable computation time.

5.5 Case Study

In this study, the transportation dataset is mainly derived from urban records of NHTS [100] (Data file named DAYPUBLL) which covers detailed travel information of 150147 U.S. households with the assumption that the user behavior of driving EV is mostly the same as people driving ICE vehicles. Specifically, columns WHYFROM and WHYTO explain the trip purpose while TRPMILES, DWELTIME and ENDTIME represent the travel distance, sojourn time and arrival time, respectively. The Nissan Leaf, with lithium-ion battery capacity of 24 kWh, is chosen as the typical private EV used in modeling. Derived from SAE J1772 [107], the charging power at home garage and public parking lot is assumed to be 3.3 kW and 19.2 kW, respectively. If not specified, the EV penetration (i.e. the proportion of EVs out of all registered sedan cars) is assumed to be about 20% to present a future smart city with EVs.

5.5.1 Influence of External Conditions

This case study considers the conditions in a typical subtropical climate. A range of 160 km for Leaf is claimed by Nissan; however, different testing results from United States Environmental Protection Agency (EPA) [108] are shown in

Table 5.1. The test proposed five driving scenarios for Nissan Leaf and its mileage ranges in a large scale from 76 km to 222 km, which indicates the great impact of AC operation and traffic jam. The fuzzy rules are then generated from Table 5.1. The resulting surface for the time-variant energy consumption per km ω is depicted in Fig. 5.3.

Table 5.1. Scenarios of charging duration at public stations

Traffic Condition	Ambient Temperature (°C)	AC on/off	Range (km)
Cruising	20	Off	222
City traffic	25	Off	169
Highway	35	In use	110
Stop and go	-10	Heater on	100
Heavy stop-and-go	30	In use	76

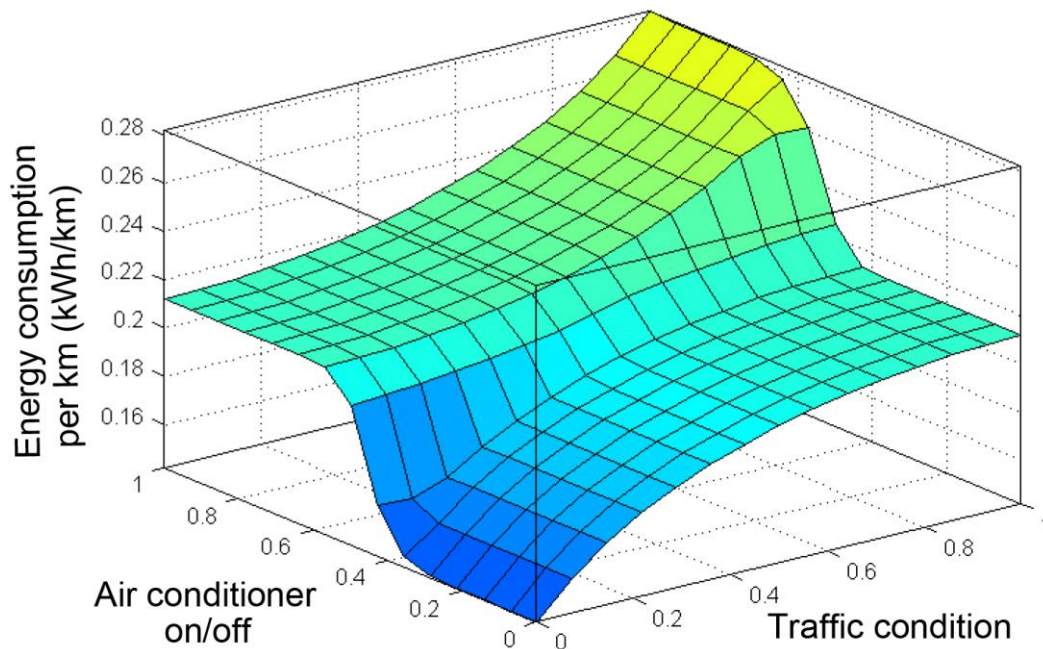


Fig. 5.3: The surface of energy consumption per km

5.5.2 Influence of Cell Balancing Strategies

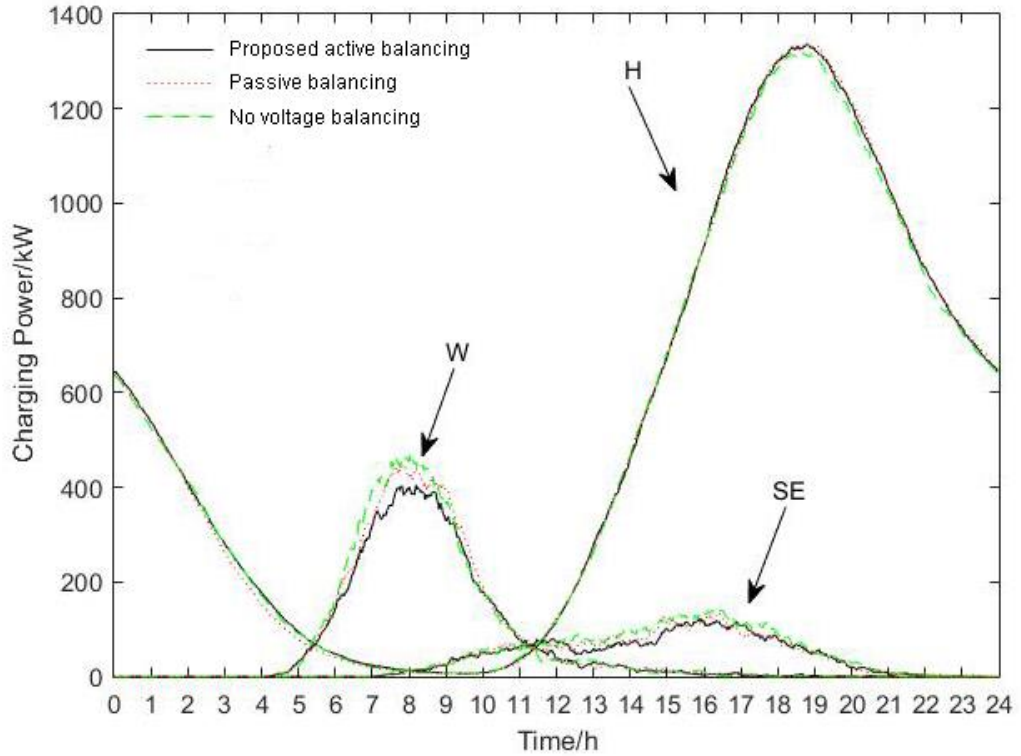


Fig. 5.4: Charging load distribution under different balancing strategies.

Chapters II, III and IV have proposed three novel active balancing circuits which effectively solved voltage balancing problems of the storage system in EV under alterable working conditions. Field experiments have demonstrated that passive balancing proposed in [67] will generate inevitable heat loss during balancing process and reduce the total usable battery capacity to 95%. Furthermore, no voltage balancing installed will largely impair the capacity of battery strings to as low as 90% for unbalanced new vehicle. Consider a case in summer weekdays, the charging load distribution at H, W, SE is compared under different voltage balancing strategies in Fig. 5.4, i.e., no voltage balancing, passive balancing and the active balancing proposed in this thesis. Assume these EV batteries are new with same State of Health (SoH) and fully charged when they leave H. When there is no balancing strategy, the usable capacity of battery strings is harshly constrained that many EVs just meet charging condition (5-7) and have

to choose charging at W or SE when they left H in a travel chain. Therefore, the charging load of no balancing case at W largely increases about 14.9% compared to the case with proposed active balancing. At the end of travel chain, charging load of no balancing at H is slightly reduced as more users have already got fully charged at public stations due to limitation of battery capacity. In other words, without balancing methods, EVs have higher probability to be forced to have extra charge than the case with proposed balancing method. Furthermore, referring to Fig. 5.9, a steep incline of charging power at W around 8 to 9 a.m. may incur larger voltage decline of the distribution power grid. Therefore, no voltage balancing and passive balancing with lower available battery capacity will block the normal usage of EVs while the novel balancing circuit proposed in this thesis is further demonstrated to be essential and applied to the following case studies.

5.5.3 Stochastic Model Results

In this case study, we consider four different scenarios, namely summer weekdays, summer weekends, winter weekdays and winter weekends. As shown in Table 5.2, these scenarios vary in ambient temperature, traffic condition, proportion of simple chains and proportion of work trips.

Table 5.2. Inputs under different scenarios

Scenario		Ambient temperature	Traffic condition	Proportion of simple chains	Proportion of work trips (%) [100]
Summer	Mon	Hot	Heavy	Medium	30.99
	Sun	Hot	Light	Medium	10.14
Winter	Mon	Cold	Heavy	More	30.99
	Sun	Cold	Light	More	10.14

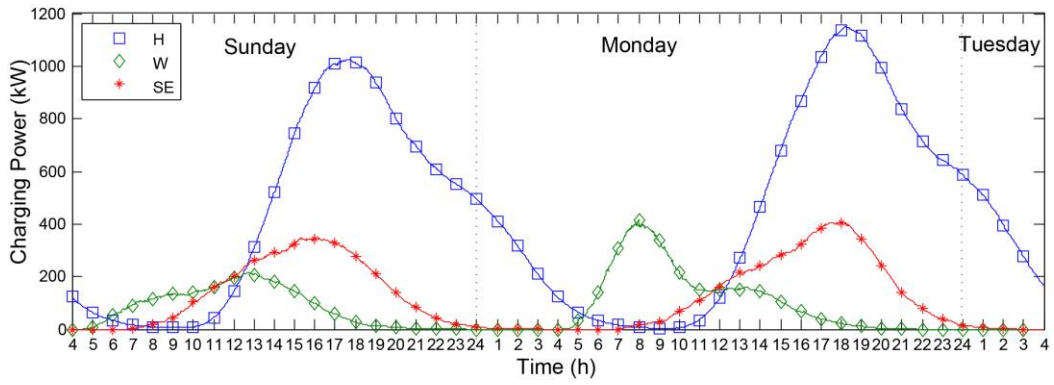


Fig. 5.5: Load demands in summer

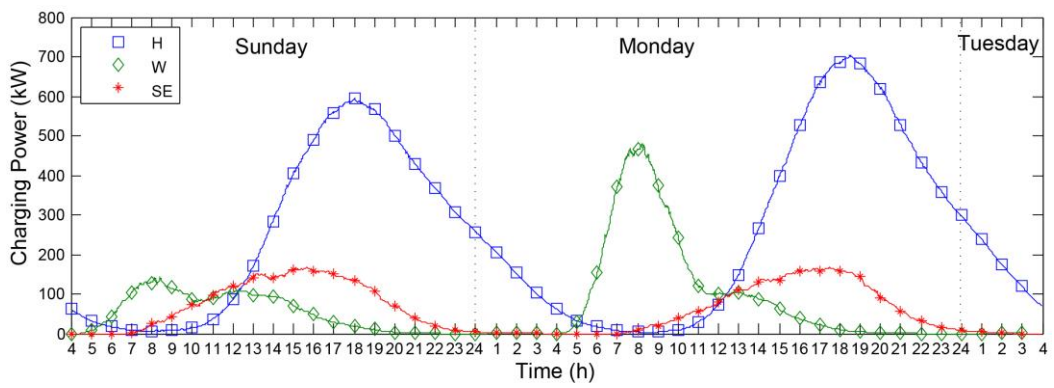


Fig. 5.6: Load demands in winter

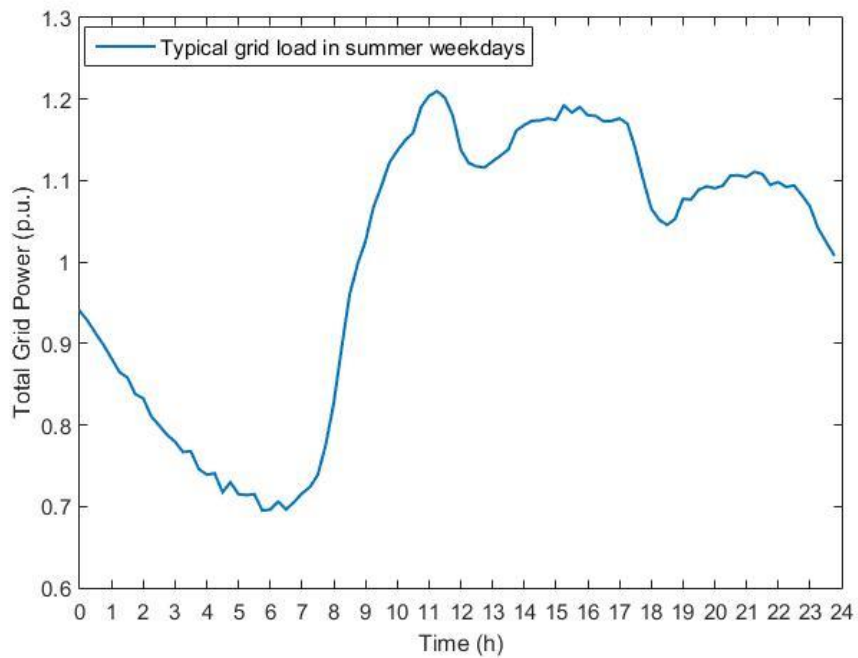


Fig.5.7: Typical total grid load in summer weekdays

The predicted daily load demand in different districts is obtained in Fig. 5.5 for summer weekdays and summer weekends while Fig. 5.6 shows demand for winter weekdays and winter weekends. Figures are plotted in consecutive Sunday, Monday and Tuesday for comparing peaks and impact of lasting charging on the next day. Their input difference lies in Table 5.3. As the properties of places SR and O are largely the same with SE, their results are not plotted for clarity.

Generally, both on-board AC and heater are turned on in typical summer and winter respectively, this influential factor is therefore not distinct. However, considering the cold weather in winter, the proportion of simple chain increases and the average daily travel distance decreases so that the total charging load in winter is much lower than that in summer [116]. Both the numbers of people going to work and people coming home after work decline in weekends, therefore the charging load demand in W is significantly lower in weekends. The peak load at W is postponed because office regulation is not that strict in weekends. Besides, due to light traffic condition in weekends, the charging demand in H is lower compared to that in weekdays with congestion.

The typical grid load of a distributed network (including charging load in Fig. 5.5) in summer weekdays is shown in Fig.5.7 [133] where there are three peak periods during 9:00-12:00, 14:00-16:00 and 19:00 -23:00 as well as one valley period during 1:00- 7:00. The peak period during evening hours coincides with the peak EV charging power depicted in Fig. 5.5. Therefore, it is more efficient to control the charging power in H for better grid optimization performance in (5-14).

5.5.4 Impact of EV Load on Power System

Fig. 5.8 presents a 33-node MV System derived from [117]. As the voltage of node 1 is assumed to be constant 1.05 p.u, the five charging places (H/W/O/SE/SR) with power factor of 0.95 are connected to five chosen nodes in

the system via 10kV/400V transformers. Different countries have laid different standards on voltage drop limit and 7% is chosen to be the maximum permissible voltage drop in this tested MV power system [118]. For security reasons, there are normally two 10kV/400V transformers with the same capacity of several hundred kilowatts at each node. The maximum allowable power load for EV charging is therefore set to be $C_{\max} = 1\text{MW}$ at every node [132]-[134]. The grid configuration is an example of an MV distribution network, so the results obtained are only valid for this case.

Table 5.3. Performance under different scenarios

Scenario/Penetration level		EV peak power (kW)	Max. voltage deviation (%)	Total line loss rate (%)		
Summer	Base load		0	4.75	5.263	
	Weekend	5%	261.9	5.68	5.561	
		10%	515.3	6.64	5.886	
		20%	1015.6	8.63	6.596	
	Weekday	5%	302.0	5.61	5.578	
		10%	578.0	6.52	5.910	
		20%	1142.0	8.18	6.624	
	Winter	Base load		0	2.91	3.927
		Weekend	5%	154.9	3.31	4.099
10%			293.5	3.68	4.258	
20%			591.8	4.47	4.613	
Weekday		5%	184.0	3.41	4.134	
		10%	354.4	3.86	4.335	
		20%	699.0	4.83	4.790	

As in many countries including China, heating is provided mainly by burning coal or natural gas in winter and, therefore, the base power load in summer is significantly higher because of the massive use of ACs. Considering the penetration levels of 5%, 10% and 20%, the maximum nodal voltage deviation, peak power and total line loss rate under different scenarios are calculated from optimization program and presented in Table 5.3 after applying the forecast power demands on the base load.

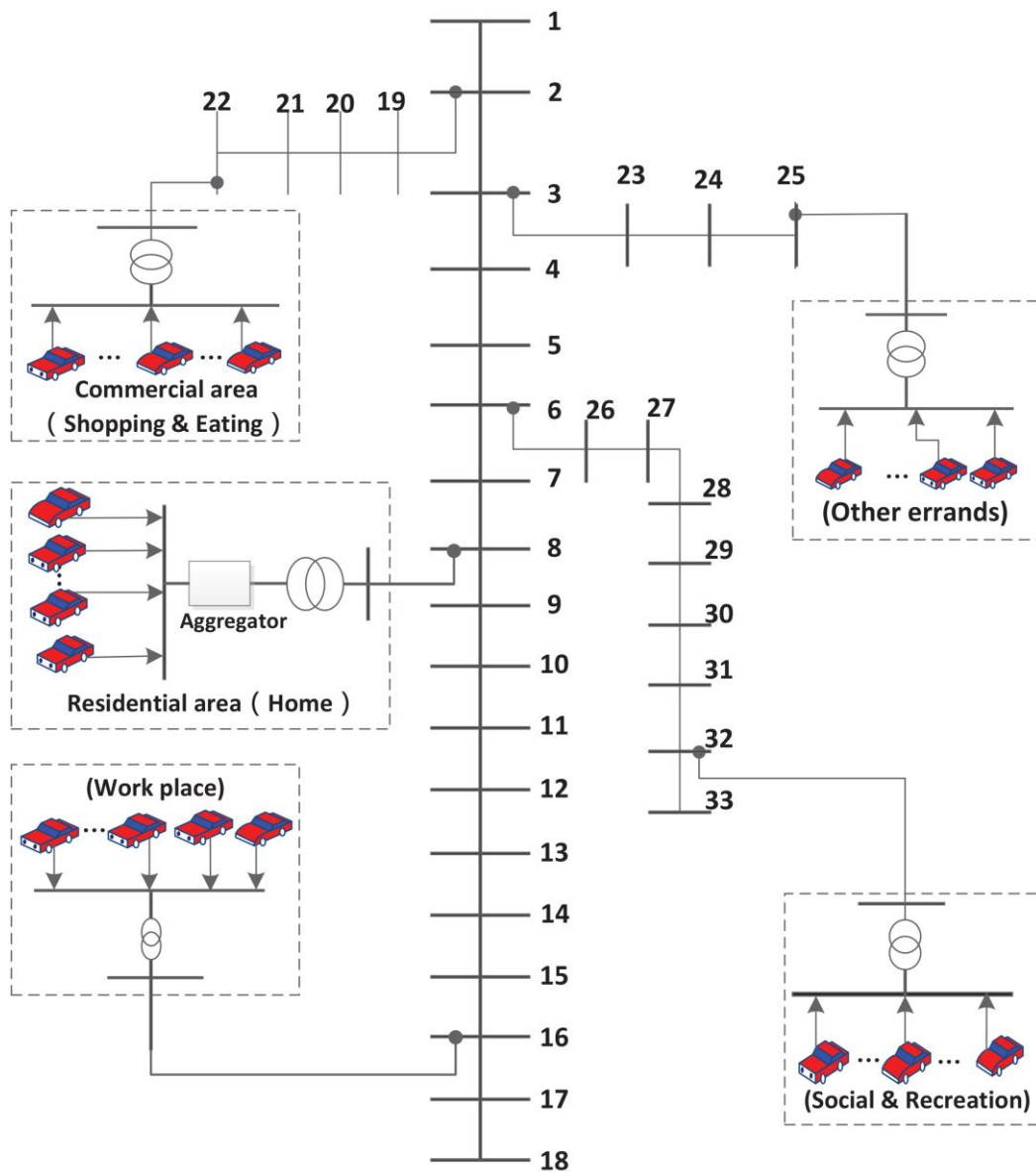


Fig. 5.8: 33-node power system topology

It is apparent that the system will become inefficient and insecure with augmentation of EV penetration. The total line loss rate increases significantly with the integration of EVs both in summer and winter. The scenario in summer weekdays with 20% penetration has the most severe impact on the regional network (EV charging power peaks at 1142 kW which exceeds the capacity of local transformer; maximum voltage deviation is calculated to be 8.18% which leads to unstable operation of regional grid). Except the period around 13:00 in summer weekends, the voltage deviation is enlarged for a short time because people may leisurely go to work late in weekends and overlap the peak of base load. For investigation of the most severe conditions during summer weekdays, voltage curves at the five nodes with charging facilities are given in Fig. 5.9. Because W is the farthest to the power supply node 1 and the heavy load H is along the line, it is shown that the voltage drop in W is the largest and severely violates the limits in the afternoon.

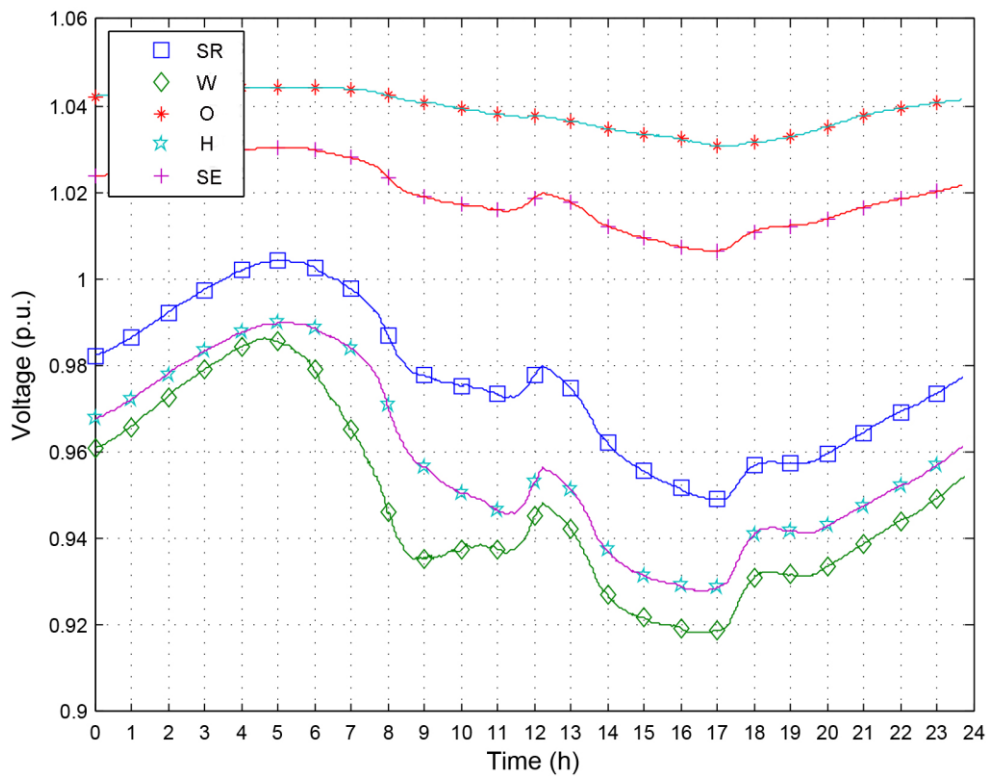


Fig. 5.9: Voltage variation in summer weekday

5.5.5 Effect of Aggregator Control

In order to investigate the improved performance of the proposed control schemes under the worst conditions, the data in summer weekdays is selected. As load demand in H is the highest shown in Fig. 5.4-5.6 and voltage in W is the lowest shown in Fig. 5.9, they both surpass the limit of grid and are checked with special attention in Fig. 5.10 and 5.11, respectively.

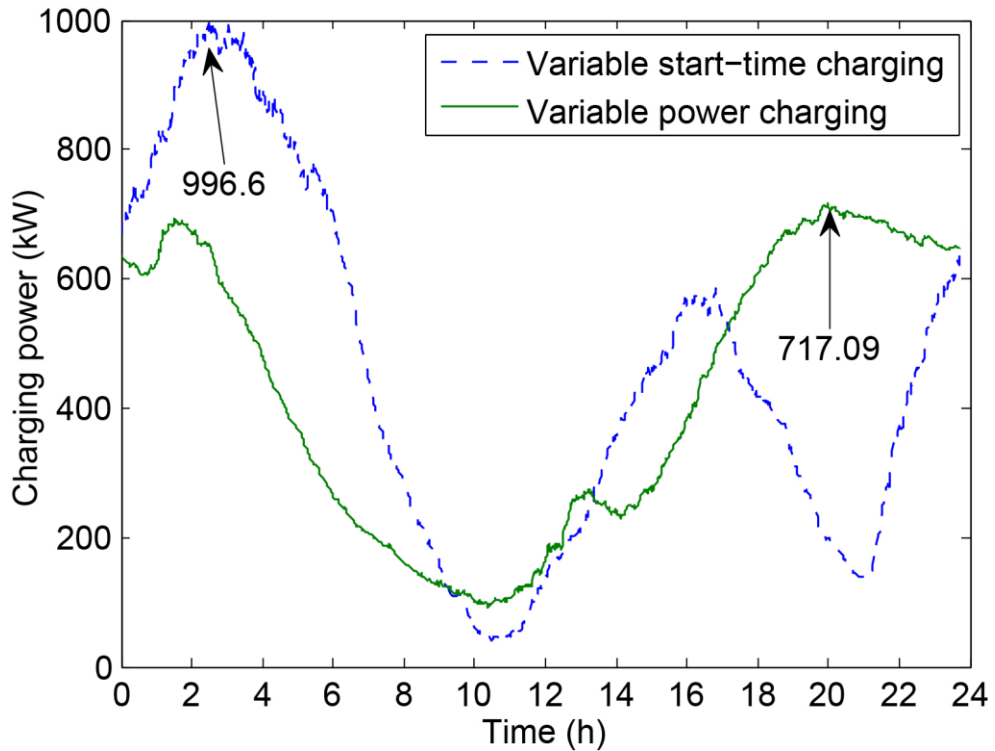


Fig. 5.10: Daily charging power in H with smart control

Considering GA efficiency and impact severity, α_1 and α_2 are selected to be 0.5 and 0.2 [105], respectively. By conducting the GA algorithm specified in Section 5.4.3, comparisons of the optimization performance for variable start-time charging and variable power charging are presented in Fig. 5.10 and Fig. 5.11 respectively.

As the control schemes are tested on the results of summer weekdays, Fig. 5.10 of the variable start-time charging is compared to curves of Mondays in Fig. 5.5. The peak load in H is decreased from 1142kW to 996.6kW (below the amount

constrained by local transformer capacity) and shifted to the time after midnight so there is a valley during 17:00 to 24:00 of variable start-time charging. If we consider total power of the grid (base power plus charging power), its daily curve successfully becomes more average. However, the largest voltage drops in W, manifested in Fig. 5.11, has been restored to be 0.9274 p.u. but still violates the limit. The fitness function finally converges to its local optimal condition, decreasing the total power loss rate from 6.624% in uncoordinated condition to now 6.382%. However, the weakness of this control scheme is also evident because shifting a peak may create another peak elsewhere and the regional network is still close to danger.

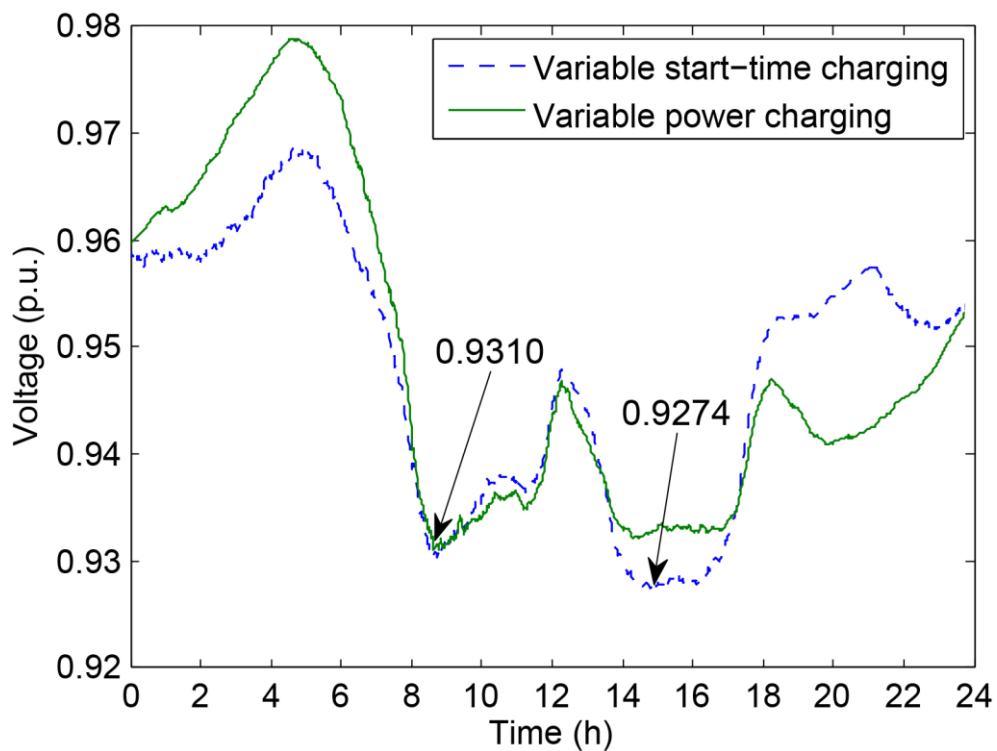


Fig. 5.11: Daily voltage variation in W with smart control

In the variable power charging, compared with the former scheme, the peak load in H is not shifted to small hours but the amount of peak is largely reduced to 717.09kW, far below the transformer capacity limit. Therefore, the daily voltage curve in W, depicted as blue dashed line in Fig. 5.11, is within the minimum

allowable limit. The optimization of daily charging power also manages to smooth the peak and valley periods of daily total power. The system line loss rate declines to 6.381% as a result, largely the same as the variable start-time charging. However, due to the prolonged charging duration, the load demand after midnight is increased and more charging services have to last till daytime than the former scheme. It can be interpreted that this variable power charging has better performance in system security but may impede the use of EVs in the morning.

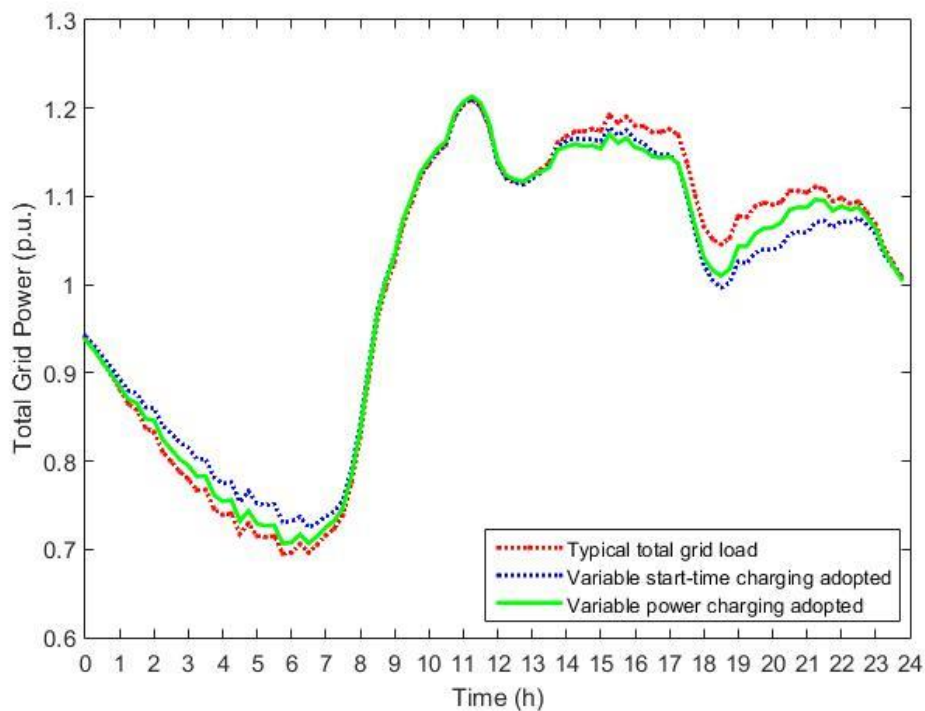


Fig. 5.12: Total grid power with smart control methods adopted

Assume the EV charging power takes up about 5% of the total power in distribution grid in the future, the charging power profiles under variable start-time charging and variable power charging methods in Fig. 5.10 are added to the total grid power in Fig. 5.7 to show the optimization performance of daily distribution power load in Fig. 5.12. It is evident that the two methods both successfully shift the peak charging power during afternoon and evening hours to valley hours

(1:00-7:00). Besides, in the afternoon, the total grid power after adopting variable power charging is the lowest, recovering the nodal voltage back within limit.

5.6 Conclusion

In this chapter, a more practical stochastic forecasting model has been proposed with inputs of historical regional travel survey and the relevant external conditions. The interrelationship among multiple trips is linked via the Markov chain. The overall impact of several geographically different charging stations is tested on MV power system and the optimization methods aiming at mitigating the influence are provided. NHTS data has been used to draw detailed temporal and spatial information of EVs' daily travel route for a case study.

On one hand a comparison for cases under different cell balancing strategies is conducted to show its great influence on the available cell capacity as well as the charging demand. It is calculated that, with no cell balancing adopted, the charging load at W largely increases about 14.9% compared to the case with proposed active balancing. On the other hand, with selection of appropriate charging control scheme, the peak load in H can be decreased from 1142kW to 717.09kW while system line loss rate from 6.624% to now 6.381%. The variable power charging is superior because variable start-time charging shifts one peak may create another peak elsewhere and the regional network is still close to danger. The proposed smart control method is demonstrated to be reliable and can be used for future charging load forecast and smart charging control with geographical and temporal considerations.

Chapter VI

Conclusions and Future Work

6.1 Conclusions

The contemporary environmental deterioration impels most of countries across the world to implement greener policies and research incentives for integration of new energy sources with energy storage systems. The intermittence and stochastic nature of new energy sources call for high standards of cell balancing and distributed power control methods. Hybrid energy sources can be combined to provide better power performance but the balancing between different types of cells becomes complicated; EVs can be regarded as mobile and distributed new energy sources and storage systems which will largely improve capability of load optimization in smart city. Therefore, investigating accurate, fast-responding and energy-saving cell balancing circuits and control methods for EV charging become the central themes of this thesis.

In Chapter II, an innovative and efficient switched-capacitor balancing circuit is proposed in this chapter to achieve cell voltage balancing for a package of hybrid energy sources. The key feature is that the balancing is not just restricted to equal cell voltage but is extended to different cell combinations that will be beneficial for non-sorted cell packages, like different types of battery cells and SCs. The mathematical derivation, software simulation and laboratory experiment have been conducted to verify the feasibility of this model. This proposed voltage equalizer is especially useful with the increasing establishment of hybrid systems which take advantages of different types of energy sources or energy storage devices.

The introduction of second-life batteries from retired electric vehicles enforces the demand of more accurate balancing systems for hybrid cells, as well as the

requirement that balancing should be extended to any preset ratio rather than 1:1. Having advantages in step-free adjustment, Chapter III proposes a novel tapped-inductor balancing circuit that allows any ratio of voltage balancing for hybrid energy storage cells that allows the coupling of the cell voltage and energy to another cell in any ratios. The analysis of the circuit, simulation and experiment results are presented to demonstrate its effectiveness in handling hybrid source balancing. It can be found that the scenario of successful balancing is extended to any voltage ratio and the ripple of currents during balancing process is small enough.

A novel zero-current switching cell balancing circuit is proposed in Chapter IV to decrease switching loss during balancing process. Furthermore, in order to adjust to different requirements of EV operation states, the multi-functional circuit is able to easily change between buck-boost and switched-capacitor pattern with flexible switching frequency and duty ratios. Simulation and experiment are conducted to demonstrate its loss reduction effect and flexibility in various situations.

Together with cell balancing, stochastic user behavior is another obstacle to efficient integration of new energy sources. In Chapter V, a more practical stochastic forecasting model of EV charging has been proposed with inputs of historical regional travel survey and the relevant external conditions. A comparison for cases under different cell balancing strategies is conducted to demonstrate that, with no cell balancing adopted, the charging load at W largely increases about 14.9% compared to the case with proposed active balancing. With selection of appropriate charging control scheme, the peak load in H can be decreased while system line loss rate is largely reduced. The methods proposed are verified to be reliable and can be used for future charging load forecast and smart charging control with geographical and temporal considerations.

The thesis has conducted a series of researches in EVs with focus on the cell balancing techniques in energy storage as well as the improved forecast and con-

trol for EV charging demand. It is demonstrated that the novel cell balancing techniques greatly promote the compatibility of hybrid cells and balancing accuracy, and reduce switching loss. The adoption of both cell balancing and smart charging control successfully saves power system loss while maintaining grid stability and customer satisfaction.

6.2 Future Work

This thesis has put forward effective cell balancing circuits for hybrid source packages and pricing control strategies with practical EV charging forecast. To extend application of the methods proposed in this thesis, following research directions may be worthy of further studying in the future:

6.2.1 Energy management for Battery/SC Hybrid Vehicle

As it is introduced in Chapter II and III, battery has much lower specific energy with high specific power. Together with the limitation of the electric motor which tender high power at low speed and lower high at higher speed so that the driving comfort of current EVs is superior to that of ICE vehicles, especially when start up. However, this feature should be deteriorated by battery as its instant power is limited. Hybridizing battery EVs with onboard SCs can be one of the promising solutions as SCs can provide high bursts of power even when EV battery capabilities have decreased, maintaining the accelerative performance. SCs can also sustain high peak currents and benefit from regenerative braking.

An effective energy management system is essential to the commercialization of battery/SC hybrid vehicle. On one hand, the management system shall ensure voltage equilibrium among hybrid cells at any energy transformation process. On the other hand, having obtained the detailed drive speed forecast and altitude of city layout, the capacity combination of batteries and SCs should be customized for optimal efficiency of the EV battery/supercapacitor hybrid system.

6.2.2 Promoting the Application of Zero-Current Switching

As it is illustrated in Chapter IV, the technique of zero-current switching has not been applied in large scale. My future work may lie in two directions: 1) Optimize the topology and reduce the cost of building ZCS circuit. 2) Modularize ZCS circuit and promote its integration to more balancing circuits, tapped-inductor circuits for example. 3) Popularize its application in more industrial products, such as EVs, various storage systems for wind, photovoltaic power stations and so on.

References

- [1] Hughes T P, Kerry J T and ÁlvarezNoriega M, “Global warming and recurrent mass bleaching of corals”, *Nature*, vol. 543, pp.373-377, 2017.
- [2] Lojowska A, Kurowicka D, Papaefthymiou G, “Stochastic Modeling of Power Demand Due to EVs Using Copula”, *IEEE Trans. on Power Syst.*, vol. 27, no. 4, pp.1960-1968, 2012.
- [3] Clement-Nyns K, Haesen E, Driesen J. “The Impact of Charging Plug-In Hybrid Electric Vehicles on a Residential Distribution Grid”, *IEEE Trans. on Power Syst.*, vol. 25, no. 1, pp.371-380, 2010.
- [4] Martinez C M, Hu X, Cao D, “Energy Management in Plug-in Hybrid Electric Vehicles: Recent Progress and a Connected Vehicles Perspective” *IEEE Trans. on Veh. Technol.* vol. 66, no. 6, pp. 4534-4549, 2017.
- [5] Tavakoli, A., Khajehoddin, S. A., & Salmon, J. “Control and analysis of a modular battery voltage balancing cell.” *IEEE Trans. on Power Electron.*, vol.pp, no.99, 2018.
- [6] Feng Ju, Weiwen Deng and Jingshan Li, “Performance Evaluation of Modularized Global Equalization System for Lithium-Ion Battery Packs” *IEEE Trans. Automat. Sci. Eng.*, vol. 13, no. 2, April 2016.
- [7] Li Xinghua, Zhang Mingkun, “Research on high-precision survey of super-capacitor ESR” *International Conference on Electronics, Communications and Control (ICECC)*, pp. 1627 – 1630, 2011.
- [8] Abhijit Choudhury, Pragasen Pillay, Sheldon S. Williamson, “Comparative Analysis Between Two-Level and Three-Level DC/AC Electric Vehicle Traction Inverters Using a Novel DC-Link Voltage Balancing Algorithm, ” *IEEE J. of Emerg. Sel. Topics Power Electron.*, vol. 2, no. 3, pp. 529 – 540, 2014.

- [9] Seima Shili, Alaa Hijazi, Ali Sari, Xuefang Lin-Shi and Pascal Venet, “Balancing circuit new control for supercapacitor storage system lifetime maximization”, *IEEE Trans. on Power Electron.*, vol. 32, no. 6, pp.4939-4948, 2017.
- [10] González A, Goikolea E, Barrena J A, “Review on supercapacitors: Technologies and materials”, *Renew. & Sust. Energy Rev.*, vol. 58, pp. 1189-1206, 2016.
- [11] Schwieters T, Evertz M, Mense M, “Lithium loss in the solid electrolyte interphase: Lithium quantification of aged lithium ion battery graphite electrodes by means of laser ablation inductively coupled plasma mass spectrometry and inductively coupled plasma optical emission spectroscopy”, *J. of Power Sources*, vol. 356, pp.47-55, 2017.
- [12] Behrouzian E, Bongiorno M, Teodorescu R. “Impact of Switching Harmonics on Capacitor Cells Balancing in Phase-Shifted PWM Based Cascaded H-Bridge STATCOM”, *IEEE Tran. on Power Electron.*, vol. pp, no. 99, pp.1-1, 2016.
- [13] Ephrem Chemali, Matthias Preindl, Pawel Malysz, Ali Emadi, “Electrochemical and Electrostatic Energy Storage and Management Systems for Electric Drive Vehicles: State-of-the-Art Review and Future Trends”. *IEEE J. of Emerg. Sel. Topics Power Electron.*, vol. 4, no. 3, pp. 1117 – 1134, 2016.
- [14] Christopher Schaef, Jason T. Stauth, “A Highly-Integrated Series-Parallel Switched-Capacitor Converter with 12-Volt-Input and Quasi-Resonant Voltage-Mode Regulation”, *IEEE J. of Emerg. Sel. Topics Power Electron.*, vol. 1, no. 1, pp. 99, 2017.
- [15] J. G.-Lozano, E. R. Cadaval, “Battery equalization active methods”, *J. Power Sources*, vol. 246, pp. 934–949, 2014.
- [16] Xiong H, Fu Y, Dong K., “A Novel Point-to-Point Energy Transmission Voltage Equalizer for Series-Connected Supercapacitors”, *IEEE Transac-*

- tions on Veh. Technol.*, vol. 65, no.6, pp.4669-4675, 2016.
- [17] Shang Y, Xia B, Lu F, “ A Switched-Coupling-Capacitor Equalizer for Series-Connected Battery Strings”, *IEEE Trans. on Power Electron.*, vol. 32, no. 99, pp.1-1, 2017.
- [18] Shang Y, Xia B, Zhang C, “An Automatic Equalizer Based on Forward-Flyback Converter for Series-Connected Battery Strings”, *IEEE Trans. on Ind. Electron.*, vol. PP, no.99, pp.1-1, 2017.
- [19] Uno M, Kukita A., “PWM Converter Integrating Switched Capacitor Converter and Series-Resonant Voltage Multiplier as Equalizers for Photovoltaic Modules and Series-Connected Energy Storage Cells for Exploration Rovers”, *IEEE Trans. on Power Electron.*, vol. PP, no.99, pp.1-1, 2016.
- [20] Oyarbide E, Bernal C, Molina P, “Voltage equalization of an ultracapacitor module by cell grouping using number partitioning algorithm”, *J. of Power Sources*, vol. 301, pp. 113-121, 2016.
- [21] A. Xu, S. Xie, and X. Liu, “Dynamic voltage equalization for series connected ultracapacitors in EV/HEV applications,” *IEEE Trans. Veh. Technol.*, vol. 58, no. 8, pp. 3981-3987, Oct. 2009.
- [22] D. V. Cadar, D. M. Petreus, and T. M. Patarau, “An energy converter method for battery cell balancing,” in *Proc. 33rd Int. Spring Semin. Electron. Technol.*, pp. 290–293, May 2010.
- [23] M. Uno and K. Tanaka, “Single-switch multioutput charger using voltage multiplier for series-connected lithium-ion battery/supercapacitor equalization,” *IEEE Trans. Ind. Electron.*, vol. 60, no. 8, pp. 3227–3239, Aug. 2013.
- [24] F. Baronti, G. Fantechi, R. Roncella, and R. Saletti, “High-efficiency digitally controlled charge equalizer for series-connected cells based on switching converter and super-capacitor,” *IEEE Trans. Ind. Informat.*, vol. 9, no. 2, pp. 1139-1147, May 2013.
- [25] C. S. Moo, Y. C. Hsieh, and I. S. Tsai, “Charge equalization for series-connected batteries,” *IEEE Trans. Aerosp. Electron. Syst.*, vol. 39, no. 2, pp.

704–710, Apr. 2003.

- [26] Yuang-Shung Lee, Ming-Wang Cheng, “Intelligent Control Battery Equalization for Series Connected Lithium-Ion Battery Strings” *IEEE Trans. on Ind. Electron.*, vol. 52, no. 5, pp.1297 – 1307, 2015.
- [27] Y. Ye, K. W. E. Cheng, J. Liu and K. Ding, “A Step-Up Switched-Capacitor Multilevel Inverter With Self-Voltage Balancing,” *IEEE Trans. Ind. Electron.*, vol. 61, no. 12, pp. 6672-6680, 2014.
- [28] R. Barzegarkhoo, H. M. Kojabadi, E. Zamiry, N. Vosoughi and L. Chang, “Generalized Structure for a Single Phase Switched-Capacitor Multilevel Inverter Using a New Multiple DC Link Producer With Reduced Number of Switches,” *IEEE Trans. Power Electron.*, vol. 31, no. 8, pp. 5604-5617, Aug. 2016.
- [29] A. C. Baughman and M. Ferdowsi, “Double-tiered switched-capacitor battery charge equalization technique,” *IEEE Trans. Ind. Electron.*, vol. 55, no. 6, pp. 2277–2285, Jun. 2008.
- [30] Y. Yuanmao, K. W. E. Cheng, and Y. P. B. Yeung, “Zero-current switching switched-capacitor zero-voltage-gap automatic equalization system for series battery string,” *IEEE Trans. Power Electron.*, vol. 27, no. 7, pp. 3234–3242, Jul. 2012.
- [31] Moon-Young Kim, Chol-Ho Kim, Jun-Ho Kim, Gun-Woo Moon, “A Chain Structure of Switched Capacitor for Improved Cell Balancing Speed of Lithium-Ion Batteries,” *IEEE Trans. Power Electron.*, vol. 61, no. 8, pp. 3989 - 3999, 2014.
- [32] Cheng, K.W.E.; Divakar, B.P.; Wu, H.; Ding, K.; Ho, H.F., “Battery-Management System (BMS) and SOC Development for Electrical Vehicles,” *IEEE Trans. Veh. Technol.*, vol. 60, pp.76–88, 2011.
- [33] Peng, X.; He, X.; Han, P.; Guo, A.; Shu, Z.; Gao, S. “Smooth switching technique for voltage balance management based on three-level neutral point clamped cascaded rectifier,” *Energies*, vol. 9, no.803, 2016.

- [34] Park, S.H.; Park, K.B.; Kim, S.H.; Moon, G.W.; Youn, M.J. “Single-Magnetic Cell-to-Cell Charge Equalization Converter With Reduced Number of Transformer Windings,” *IEEE Trans. Power Electron.*, vol. 27, pp. 2900–2911, 2012.
- [35] Gao, Z.C.; Chin, C.S.; Toh, W.D.; Chiew, J.; Jia, J. “State-of-Charge Estimation and Active Cell Pack Balancing Design of Lithium Battery Power System for Smart Electric Vehicle,” *J. Adv. Transp.* 2017.
- [36] Daowd, M.; Antoine, M.; Omar, N.; Bossche, P.V.D.; Mierlo, J.V. Single “Switched capacitor battery balancing system enhancements,” *Energies*, vol. 6, pp. 2149–2174, 2013.
- [37] Law, K.K.; Cheng, K.W.E. “Examination of the frequency modulation and lifting techniques for the generalized power factor correction switched-capacitor resonant converter,” *Int. J. Circuit Theory Appl.*, vol. 7, pp. 839–855, 2008.
- [38] Ye, Y.; Cheng, K.W.E.; Fong, Y.C. “Topology, Modeling, and Design of Switched-Capacitor-Based Cell Balancing Systems and Their Balancing Exploration,” *IEEE Trans. Power Electron.*, vol. 32, pp. 4444–4454, 2017.
- [39] Feng, F.; Lu, R.; Zhu, C. “Equalisation strategy for serially connected LiFePO₄ battery cells,” *IET Electr. Syst. Transp.*, vol. 6, pp.246–252, 2016.
- [40] Lambert, S.M.; Pickert, V.; Atkinson, D.J.; Zhan, H. “Transformer-Based Equalization Circuit Applied to n-Number of High Capacitance Cells,” *IEEE Trans. Power Electron.*, vol. 31, pp. 1334–1343, 2016.
- [41] Chen, Y.; Liu, X.; Cui, Y.; Zou, J.; Yang, S. A , “MultiWinding Transformer Cell-to-Cell Active Equalization Method for Lithium-Ion Batteries With Reduced Number of Driving Circuits,” *IEEE Trans. Power Electron.*, vol. 31, pp. 4916–4929, 2016.
- [42] Liu, M.; Fu, M.; Wang, Y.; Ma, C. , “Battery Cell Equalization via Megahertz Multiple-Receiver Wireless Power Transfer,” *IEEE Trans. Power Electron.*, vol 33, pp. 4135–4144, 2018.

- [43] Cheng, K.W.E., "Review of battery management systems for electric vehicles. In Energy Systems for Electric and Hybrid Vehicles," *IET*: London, UK, 2016.
- [44] Xiong, R.; He, H.; Sun, F.; Zhao, K., "Online estimation of peak power capability of Li-ion batteries in electric vehicles by a hardware-in-loop approach," *Energies*, vol. 5, pp.1455–1469, 2012.
- [45] Monem, M.A.; Hegazy, O.; Omar, N.; Trad, K.; Breucker, S.D.; Bossche, "P.V.D. Design and analysis of generic energy management strategy for controlling second-life battery systems in stationary applications," *Energies*, vol. 9, no.889, 2016.
- [46] Mukherjee, N.; Strickland, D. , "Control of Second-Life Hybrid Battery Energy Storage System Based on Modular Boost-Multilevel Buck Converter," *IEEE Trans. Ind. Electron.*, vol.62, pp.1034–1046, 2015.
- [47] Mukherjee, N.; Strickland, D. , "Analysis and Comparative Study of Different Converter Modes in Modular Second-Life Hybrid Battery Energy Storage Systems," *IEEE J. Emerg. Sel. Top. Power Electron.*, vol.4, pp.547–563, 2016.
- [48] Chan, H.L.; Cheng, K.W.E.; Sutanto, D. , "Bidirectional phase-shifted DC-DC converter," *IEE Electron. Lett.*, vol. 35, pp.523–524, 1999.
- [49] Cheng, K.W.E.; Evans, P.D. , "Parallel-mode extended-period quasiresonant convertor," *IEE Proc. B*, vol.138, pp.243–251, 1991.
- [50] Shi, Z.H.; Cheng, K.W.E.; Ho, S.L. , "Static performance and parasitic analysis of tapped-inductor converters," *IET Power Electron.*, vol.7, pp.366–375, 2014.
- [51] Li, S.; Cheng, K.W.E.; Ye, Y.; Shi, Z. , "Wide input and wide output topology analysis for tapped-inductor converters with consideration of parasitic elements," *IET Power Electron.*, vol. 9, pp. 1952–1961, 2016.
- [52] Grant, D.A.; Darroman, Y. , "Watkins-Johnson converter completes tapped inductor converter matrix," *Electron. Lett.*, vol. 39, pp. 271–272, 2003.

- [53] Yuanmao Ye, Ka Wai E. Cheng, “Modeling and Analysis of Series–Parallel Switched-Capacitor Voltage Equalizer for Battery/Supercapacitor Strings,” *IEEE J. of Emerg. Sel. Topics Power Electron.*, vol. 3, no. 4, pp. 977 – 983, 2015.
- [54] K. Wang, Y. Li, Z. Zheng, and L. Xu, “Voltage balancing and fluctuation suppression methods of floating capacitors in a new modular multilevel converter,” *IEEE Trans. Ind. Electron.*, vol. 60, no. 5, pp. 1943–1954, May 2013.
- [55] P. N. Tekwani, R. S. Kanchan, K. Gopakumar, “A Dual Five-Level Inverter-Fed Induction Motor Drive With Common-Mode Voltage Elimination and DC-Link Capacitor Voltage Balancing Using Only the Switching-State Redundancy—Part II,” *IEEE Trans. Ind. Electron.*, vol. 54, no. 5, pp. 2609 - 2617, 2007.
- [56] Mahmoud Shousha; Timothy McRae; Aleksandar Prodić; Victor Marten; John Milios, “Design and Implementation of High Power Density Assisting Step-Up Converter With Integrated Battery Balancing Feature” *IEEE J. of Emerg. Sel. Topics Power Electron.*, vol. 5, no. 3, pp.1068 - 1077, 2017.
- [57] Y.Beck; S.Singer; L.M.-Salamero, “Modular Realization of Capacitive Converters Based on General Transposed Series–Parallel and Derived Topologies,” *IEEE Trans.Ind. Elect*, vol. 61, no.3, 2014.
- [58] Y. C. Fong; Yuanmao Ye; S. Raghu Raman; K. W. E. Cheng, “A hybrid multilevel inverter employing series-parallel switched-capacitor unit,” *IEEE Applied Power Electronics Conference and Exposition (APEC)*, 2017.
- [59] L. Zubieta, and R. Boner, “Characterization of double-layer capacitors for power electronics applications,” *IEEE Trans. on Industry Applications*, vol. 36, no. 1, pp. 199-205, Feb. 2000.
- [60] Z. Cerovsky; P. Mindl, “Regenerative braking by electric hybrid vehicles using super capacitor and power splitting generator” *European Conference on Power Electronics and Applications*, 2005

- [61] Pahlevani M, Eren S, Guerrero J M, “A Hybrid Estimator for Active/Reactive Power Control of Single-Phase Distributed Generation Systems with Energy Storage,” *IEEE Trans. on Power Electron.*, vol. 31, no. 4, pp. 2919-2936, 2015.
- [62] Hu Y, Cheng H, Tao S. , “Retired Electric Vehicle (EV) Batteries: Integrated Waste Management and Research Needs,” *Environ. Sci. & Technol.*, vol. 51, no.19, 2017.
- [63] Hu X, Murgovski N, Johannesson L, “Energy efficiency analysis of a series plug-in hybrid electric bus with different energy management strategies and battery sizes,” *Appl. Energ.*, vol. 111, no. 4, pp. 1001-1009, 2013.
- [64] Dufo-López R, Lujano-Rojas J M, Bernal-Agustín J L., “Comparison of different lead–acid battery lifetime prediction models for use in simulation of stand-alone photovoltaic systems,” *Appl. Energ.*, vol. 115, no.4, pp.242-253, 2014.
- [65] Deng Y, Li J, Shin K H, “Improved Modulation Scheme for Loss Balancing of Three-Level Active NPC Converters,” *IEEE Trans. on Power Electron.*, vol. 32, no. 4, pp. 2521-2532, 2017.
- [66] Jiao Y, Lee F C, Lu S., “Space Vector Modulation for Three-Level NPC Converter With Neutral Point Voltage Balance and Switching Loss Reduction,” *IEEE Trans. on Power Electron.*, vol. 29, no.10, pp.5579-5591, 2014.
- [67] J. Cao, N. Schofield, and A. Emadi, “Battery balancing methods: A comprehensive review,” in Proc. *IEEE Veh. Power Propulsion Conf.*, Harbin, China, Sep. 3–5, pp. 1–6, 2008.
- [68] Yunlong Shang, Chenghui Zhang, Naxin Cui and Josep M. Guerrero “A Cell-to-Cell Battery Equalizer With Zero-Current Switching and Zero-Voltage Gap Based on Quasi-Resonant LC Converter and Boost Converter” *IEEE Trans. on Power Electron.*, vol. 30, no. 7, pp 3731-3747, July 2015.
- [69] Yuang-Shung Lee, Ming-Wang Cheng, “Intelligent Control Battery Equal-

- zation for Series Connected Lithium-Ion Battery Strings,” *IEEE Trans. on Ind. Electron.*, vol. 52, no. 5, pp.1297 – 1307, 2015.
- [70] Y. Ye, K. W. E. Cheng, J. Liu and K. Ding, “A Step-Up Switched-Capacitor Multilevel Inverter With Self-Voltage Balancing,” *IEEE Trans. Ind. Electron.*, vol. 61, no. 12, pp. 6672-6680, 2014.
- [71] R. Barzegarkhoo, H. M. Kojabadi, E. Zamiry, N. Vosoughi and L. Chang, “Generalized Structure for a Single Phase Switched-Capacitor Multilevel Inverter Using a New Multiple DC Link Producer With Reduced Number of Switches,” *IEEE Trans. Power Electron.*, vol. 31, no. 8, pp. 5604-5617, Aug. 2016.
- [72] A. C. Baughman and M. Ferdowsi, “Double-tiered switched-capacitor battery charge equalization technique,” *IEEE Trans. Ind. Electron.*, vol. 55, no. 6, pp. 2277–2285, Jun. 2008.
- [73] Moon-Young Kim, Chol-Ho Kim, Jun-Ho Kim, Gun-Woo Moon, “A Chain Structure of Switched Capacitor for Improved Cell Balancing Speed of Lithium-Ion Batteries,” *IEEE Trans. Power Electron.*, vol. 61, no. 8, pp. 3989 - 3999, 2014.
- [74] C. Pascual and P.T. Krein, “Switched capacitor system for automatic series battery equalization,” in *Proc. Appl. Power Electron. Conf. Expo.*, pp. 848–854, Feb. 1997.
- [75] A. C. Baughman and M. Ferdowsi, “Double-tiered switched-capacitor battery charge equalization technique,” *IEEE Trans. Ind. Electron.*, vol. 55, no. 6, pp. 2277–2285, Jun. 2008.
- [76] M.-Y. Kim, C.-H. Kim, J.-H. Kim, and G.-W. Moon, “A chain structure of switched capacitor for improve cell balancing speed of lithium-ion batteries,” *IEEE Trans. Ind. Electron.*, vol. 61, no. 8, pp. 3989–3999, Aug. 2014.
- [77] Masoud Jabbar and Uosef Dadkhah Tehrani, “Double-boost switched-resonator converter,” *IET Power Electron.*, vol. 11, no. 8, pp. 1382 – 1388, 2018.

- [78] K.W.E.Cheng and P.D.Evans, "Parallel-mode extended-period quasi-resonant convertor," *IEE Proceedings-B*, vol. 138, no. 5, pp. 243-251, September 1991.
- [79] Bor-Ren Lin, Jeng-Yu Chen, "Interleaved resonant converter with the balanced flying capacitors," *IET Power Electron.*, vol. 8, no. 3, pp. 447-457, 2015.
- [80] Oswald N, Anthony P, Mcneill N, "An Experimental Investigation of the Tradeoff between Switching Losses and EMI Generation With Hard-Switched All-Si, Si-SiC, and All-SiC Device Combinations," *IEEE Trans. on Power Electron.*, vol. 29, no. 5, pp.2393-2407, 2014.
- [81] Fujii K, Koellensperger P, Doncker R W D. , "Characterization and Comparison of High Blocking Voltage IGBTs and IEGTs Under Hard- and Soft-Switching Conditions," *IEEE Trans. on Power Electron.*, vol. 23, no. 1, pp. 172-179, 2008.
- [82] Ahmed M R, Todd R, Forsyth A J., "Predicting SiC MOSFET Behaviour Under Hard-Switching, Soft-Switching and False Turn-On Conditions," *IEEE Trans. on Ind. Electron.*, 2017, PP(99):1-1.
- [83] Thounthong P, Raël S, Davat B., "Energy management of fuel cell/battery/supercapacitor hybrid power source for vehicle applications," *J. of Power Sources*, vol. 193, no.1, pp. 376-385, 2009.
- [84] Jiang Z, Gao L, Dougal R A. , "Adaptive Control Strategy for Active Power Sharing in Hybrid Fuel Cell/Battery Power Sources," *IEEE Trans. on Energy Convers.*, vol. 22, no. 2, pp. 507-515, 2007.
- [85] Thounthong P, Raël S, Davat B., "Energy management of fuel cell/battery/supercapacitor hybrid power source for vehicle applications," *J. of Power Sources*, vol. 193, no.1, pp. 376-385, 2009.
- [86] Mukherjee S, Giri S K, Kundu S, "A modified PWM scheme for three-level inverters with neutral point voltage balancing for EV applications," *IEEE Transportation Electrification Conference*, pp. 1-6, 2017.

- [87] Evzelman M, Rehman M M U, Hathaway K, “ Active Balancing System for Electric Vehicles with Incorporated Low-Voltage Bus,” *IEEE Trans. on Power Electron.*, vol. 31, no. 11, pp.7887-7895, 2016.
- [88] Sánchez-Martín P, Lumbreras S, Alberdi-Alén A. , “Stochastic Programming Applied to EV Charging Points for Energy and Reserve Service Markets,” *IEEE Trans. on Power Syst.*, vol. 31, no. 1, pp. 198-205 2015.
- [89] Yang T, Xu X, Guo Q, “EV charging behaviour analysis and modelling based on mobile crowdsensing data,” *IET Gener. Transm. & Dis.*, vol. 11, no. 7, pp.1683-1691, 2017.
- [90] Arias M B, Kim M, Bae S. , “Prediction of electric vehicle charging-power demand in realistic urban traffic networks,” *Applied Energy*, vol. 195, pp. 738-753. , 2017
- [91] H. Huang, C. Y. Chung and K. W. Chan, “Quasi-Monte Carlo based probabilistic small signal stability analysis for power systems with plug-in electric vehicle and wind power integration,” *IEEE Trans. Power Syst.*, vol. 28, no. 3, pp. 3335-3343, Aug. 2013.
- [92] K. Qian, C. Zhou, and M. Allan, “Modeling of load demand due to EV battery charging in distribution systems, ” *IEEE Trans. Power Syst.*, vol. 26, no. 2, pp. 802-810, May 2011.
- [93] P. Zhang, K. Qian, and C. Zhou, “A methodology for optimization of power systems demand due to electric vehicle charging load, ” *IEEE Trans. Power Syst.*, vol. 27, no. 3, pp. 1628-1636, Aug. 2012.
- [94] A. Ashtari, E. Bibeau and S. Shahidinejad, “PEV charging profile prediction and analysis based on vehicle usage data, ” *IEEE Trans. Smart Grid*, vol. 3, no. 1, pp. 341-350, Mar. 2012.
- [95] L. Zhao, P. Awater, and A. Schafer, “Scenario-based evaluation on the impacts of electric vehicle on the municipal energy supply systems, ” *Power and Energy Society General Meeting*, 2011 IEEE.
- [96] M. Hübner, L. Zhao, and T. Mirbach, “Impact of large-scale electric vehi-

- cle application on the power supply, ” *Electrical Power & Energy Conference (EPEC)*, 2009 IEEE
- [97] M. F. Shaaban, Y. M. Atwa, and E. F. El-Saadany, “PEVs modeling and impacts mitigation in distribution networks, ” *IEEE Trans. Power Syst.*, vol. 28, no. 2, pp. 1122-1131, May. 2011.
- [98] D. Steen, L. A. Tuan, O. Carlson, and L. Bertling, “Assessment of electric vehicle charging scenarios based on demographical data, ” *IEEE Trans. Smart Grid*, vol. 3, no. 3, pp. 1457-1468, Sep. 2012.
- [99] S. Acha, K. H. van Dam, and N. Shah, “Modelling spatial and temporal agent travel patterns for optimal charging of electric vehicles in low carbon networks,” *Power and Energy Society General Meeting*, 2012 IEEE
- [100] "National Household Travel Survey", Department of Transportation. [online]. Available: <http://nhts.ornl.gov/>, Apr. 9, 2009, USA.
- [101] V. G. Kulkarni, "Discrete-time Markov Models," in *Modeling, Analysis, Design, and Control of Stochastic Systems*, Springer, pp. 106-109, May 1999.
- [102] S. N. Mandal, J. P. Choudhury, and S. R. B. Chaudhuri, "In search of suitable fuzzy membership function in prediction of time series data," *International Journal of Computer Science Issues*, vol. 9, no. 3, pp. 293-302, May 2012.
- [103] C. W. Tao and J. S. Taur, "Alternative Equivalent Designs of Fuzzy Controllers." *Proceedings of the Fifth IEEE International Conference on Fuzzy Systems*, vol. 1, pp. 439-443, Sep. 1996
- [104] S. Teleke, M. E. Baran and S. Bhattacharya, "Optimal control of battery energy storage for wind farm dispatching," *IEEE Trans. Energy Convers.*, vol. 25, no. 3, pp. 787-794, Sep. 2010.
- [105] Y. H. Song, A. Johns and R. Aggarwal, "Genetic algorithm in power system optimization," in *Computational Intelligence Applications to Power Systems*, Springer, pp. 135-137, Nov. 1996.

- [106] S. Boyd and L. Vandenberghe, *Convex Optimization*, Cambridge University Press, pp. 9-10, 2004.
- [107] SAE electric vehicle and plug-in hybrid electric vehicle conductive charge coupler, *SAE Standard J1772*, Jan. 2010.
- [108] Urban Dynamometer Driving Schedule (UDDS). [online]. Available: www.epa.gov.
- [109] M. E. Baran, and F. F. Wu, "Network reconfiguration in distribution systems for loss reduction and load balancing," *IEEE Trans. Power Del.*, Vol. 4, No. 2, pp. 1401-1407, Apr. 1989.
- [110] S. Prousch, C. Breuer, and L. Zhao, "Operational optimization of municipal energy supply systems." *Power and Energy Society General Meeting*, 2010 IEEE.
- [111] V. G. Kulkarni, "Discrete-time Markov Models," in *Modeling, Analysis, Design, and Control of Stochastic Systems*, Springer, pp. 106-109, May 1999.
- [112] K. Clement-Nyns, E. Haesen, and J. Driesen, "The impact of charging plug-in hybrid electric vehicles on a residential distribution grid," *IEEE Trans. Power Syst.*, vol. 25, no. 1, pp. 371-380, Feb. 2010.
- [113] B. Geng, J. K. Mills and D. Sun, "Two-stage charging strategy for plug-in electric vehicles at the residential transformer level," *IEEE Trans. Smart Grid*, vol. 4, no. 3, pp. 1442-1452, Sept. 2013.
- [114] G. Zhang, T. Tan and G. Wang, "Real-time smart charging of electric vehicles for demand charge reduction at non-residential sites," *IEEE Trans. Smart Grid*, early access.
- [115] T. Tran-Quoc and L. Nguyen-Van, "Integration of electric vehicles into an industrial grid: Impact assessment and solutions." *Power and Energy Society General Meeting*, 2016 IEEE
- [116] H. N. T. Nguyen, C. Zhang and J. Zhang, "Dynamic demand control of electric vehicles to support power grid with high penetration level of re-

- newable energy," *IEEE Trans. Transport. Electrification*, vol. 2, no. 1, pp. 66-75, Mar. 2016.
- [117] W. Yao, J. Zhao and F. Wen, "A hierarchical decomposition approach for coordinated dispatch of plug-in electric vehicles," *IEEE Trans. Power Syst.*, vol. 28, no. 3, pp. 2768-2778, Aug. 2013.
- [118] E. S. Rigas S. D. Ramchurn and N. Bassiliades, "Managing Electric Vehicles in the Smart Grid Using Artificial Intelligence: A Survey," *IEEE Trans. Intell. Transp. Syst.*, vol. 16, no. 4, pp. 1619-1635, Aug. 2015.
- [119] W. Yao, C. Y. Chung, F. Wen, M. Qin and Y. Xue, "Scenario-based comprehensive expansion planning for distribution systems considering integration of plug-in electric vehicles," *IEEE Trans. Power Syst.*, vol. 31, no. 1, pp. 317-328, Jan. 2016.
- [120] S. Bashash and H. K. Fathy, "Cost-optimal charging of plug-in hybrid electric vehicles under time-varying electricity price signals," *IEEE Trans. Intell. Transp. Syst.*, vol. 15, no. 5, pp. 1958-1968, Oct. 2014.
- [121] Y. He, B. Venkatesh and L. Guan, "Optimal scheduling for charging and discharging of electric vehicles," *IEEE Trans. Smart Grid*, vol. 3, no. 3, pp. 1095-1105, Sept. 2012.
- [122] A. O. Kotb, Y.-C. Shen, X. Zhu and Y. Huang, "iParker—A new smart car-parking system based on dynamic resource allocation and pricing," *IEEE Trans. Intell. Transp. Syst.*, vol. 17, no. 9, pp. 2637-2647, Sept. 2016.
- [123] Y. Mou, H. Xing, Z. Lin and M. Fu, "Decentralized optimal demand-side management for PHEV charging in a smart grid," *IEEE Trans. Smart Grid*, vol. 6, no. 2, pp. 726-736, Mar. 2015.
- [124] A. Fawaz, R. Berthier and W. H. Sanders, "A Response Cost Model for Advanced Metering Infrastructures," *IEEE Trans. Smart Grid*, vol. 7, no. 2, pp. 543-553, Mar. 2016.
- [125] P. Grahn, K. Alvehag and L. Söder, "PHEV utilization model considering type-of-trip and recharging flexibility," *IEEE Trans. Smart Grid*, vol. 5, no.

- 1, pp. 139-148, Jan. 2014.
- [126] Q. Wu, "EVs and the Current Nordic Electricity Market," in *Grid Integration of Electric Vehicles in Open Electricity Markets*, Wiley, Jun. 2013, pp. 34-37.
- [127] R. Li, Q. Wu, and S. S. Oren, "Distribution locational marginal pricing for optimal electric vehicle charging management," *IEEE Trans. Power Syst.*, vol. 29, no. 2, pp. 203-211, Jan. 2014.
- [128] C. D. Korkas, S. Baldi, P. Michailidis and E. B. Kosmatopoulos, "a cognitive stochastic approximation approach to optimal charging schedule in electric vehicle stations", *25th Mediterranean Conference on Control and Automation*, 2017.
- [129] B. Skugor and J. Deur, "Dynamic programming-based optimization of electric vehicle fleet charging." *IEEE International Electric Vehicle Conference (IEVC)*, 2014
- [130] P. Martín and A. Sierra, "Improving Power System Static Security Margins by Means of a Real Coded Genetic Algorithm," *IEEE Trans. Power Syst.*, vol. 31, no. 3, pp. 1915-1924, May 2016.
- [131] A. M. Eldurssi and R. M. O'Connell, "A Fast Nondominated Sorting Guided Genetic Algorithm for Multi-Objective Power Distribution System Reconfiguration Problem," *IEEE Trans. Power Syst.*, vol. 30, no. 2, pp. 593-601, Mar. 2015.
- [132] B. Pal and B. Chaudhuri, "Test System Model," in *Robust control in power systems*, Springer, pp. 39-41, 2005.
- [133] U.S. Energy Information Administration (EIA). [online]. Available: <http://www.eia.gov/electricity/>.
- [134] The New York Independent System Operator (NYISO). [online]. Available: http://www.nyiso.com/public/markets_operations/.